Gold Nanorods: From Synthesis and Properties to Biological and Biomedical Applications

By *Xiaohua Huang, Svetlana Neretina,* and *Mostafa A. El-Sayed**

Noble metal nanoparticles are capable of confining resonant photons in such a manner as to induce coherent surface plasmon oscillation of their conduction band electrons, a phenomenon leading to two important properties. Firstly, the confinement of the photon to the nanoparticle's dimensions leads to a large increase in its electromagnetic field and consequently great enhancement of all the nanoparticle's radiative properties, such as absorption and scattering. Moreover, by confining the photon's wavelength to the nanoparticle's small dimensions, there exists enhanced imaging resolving powers, which extend well below the diffraction limit, a property of considerable importance in potential device applications. Secondly, the strongly absorbed light by the nanoparticles is followed by a rapid dephasing of the coherent electron motion in tandem with an equally rapid energy transfer to the lattice, a process integral to the technologically relevant photothermal properties of plasmonic nanoparticles. Of all the possible nanoparticle shapes, gold nanorods are especially intriguing as they offer strong plasmonic fields while exhibiting excellent tunability and biocompatibility. We begin this review of gold nanorods by summarizing their radiative and nonradiative properties. Their various synthetic methods are then outlined with an emphasis on the seed-mediated chemical growth. In particular, we describe nanorod spontaneous self-assembly, chemically driven assembly, and polymer-based alignment. The final section details current studies aimed at applications in the biological and biomedical fields.

1. Introduction

The physical and chemical properties of matter are, to a large degree, determined by the type of motion its electrons are allowed to execute. The electronic motion, in turn, is dependent on the type of material and the space accessible to its electrons (i.e., the degree of confinement). The spatial effect becomes pronounced when the electrons are confined to the nanometer scale. Thus, when materials are reduced to these mesoscopic dimensions (in the 1–100 nm range), new properties appear due to the restrictions imposed on their electronic motion, an effect which also strongly depends on the overall shape of the material. When the size of semiconductor nanocrystals reaches the 2–10 nm range, which is often comparable to or smaller than their exciton Bohr radius, the motion of their charge carriers becomes confined (quantum confinement) leading to unique absorption and fluorescence properties that are dependent on both the particle's size and shape. In metals, when the particle size becomes comparable to, or smaller than the electron mean free path, surface effects become important, often dominating the response, giving rise to properties quite different from the bulk. Transition metal nanoparticles have shown great functionality, finding their way in nanocatalysis applications, which rely on the large surface to volume ratios available as well as the improved catalytic efficiencies achieved through size and shape dependencies.[1,2] Noble metal (plasmonic) nanoparticles, on the other hand, have distinguished themselves as a distinct class of metallic nanoparticles. In addition to their useful catalytic property,[3] they have the ability to confine resonant photons within their small particle size to induce the localized surface plasmon oscillations of the

[*] Prof. M. A. El-Sayed
Laser Dynamics Laboratory
School of Chemistry and Biochemistry
Georgia Institute of Technology
Atlanta, GA 30332 (USA)
E-mail: melsayed@gatech.edu
Dr. X. Huang
Laser Dynamics Laboratory
School of Chemistry and Biochemistry
Georgia Institute of Technology, Atlanta, GA 30332 (USA)

Dr. X. Huang
Emory-Georgia Tech Cancer Center for Nanotechnology Excellence
Department of Biomedical Engineering
Emory University and Georgia Institute of Technology
Atlanta, GA 30332 (USA)
Dr. S. Neretina
Laser Dynamics Laboratory
School of Chemistry and Biochemistry
Georgia Institute of Technology
Atlanta, GA 30332 (USA) and
Dr. S.Neretina
Department of Mechanical Engineering
Temple University
1947 N. 12th St., Philadelphia, PA 19122 (USA)

DOI: 10.1002/adma.200802789

conduction band electrons. This photon confinement increases the amplitude of the light wave by orders of magnitude, which dramatically increases the light intensity by virtue of the fact that the intensity is proportional to the square of the wave's amplitude. In this manner, noble metal nanoparticles, through plasmonic confinement, effectively focus resonantly coupled light. As a result, all radiative properties, such as light absorption, fluorescence, Rayleigh scattering (Mie), and Raman scattering are enhanced by orders of magnitude. The strong scattering from these nanoparticles greatly increases their functionality in optical imaging. Furthermore, the optical imaging resolving power using these nanoparticles has greatly increased. This is due to the fact that the optical detection of objects attached to the scattering nanoparticles is determined, not by the diffraction-limited photon wavelength, but by the much smaller size of the nanoparticle.

Once resonant photons are confined within a plasmonic nanoparticle, they excite the localized surface plasmon oscillations, which give rise to strong surface electromagnetic fields that propagate around the particle and decay exponentially over a distance comparable to the particle size.[4] This plasmonic near-field can affect the properties of materials in proximity to the nanoparticles. Examples of this field effect are: i) the large enhancement of the Raman scattering by species adsorbed onto the surface of the particles (surface-enhanced Raman spectroscopy—SERS);[5,6] ii) the decrease of the retinal photoisomerization rate in the photocycle of bacteriorhodopsin—the other photosynthetic system in nature;[7] iii) the increased rate of nonradiative relaxation of hot electrons in CdTe semiconductor nanowires;[8] iv) the elongation of the coherent phonon oscillation of the nanoparticles;[9] v) the dramatic increase of the Raman scattering from surrounding species, the so-called ''hot spot'' effect,[10] due to field coupling when two or more plasmonic nanoparticles are close to one another; and vi) the red-shift of the surface plasmon resonance (SPR) band due to field coupling, as observed by the distinct color change when plasmonic nanoparticles come close together in a bulk solution, a phenomenon used for colorimetric detection.[11] In fact, the dependence of the fractional shift of the plasmon wavelength from coupled pairs of nanoparticles on the interparticle distance (in units of the particle size) has recently been used as a ''molecular ruler'' to measure intersite distances in biological systems.[12–14] This spectral shift exhibits a universal scaling behavior that is independent of the particle's size but not of its shape.[4,15–19]

When plasmonic nanoparticles (gold or silver) are exposed to laser light resonant with their surface plasmon oscillation, they can strongly absorb the light and rapidly convert it into heat via a series of photophysical processes.[20–22] By adjusting the rate of absorption (which is determined by the absorption cross-section and the laser pulse width and energy) relative to the rate of cooling, the nanoparticles exhibit a number of varied responses, where each is suitable to particular applications. Lower rates of excitation lead to photothermal heating of the nanoparticles and its surrounding medium. If, in this regime, the nanoparticles are selectively attached to a diseased (e.g., cancerous) cell, then the heat can selectively melt its membrane. This has been demonstrated to be an effective selective photothermal therapeutic method capable of destroying cancerous cells both in vitro and in vivo.[23,24] If nanosecond laser pulses are used to obtain an increased rate of optical excitation, then melting of the plasmonic nanoparticles occurs. Indeed, prismatic nanoparticles have been shown to melt into spheres with many of them flying away from the substrate, an effect which provides a potential means of propulsion for nanomotor applications.[25] When femtosecond pulses are used, ablation leads to a pressure build-up underneath the nanoparticle, which results in a high-speed ejection, but the nanoparticle shape is preserved.[26] If the fluence is significantly

Xiaohua Huang received her B.S. degree in Chemistry from Jilin University, China in 1996 and her Ph.D. in Analytical Chemistry from the Georgia Institute of Technology in 2006. Currently, she is a distinguished CCNE Postdoctoral Fellow in the Emory-Georgia Cancer Nanotechnology Center, Department of Biomedical Engineering at Emory and Georgia Tech, supervised by Prof. Mostafa A. El-Sayed and Prof. Shuming Nie. Her research is focused on cancer imaging, diagnosis, and photothermal therapy using gold nanoparticles and some other advanced nanomaterials.

Svetlana Neretina received her Ph.D. in Engineering Physics from McMaster University, Canada in 2007. She has since worked as a postdoctoral researcher at the Georgia Institute of Technology. Her current research is directed toward the nanofabrication and characterization of coupled semiconductor-plasmonic structures with potential biomedical applications.

Mostafa A. El-Sayed received his B.S. degree from Ain Shams University, Egypt and Ph.D. degree from Florida State university. He taught at UCLA until 1994, when he became the Julius Brown Chair, Regents Professor and Director of the Laser Dynamics Lab at Georgia Tech. He is an elected member of the National Academy of Sciences and a recipient of the 2007 National Medal of Science. His current research is focused on the properties of metal nanoparticles and their applications in nanocatalysis, nanophotonics, and nanomedicine.

lowered, then the femtosecond pulses induce a coherent oscillation of the nanoparticle's lattice.[27,28] These oscillations can have a frequency, which depends on the nanoparticle's size, shape, and interparticle distance.[29–31] Such oscillating nanoparticles could be used to modulate scattered laser light for future optical communication devices.

Another remarkable feature of plasmonic nanoparticles is the degree by which their optical properties can be tuned through changes in their size, shape, composition, structure, and morphology, and, when assembled, their relative interparticle orientation and separation.[32] Silver colloids exhibit significantly shorter SPR wavelengths than do gold colloids, with both metals showing a trend toward longer resonant wavelengths as the particle size is increased.[33] Changing the structure of the gold particles from a solid sphere to a shell formed on a silica nanoparticle[34] or to a hollow cage[35] results in a shift of the optical extinction band from the visible to near-infrared region. Such structural and compositional tuning is quite useful in potential in vivo applications where tissue absorption in the near-infrared window (650–900 nm) is minimal, and thus, favorable to optimal light penetration.[36] Gold nanorods also offer a means of tailoring the SPR to a particular wavelength,[37,38] but with significant advantages. The synthetic routes, especially the seed-mediated growth protocol, are both facile and well established, producing stable structures with high yield and monodispersity. Nanorods, unlike more symmetrically shaped nanoparticles (i.e., spheres, shells, cubes, or cages), also have the ability to assemble into a number of alternatively aligned configurations, a property which gives rise to optical anisotropies that should prove useful to a number of potential photonic devices.

The recent and rapid upsurge in research activities devoted to gold nanorods in biological and biomedical applications is, to a large extent, a result of the unique nature of these rod-shaped nanostructures. The sensitivity of the SPR bands to the local environment is quite important in terms of biological sensing. The radiative elastic Rayleigh scattering, inelastic Raman scattering, two-photon- induced luminescence, and photoacoustic properties offer multiple modalities for molecular imaging and disease diagnostics. The nonradiative photothermal property,[20–22] often used to characterize the thermal properties of nanomaterials, can be utilized in drug and gene delivery and in photothermal therapy of cancer and other diseases. Here, we present a broad-based review covering selected topics of importance to gold nanorod properties, fabrication, and applications. We summarize both the radiative and nonradiative properties of gold nanorods. Routes to synthesis, which include bottom-up and top-down approaches, are outlined with a further discussion of techniques devoted to nanorod assembly. The final section details current applications of gold nanorods in the biological and biomedical fields.

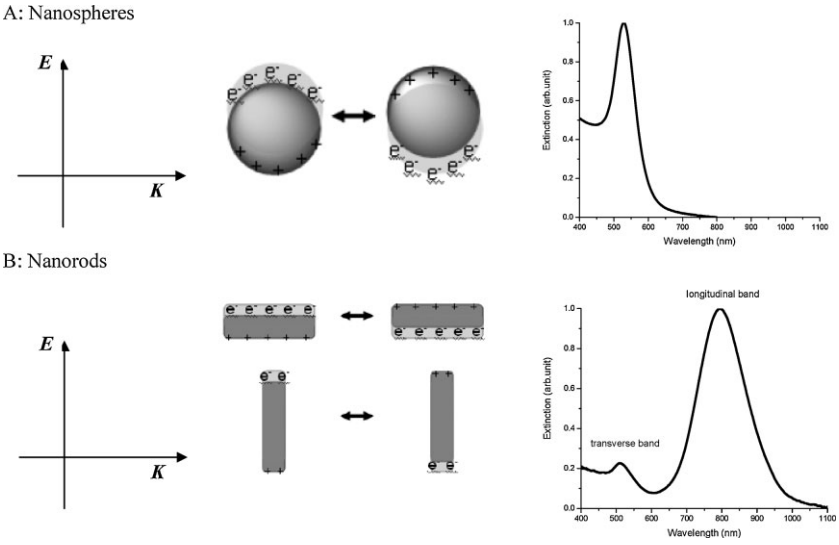

Figure 1. Schematic illustration of the interaction of polarized light and gold nanospheres (A) and nanorods (B) to form the electronic coherent surface plasmon resonance (SPR) oscillation. The electric field (*E*) of incident light (propagating along the *K* direction) induces coherent collective oscillation of conduction band electrons with respect to the positively charged metallic core. This dipolar oscillation is resonant with the incoming light at a specific frequency that depends on particle size and shape. While gold nanospheres show one SPR band in the visible region, gold nanorods show two bands: a strong longitudinal band in the near-infrared region corresponding to electron oscillation along the long axis and a weak transverse band, similar to that of gold nanospheres, in the visible region corresponding to electron oscillations along the short axis.

2. Properties

2.1. Radiative Properties

2.1.1. Surface Plasmon Resonance Absorption, Scattering, and Total Extinction

The intriguing optical properties of metal nanoparticles, as reflected by their intense color, are attributed to their unique interaction with incident light. In the presence of the oscillating electromagnetic field of light, the conduction band electrons of a metal nanoparticle undergo a collective coherent oscillation in resonance with the frequency of light, which is called the SPR.[39–43] This oscillation induces a charge separation between the free electrons and the ionic metal core, which in turn exerts a restoring Coulomb force to make the electrons oscillate back and forth on the particle surface resulting in a dipole oscillation in the simplest case (Fig. 1A). The SPR oscillation induces a strong absorption of light, as seen in the UV–vis spectrum, which is the origin for the observed color of the colloidal solution as explained by Mie theory.[39] The SPR condition is dependent on the particle size, shape, structure, the dielectric properties of the metal, and the surrounding medium, as these factors affect the electron charge density on the particle surface.[20,22,39–46] Spherical gold, silver, and copper nanoparticles show a strong SPR band in the visible region while other metals show broad and weak bands in the UV region.[47,48] Hollow[49–51] or core/shell structures[34] show a very large red-shift of the SPR wavelength compared to solid structures. Anisotropic nanoparticles, such as triangular[52] and

branched[53] structures, also exhibit a red-shifted SPR band compared to their spherical analogs.

In the case of gold nanorods, electron oscillation can occur in one of two directions depending on the polarization of the incident light: the short and long axes (Fig. 1B). The excitation of the surface plasmon oscillation along the short axis induces an absorption band in the visible region at wavelength similar to that of gold nanospheres, referred to as the transverse band. The excitation of the surface plasmon oscillation along the long axis induces a much stronger absorption band in the longer wavelength region, referred to as the longitudinal band. While the transverse band is insensitive to the size of the nanorods, the longitudinal band is red-shifted largely from the visible to near-infrared region with increasing aspect ratio (length/width). This optical behavior can be well understood according to Gans[54] theory which was developed for the explanation of optical properties of ellipsoid particles based on a dipole approximation. In aqueous solution, the SPR absorption maximum (λ_{max}) is linearly proportional to the aspect ratio (R) by the following relationship:[55–58]

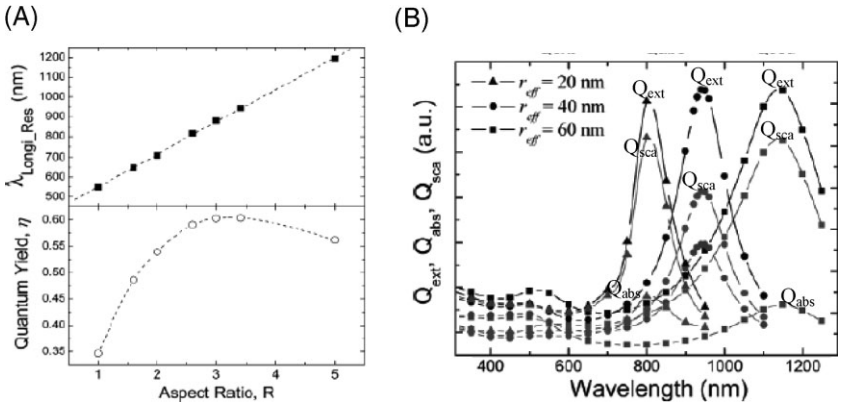

Figure 2. A) Dependence of the wavelength and scattering quantum yield of the longitudinal SPR on the aspect ratio. Unlike the resonance wavelength, which shows a linear relationship with R, the scattering quantum yield increases with increasing R, reaching a maximum at 3.4, and begins to decrease with further increases. B) Dependence of the relative contributions of light scattering and absorption to the total extinction efficiency on the size of the rods at a fixed aspect ratio of 3.4. Reproduced with permission from [71]. Copyright 2006, the American Chemical Society (ACS).

$$\lambda_{max} = 95R + 420 \quad (1)$$

This provides the possibility of optically tuning gold nanorods by simply varying the aspect ratio of the particles, which is different from spheres for which the SPR only slightly red-shifts with increasing particle size. Gans theory also enables the determination of the statistical distribution of aspect ratios of a nanorod solution by fitting the observed inhomogeneously broadened SPR absorption spectrum of gold nanorods in solution with a convolution of homogeneously broadened spectra of nanorods, each with a specific aspect ratio and population contributions.[59] Such a method provides a relatively convenient alternative to conventional transmission electron microscopy (TEM).

Due to the SPR excitation, light absorption by gold nanoparticles is strongly enhanced on the scale of 5–6 orders of magnitude larger than that of dye molecules.[60] The same fact exists for light scattering, the other process contributing to total light extinction. This can be seen from the quantitative description of the cross-sections of absorption (C_{abs}), scattering (C_{sca}), and total extinction (C_{ext}) derived from Gans theory:[61–63]

$$C_{abs} = \frac{2\pi}{3\lambda}\varepsilon_m^{3/2} V \sum_i \frac{\varepsilon_2/\left(n^{(i)}\right)^2}{\left(\varepsilon_1 + [(1-n^{(i)})/n^{(i)}]\varepsilon_m\right)^2 + \varepsilon_2^2} \quad (2)$$

$$C_{sca} = \frac{8\pi^3}{9\lambda^4}\varepsilon_m^2 V^2 \sum_i \frac{(\varepsilon_1 - \varepsilon_m)^2 + \varepsilon_2^2/\left(n^{(i)}\right)^2}{\left(\varepsilon_1 + [(1-n^{(i)})/n^{(i)}]\varepsilon_m\right)^2 + \varepsilon_2^2} \quad (3)$$

$$C_{ext} = C_{abs} + C_{sca} \quad (4)$$

where λ is the wavelength of light, V the unit volume of the nanoparticle, ε_m the dielectric constant of the surrounding medium, ε the dielectric constant of the metal given by $\varepsilon = \varepsilon_1 + i\varepsilon_2$ (in which, ε_1 and ε_2 are the real and imaginary components of the dielectric constant), and $n^{(i)}$ the depolarization factor, defined by:

$$n^{(a)} = \frac{2}{R^2-1}\left(\frac{R}{2\sqrt{R^2-1}}\ln\frac{R+\sqrt{R^2-1}}{R-\sqrt{R^2-1}} - 1\right) \quad (5)$$

$$n^{(b)} = n^{(c)} = \left(1 - n^{(a)}\right)/2 \quad (6)$$

where a, b, and c are the three axes of the nanoparticle, $a > b = c$, and the aspect ratio, R, is equivalent to a/b. For spheres, $n^{(i)}$ is equal to 1/3. The SPR occurs at $\varepsilon_1 = -(1-n^{(i)}) \times \varepsilon_m/n^{(i)}$, where $i = a$ for the longitudinal resonance and $i = b,c$ for the transverse resonance. At such resonance wavelengths, the absorption, scattering, and total extinction are all strongly enhanced, which is the basis for their application in biological and biomedical imaging and therapeutics.

The absorption, scattering, and total extinction of gold nanorods not only depend on the wavelength of the light, but also the particle aspect ratio and size. The relative contribution of the absorption and scattering to the total extinction at different aspect ratios and sizes has been well studied theoretically by Lee and El-Sayed[64] using discrete dipole approximation (DDA),[65–69] which is a powerful tool for calculating optical properties, especially the scattering problem of targets with arbitrary geometry. In their studies, they define a scattering quantum yield, η:

$$\eta = \left.\frac{Q_{sca}}{Q_{ext}}\right|_{Res} \quad (7)$$

which is the ratio of scattering efficiency (Q_{sca}) to the total extinction efficiency (Q_{ext}) at their respective resonance maxima.

The quantum yield increases dramatically with increasing aspect ratio, but it drops slightly for further increases in elongation at $R > 3.4$ for rods with an effective radius (r_{eff}) of 40 nm (Fig. 2A). Their studies also show that the scattering quantum yield is enhanced from 0.326 for a sphere to 0.603 for a rod by only elongating the shape. This is probably because of the dramatic reduction of plasmon dephasing in nanorods compared to nanospheres (e.g., suppression of interband damping[70]). At a fixed aspect ratio, the absorption efficiency is dominant for smaller rods and the scattering efficiency is dominant for larger rods (Fig. 2B,[64]). Similar phenomena apply to gold nanospheres.[60] These studies offer a golden standard for choosing gold nanoparticles for biomedical applications. For imaging, larger nanoparticles are preferred because of their higher scattering efficiency, whereas for photothermal therapy, smaller nanoparticles are preferred as light is mainly adsorbed by the particles, and thus, efficiently converted to heat for cell and tissue destruction.

The SPR band is also sensitive to the dielectric constant of the surrounding medium, as can be seen from Equations 2, 3, and 4. The sensitivity, defined as a shift in the SPR wavelength relative to the refractive index change of the surrounding medium, increases linearly with the increasing aspect ratios.[71,72] The sensitivity is more prominent for nanorods with higher aspect ratios, but the resolution might decrease due to broadening of the absorption bandwidth, resulting from the contributions of the multipolar electron oscillations. Experimental comparison of the sensitivity of nanoparticles of various shapes found that gold nanorods show much higher sensitivity than nanospheres, but lower sensitivity than gold nanobranches.[72]

2.1.2. Surface Plasmon Resonance Linewidths and Lifetimes

The SPR linewidth plays an important role in the sensitivity of SPR to local environmental changes.[73] Narrow linewidths give higher sensitivity. Also associated with narrow linewidths is large near-field enhancement, a property crucial to the occurrence of sizable nonlinear optical and surface-enhanced Raman scattering effects. It is, thus, paramount to these burgeoning technologies that the factors governing the resonant linewidth are well understood and characterized.

The spectroscopies most commonly used to characterize plasmon resonances rely on the collective response of an ensemble of nanostructures. Because such ensembles show significant size and shape distributions, the measured resonant linewidth provides more information about the ensemble's inhomogeneities than it does the intrinsic linewidth of individual nanostructures. As a result, studies of the intrinsic linewidth have had to rely almost exclusively on spectroscopies that are able to probe single nanoparticles. Spectra have been obtained for individual nanostructures by probing the total internal reflection,[74] the dark-field light scattering,[75,76] or the absorptive response[77] of the structure.

When a plasmon is created, it is subject to a number of processes that damp the collective oscillation. It is this ''dephasing'' of the oscillation that ultimately results in the plasmon's decay. The resonance linewidth provides a measure of this process as it is inversely proportional to the lifetime of the plasmon. Damping can occur either through radiative or nonradiative processes. Radiative damping occurs when the oscillating dipole moment of the plasmon gives rise to photon emission. Nonradiative damping occurs when the plasmon excites intraband or interband electronic transitions or through electron scattering processes at the surface of the nanostructure. Sönnichsen et al.[70] obtained spectra for individual nanospheres of various radii and for nanorods having various aspect ratios. They extracted both the plasmon linewidth and lifetimes for each structure. The result, shown in Figure 3, clearly demonstrates that nanorods with a high aspect ratio show the narrowest linewidths and, hence, the longest lifetimes. The reduction in linewidth for the nanorods compared to nanospheres was attributed to a decrease in the nonradiative damping associated with interband transitions between the d-band and conduction band of gold. The excitation of such transitions requires a threshold energy of approximately 1.8 eV, an energy that is unavailable to plasmons red-shifted to energies below this value. Nanospheres, with plasmon resonances below this threshold value, also experience the same reduction in nonradiative damping, but it is more than offset by the increased radiative damping that accompanies the large volume nanospheres required to obtain these substantial red-shifts. As an aside, it is noted that hollow nanocubes, often termed nanoboxes or nanocages, while having significantly less gold per unit volume than gold nanospheres, still show very broad plasmon resonances due to significant radiation damping as well as enhanced surface scattering from the thin walls.[76]

The numerous decay routes available to the longitudinal plasmons in nanorods have prompted investigations aimed at determining the nanorod geometry that gives rise to the longest

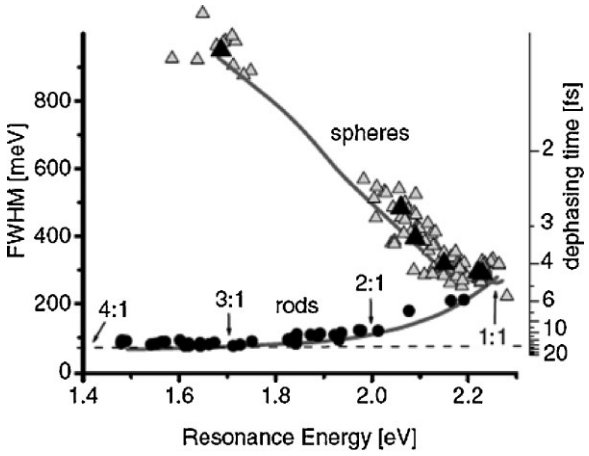

Figure 3. The dependence of the linewidth, Γ, and dephasing time of plasmon resonance of light scattering spectra on the resonant energy for single gold nanorods (dots) and nanospheres (open triangles) of various dimensions. Black triangles: averages for spherical particles of the same nominal size (150, 100, 80, 60, 40, and 20 nm from left to right). Lines: theoretical results. Some selected aspect ratios, a/b, are indicated. The plasmon dephasing time ranges from 1.4 to 5 fs for nanospheres and from 6 to 18 fs for nanorods. The dephasing rate ($1/T_2$ where T_2 is the dephasing time.) of nanospheres increases for larger particles due to increased radiation damping for increased particle volume. In contrast, the dephasing rate of nanorods decreases drastically with increasing aspect ratios due to reduced nonradiative plasmon decay. Reproduced with permission from [70]. Copyright 2007 the American Physical Society (APS).

plasmon lifetimes.[75,76] With the aforementioned high aspect ratio being an obvious requirement, studies were undertaken to examine plasmon linewidths for nanorods of various widths, but with identical aspect ratios. As expected, due to the increased radiative damping associated with larger volumes, linewidth broadening was observed as the width of the nanorod was increased. However, increased broadening for small nanorod widths was also observed due to the surface scattering occurring when the nanorod dimension became significantly smaller than the electronic mean free path in gold (~20 nm). These two competing processes lead to an optimum nanorod width in the range of 10–20 nm where the resonance is sharpest, the lifetime is the longest, and the near-fields are the greatest.

As a final commentary, two interesting studies performed on more intricate nanostructures will be discussed. The first, conducted by Becker et al.[78] examined the linewidth of both ensembles and individual gold nanorods coated with silver. Comparing the spectra from these core/shell structures to stand-alone gold nanorods they observed a blue-shift in the plasmon resonance for both individual core/shell structures and the ensembles. Significant was the fact that the observed linewidth for individual core/shell structures was narrower when compared to gold nanorods with the same resonant energy. Also noteworthy is that a stronger blue-shift occurs for gold nanorods having plasmon resonances at longer wavelengths. Thus, when an ensemble of gold nanorods is coated with silver all resonances exhibit a blue-shift that is weighted for nanorods having long wavelength resonances. The net result is an overall narrowing of the ensemble's plasmonic linewidth, an effect referred to as ''plasmonic focusing.'' The second study, conducted by Ueno et al.,[79] fabricated closely spaced gold nanoblock structures of various lengths with the nanoblocks aligned along the diagonal of the block's top surface. The longitudinal plasmonic resonances formed along this diagonal, in many ways, mimic those of nanorods of similar length, but lack the undesirable multipolar modes. These nanoblock structures, despite having volumes significantly larger than the comparable nanorods, showed similar radiative plasmon damping.

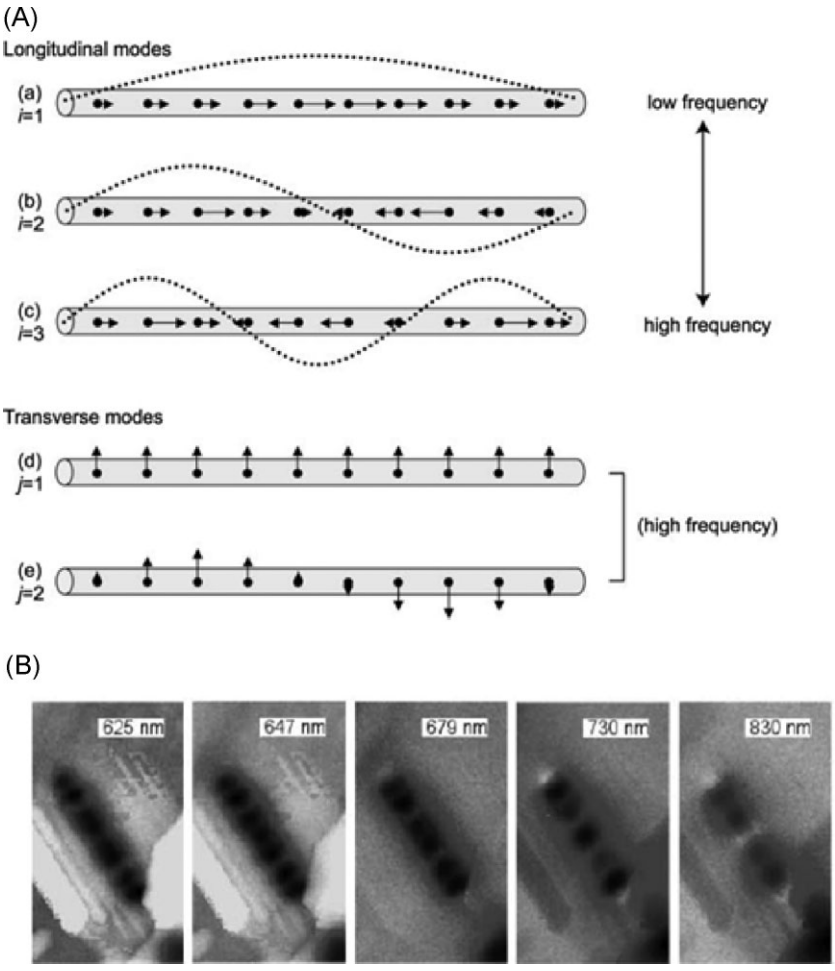

Figure 4. A) Schematic representation of the longitudinal and transverse plasmon modes for a nanorod. The standing waves describe the spatial distribution of the amplitude of the oscillating electrons. The longitudinal and transverse fundamental modes correspond to $i = 1$ and $j = 1$, respectively. B) Near-field transmission images measured for a resonantly excited gold nanorod (length = 510 nm, diameter = 20 nm). The images are acquired through the detection of transmitted and scattered light from a resonantly excited gold nanorod using a near-field technique. Note that the number of antinodes decreases from 8 to 4 as the resonant wavelength is increased from 625 to 830 nm. Reproduced with permission from [81]. Copyright 2007 the Royal Society of Chemistry (RSC).

2.1.3. Imaging Plasmonic Electron Density Distribution Using Near-Field Emission Techniques

A spatial distribution of the amplitude of surface plasmon mode in plasmonic nanoparticles is characterized by a standing wave pattern. Like any standing wave, plasmons can be in resonance at the fundamental frequency or any of its overtones, a response that is well established for long gold nanorods.[80] Figure 4A schematically displays both the fundamental mode and some of the smaller wavelength overtones for the longitudinal and transverse plasmon modes in gold nanorods.[81] The oscillating electrons constituting these standing wave modes generate the local electric fields that form the essence of the plasmonic wavefunction. These electric field strengths can be mapped using near-field optical techniques.

Near-field optical techniques are quite different from conventional spectroscopies in that the sample under investigation is illuminated with the light source from a nearby nanometer-scale aperture, making it possible to utilize a single-mode fiber-optic cable. The aperture's close proximity allows for a measured response in the optical near-field. Unlike conventional spectroscopies, where the measured response is in the optical far-field, near-field techniques are able to overcome the diffraction limit achieving spatial resolutions on the nanometer scale. Thus, by

scanning the aperture over a gold nanorod's surface, a point-by-point response is obtained and collectively gives rise to an image having a direct likeness to the square moduli of the plasmonic wavefunction. Figure 4B shows a number of near-field images acquired through the detection of transmitted and scattered light from a resonantly excited gold nanorod.[81,82] The images show a series of bright and dark spots which correspond to the nodes and antinodes of the plasmonic wavefunction, respectively. A compilation of such images for nanorods of various sizes indicates that the resonances fall on a single dispersion curve for nanorods of identical diameter.[83]

Advancements to this spectroscopic technique now allow for spectra which, instead of measuring the near-field transmission/scattering from a nanorod, measure the near-field two-photon photoluminescence generated by intense infrared pulses from a Ti/sapphire laser.[84] Unfavorable to this technique is the fact that the resonance condition must be obtained through appropriately chosen nanorod lengths as the excitation wavelength is fixed. The advantage to this technique is the enhanced image-contrast associated with the measurement of a nonlinear optical effect. This technique has shown its effectiveness by providing images considerably sharper than those in Figure 4. It has also been used to observe the lightening rod effect, where a narrowing of the nanowire's end gives rise to a build-up of intense fields.[85] High spatial resolution has also been obtained using a near-field mapping technique commonly referred to as photoemission electron microscopy (PEEM).[86]

In one of the more impressive demonstrations in the field of plasmonics, Imura et al.[87] incorporated ultrafast pump-probe techniques into these near-field methodologies. It allowed them to simultaneously monitor the spatial and temporal response of a nanorod once its localized surface plasmon mode was resonantly excited by an infrared pulse. A series of near-field images taken for progressively longer pump-probe delay times shows that the plasmon dissipation processes varied along the length of the nanorods and that there exists dramatic differences in the temporal response for the various positions. Striking differences were also observed between the nodal and antinodal positions, with relaxation processes occurring more rapidly near the nanorod ends. Analysis of the results allowed the authors to describe the response in terms of spatially uniform electron–electron processes and spatially dependent electron–phonon processes. Differences in the nodal and antinodal response were attributed to the longer electron–phonon coupling times arising from the higher electronic temperatures at the antinodes. In a follow-up report,[88] they explored the possibility of using these elevated electronic temperatures as a means of obtaining optical control over these plasmonic materials.

2.1.4. Near-Field Effect and Coupling

Near-Field Effect: The strongly resonant surface plasmon oscillation can simply be visualized as a photon confined to the small nanoparticle size. This strong confinement of the photon oscillation with the frequency of light in resonance with SPR leads to a large decrease in its wavelength (to fit within the nanoparticle). As a result, the amplitude of the photon wave increases greatly. Since the electromagnetic field is proportional to the square of the amplitude of the light wave, this will have the effect of greatly increasing the field intensity. Thus, effectively, capturing the photon within the plasmonic nanoparticles causes strong focusing of the electromagnetic field within the expected plasmonic nanoparticles.

The field strength depends on the particle type, size, and shape.[10] Silver is known to give higher field effects due to less plasmon damping by interband electron transitions. This is because the SPR and interband absorptions are further apart in silver nanoparticles than in gold nanoparticles. The field increases with increasing particle size, but further increases in size might decrease the field due to increased radiative damping for larger particles. This is most likely the reason why 60 nm spheres give larger enhancement than other sizes.[89] The field decays within a distance comparable to the size of the nanoparticle.[4] High curvature nanoparticles give a strong field enhancement (lightening-rod effect[90]). Using DDA calculations, Schatz and co-workers[91,92] have compared the field enhancement for various nanoparticle shapes. The results showed that prisms, rods, and spheroids with similar size dimension show similar enhancement with $|E|^2/|E_0|^2$ on the scale of $>10^3$, which is significantly higher than spheres ($\sim 10^2$) and E_0 is the electrical field of incident light. The nanorod shows much higher electric fields at the end of the long axis and weakest fields at the center of the rods. The *E*-field enhancement at their resonance wavelength increases with increasing aspect ratio for the same total particle volume.

The strong fields are the reason for the observed fluorescence from gold nanorods,[93] as well as a series of nonlinear optical processes described later in this review. It exerts effects on many properties of surrounding species, with the most noteworthy example being Raman enhancement of adsorbed species, known as surface-enhanced Raman scattering. Recently, the plasmonic field effect on biological processes has been reported by El-Sayed and co-workers,[7] who found that the field from gold nanoparticles slows down the rate of the dynamics of the primary step in the photocycle of bacteriorhodopsin (bR), a photosynthetic protein in nature besides chlorophyll. Another influence is the enhancement of the relaxation rate of hot electrons in an electronically quantized system.[8] Femtosecond transient spectroscopy measurements, carried out on CdTe nanowires (width = 75 nm, height = 200 nm) coated with a 15 nm gold nanoshell, showed an enhanced rate of electronic relaxation in the semiconductor when the states were excited resonantly with the surface plasmon band of the gold nanoshell. It should be recognized that the observed enhancement factor of less than two is nowhere near as great as the aforementioned radiative enhancements. The authors proposed several possible mechanisms for the enhancement, with some of them being directly linked to enhanced radiative processes in the CdTe nanowire brought on by the plasmonic field.

Near Field Coupling: It should be not surprising that when plasmonic nanostructures are brought in close proximity to one another the same near-fields result in interparticle interactions. Thus far, the most revealing work, in terms of the electromagnetic coupling between gold nanostructures, has been conducted on lithographically generated gold nanodisk pairs.[4,94,95] As expected, these investigations demonstrate that near-fields give rise to a collective extinction response that is quite different from that of isolated nanodisks, which can be seen in Figure 5A and B. Along the axis formed between the centers of the two disks, there

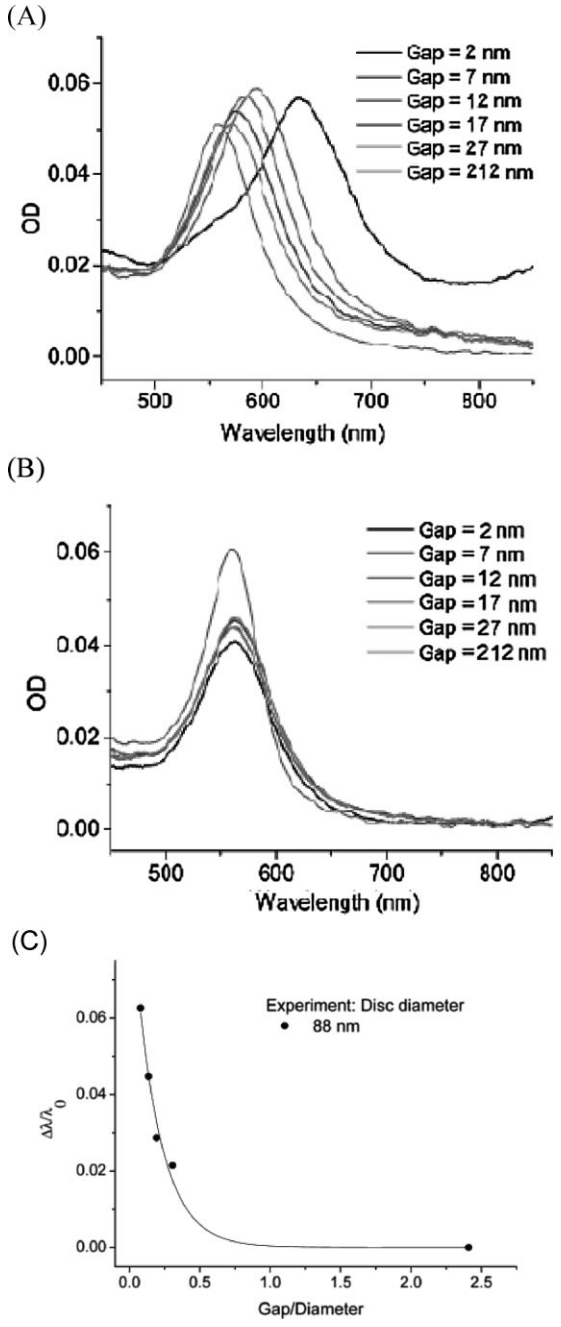

Figure 5. Microabsorption spectra for gold nanodisk pairs for various gap spacings with the polarization of the incident light along (A) and orthogonal (B) to the axis formed between the centers of the two disks. Isolated nanodisks show spectra near that of the largest spacing. The SPR wavelength red-shifts dramatically with decreasing interparticle distance when the light is polarized along the axis. It does not change obviously when the light is polarized orthogonal to the axis. (OD is optical density) C) Calculated fractional shift in the plasmon wavelength maximum as a function of the interparticle gap for side-by-side nanodisks with the light polarized along the axis formed between the centers of the two disks. The plot of the plasmon shift versus the interparticle gap follows nearly an exponential decay. Reproduced with permission from [4]. Copyright 2007 ACS.

exists a red-shift ($\Delta\lambda$) in the plasmon resonant wavelength (λ_0) which increases in size as the interparticle distance is reduced. A plot of the calculated fractional plasmon wavelength shift, $\Delta\lambda/\lambda_0$, versus the ratio of the interparticle spacing to particle size (Fig. 5C) shows near exponential behavior, with a decay length that is approximately 0.2 times the interparticle gap. Spectra taken for the orthogonal direction show only slight deviations from the response observed for isolated nanodisks, exhibiting a small blue-shift for the smallest interparticle spacings.

Even though studies utilizing the nanodisk geometry are more advanced, coupled nanorods provide a more attractive geometry due to the large oscillator strength and tunability of the longitudinal plasmon mode. Controlled studies of such effects necessitate the formation of well-defined geometries, such as the side-by-side or end-to-end configurations. These configurations allow one to probe the coupling effects on longitudinal and transverse modes by polarizing the light parallel or perpendicular to the long axis of the nanorods, respectively.[96] The responses from the two configurations were quite different. The side-by-side geometry showed a blue-shift in the longitudinal mode and a red-shift in the transverse mode while the end-to-end geometry showed a red-shift in the longitudinal mode with little change in the transverse mode. These optical changes have been explained by Jain et al.[97] in terms of simple dipole–dipole ''selection rules'' for the plasmon coupling. DDA calculations[17] show that the maximum coupling between two nanorods arises when they are end-to-end, closely spaced, identical in size, of high aspect ratios, and with large end-curvatures. It also shows an increased coupling for trimer structures formed when three nanorods are placed end-to-end or side-by-side. Fabricated gold nanorod arrays show similar trends as the assembled colloidal rods.[98–100]

The sizeable amount of data and theoretical modeling, describing the coupling between various shaped nanostructures, has made possible numerous comparisons. In their study of gold nanoparticles, Su et al.[95] demonstrated that the plasmon shift, due to field coupling, increased exponentially as the interparticle dimension decreased. Moreover, they realized that nanoparticles of different size could all be described by an identical relationship if the shift in the plasmon wavelength, $\Delta\lambda$, was scaled by the plasmon wavelength, λ_0, and the particle size, D. The relationship is given by:

$$\Delta\lambda/\lambda_0 = \kappa \exp^{-s/\tau D} \quad (8)$$

where κ is a proportionality constant, s is the interparticle distance, and τ is a decay length with a value near 0.2. It was later shown that this relationship was also followed by other coupled nanostructures, such as nanodisks[4] (as in Fig. 5), nanoshells,[16] and nanorods[17] when scaled with the disk diameter, the metal shell thickness, and the long axis dimension, respectively. It was further pointed out that the relationship holds regardless of the nanoparticle's surrounding medium and for plasmonic nanostructures formed from metals other than gold.[4] This shared behavior, now termed as the ''Universal Scaling Law,'' allows for a predictable coupling response from a wide variety of nanostructures. The origin of this scaling law relies on the interplay between the nanoparticle's polarizability, which varies as the cubic power of the particle's size, and the plasmonic near-field coupling, which varies as the inverse cubic power of the distance.

Thus, as the nanoparticle's size is increased, its increased polarizability supports enhanced coupling, but at the same time, the near-field's influence on the adjacent particle is diminished due to the increased length-scales associated with larger nanoparticles. As a result, there are two competing factors that are inextricably linked due to the geometries of these coupled systems. The Universal Scaling Law exists due to the inherent scaling associated with these two competing parameters. It should be understood, however, that the scaling law makes no predictions with regard to the coupled particle's plasmon strength.

Coupled nanostructures hold tremendous promise from an applications point of view. Quite obvious from this simple example is the potential for coupled nanostructures to be used in detection systems. A more sophisticated example, which utilizes the same basic principle, is in the detection of a biomolecular event that results only when a biological species is trapped between two functionalized nanoparticles. The event is detected by the shift in the plasmon wavelength that arises due to the nanoparticle coupling. Sönnichsen et al.[14] were able to monitor such events using a dark-field microscope in transmission mode. Through the use of linkers, they were able to bind gold nanospheres to a glass surface. Once a biological species was trapped between this bound nanosphere and another gold nanosphere, they were able to monitor a single coupled pair for as long as 3000 s. For such a coupled system, it is also possible to extract information about the size of the trapped species as the plasmon wavelength has an exponential dependence upon the interparticle spacing. In their report, they anticipated that such a ''plasmon ruler'' would be able to monitor distances up to 70 nm with better than 1 nm resolution. Like any system of measurement, however, the plasmon ruler requires calibration.[12] Fortunately, an elaborate calibration scheme is not required due to the aforementioned Universal Scaling Law. Utilizing this law, Jain et al.[4] was able to derive a simple empirical ''plasmon ruler equation,'' which can be used to estimate the interparticle separation based on the observed plasmon shift. The existence of such a simple calibration scheme greatly enhances the functionality of such a measurement system.

While coupled gold nanorod prototype devices have not yet been demonstrated, the potential does exist. Coupled rods should support some of the largest near-fields attainable. This property alone is of great interest to surface-enhanced Raman scattering applications. A positive step toward such applications is the recent fabrication of a gold nanorod array on the end of a fiber optic.[100] This configuration offers intriguing possibilities as the light delivery capability of the fiber provides a means of excitation for remote biological and chemical sensing carried out at the fiber's end. Even though the research into coupled plasmonic structures is still in its infancy, the impressive progress made to date clearly demonstrates that this is an emerging field. The simplicities offered by the Universal Scaling Law combined with intense near-fields available in these systems make it quite likely that coupled plasmonic structures will form the basis for advanced detection systems.

2.1.5. Photoluminescence Properties

Due to the rapid nonradiative electron–hole recombination processes, bulk metal (Au, Ag, and Cu) has extremely weak fluorescence[101] (quantum yield of $\sim 10^{-10}$). Theoretical studies show that silver nanorods have the largest surface plasmon fields, a conclusion expected to hold for gold nanoparticles.[92] These are the fields that are expected to give rise to an enhancement in the radiative processes to the extent that they are able to compete with the efficient nonradiative processes. It has been observed that for nanorods with aspect ratios less than 3, the quantum efficiency of the photoluminescence (PL) is in the range of 10^{-4} to 10^{-3}, which is six orders of magnitude greater than that found in the bulk.[93] Furthermore, the PL wavelength maximum is found to increase linearly with increasing aspect ratio (Fig. 6A). At the same time, the quantum efficiency increases quadratically for aspect ratios below three and then begins to diminish thereafter. A detailed examination of the enhanced emission intensity was carried out for nanorods including high aspect ratios by Eustis and El-Sayed.[102] The studies show that as the aspect ratio increases beyond 3.5, the intensity of the enhanced emission decreases. The authors used simulations to demonstrate that the emission depends on: i) the strength of the plasmonic field of the longitudinal band, ii) the enhancement of the interband absorption of light by this field, which depends on the extent of the overlap between the interband absorption band and the SPR absorption, and iii) the enhancement of the outgoing emitted fluorescence light by the plasmon field, which depends on the overlap of the fluorescence spectrum of gold and the SPR absorption band. Because the SPR absorption shifts to longer wavelengths as the nanorod aspect ratio is increased, the extent of the overlap between the interband processes and the SPR absorption band will be constantly changing. Initially, increases to the aspect ratio result in greater overlap responsible for an emission enhancement. At some point, however, further increases diminish the degree of overlap resulting in an emission decline. However, as shown by Li et al.[103] the quantum efficiency of long rods (length over 200 nm) rapidly increases such that the solution shows similar appearance as fluorescent quantum dots (Fig. 6B).

Like bulk metal, the PL response in nanorods has been assigned to a three-step process:[93,101,104,105] i) excitation of d-band electrons to the sp band to generate electron–hole pairs, ii) electrons lose energy to the phonon lattice via electron and hole scattering processes, which relax to lower energy levels above the Fermi level, and iii) excited electrons in the sp band recombine with holes in the d-band, resulting in photon emissions. The effect's strong dependency on the nanorod's length, combined with the fact that similar enhancements are not observed for nanospheres, provided strong evidence that the strong surface fields of the longitudinal surface plasmon oscillations are the origin of the fluorescence enhancement. This is also supported by the polarization of the emission being along the long rod axis. The excitation of interband absorption simultaneously excites the longitudinal surface plasmon of gold nanorods, which results in enhanced local electric fields amplifying both exciting and emission fields.

Supportive of these conclusions is the two-photon luminescence (TPL).[84,106] The increased sensitivity obtained from two-photon processes, originating from a response that increases quadratically with intensity, allows for a PL investigation of individual nanorods. Similar to single-photon luminescence, the TPL wavelength is red-shifted with increasing aspect ratio (Fig. 6C, left).[106] TPL of gold nanorods is more intense than

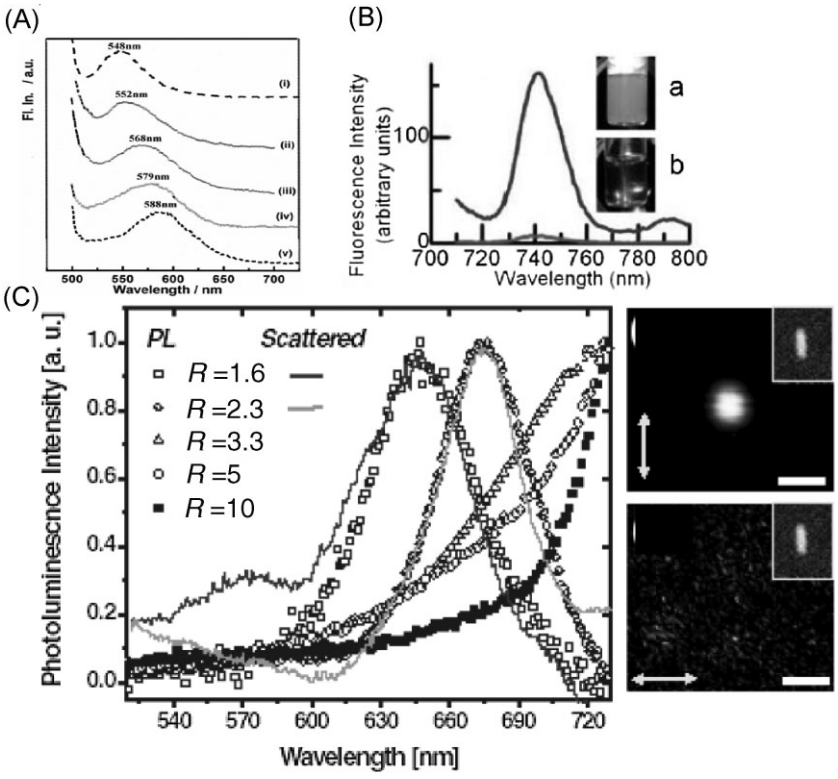

Figure 6. A) The emission spectra for gold nanorods with average aspect ratios of i) 2.0, ii) 2.6, iii) 3.3, iv) 4.3, and v) 5.4. The emission maximum red-shifts with increasing aspect ratios. (Fl. In. = Fluorescence Intensity) Reprinted from [93] with permission. Copyright 2000 Elsevier. B) Emission of nanorods with a length of 230 (black) and 30 nm (grey) excited at 690 nm. The inset shows the illumination photographs of long rods (a) and short rods (b) in aqueous solution. Compared to shorter rods, longer rods show much stronger fluorescence. Reprinted with permission from [103]. Copyright 2005 RSC. C) Left: Two-photon-induced emission spectra of gold nanorods with different aspect ratios. The emission maximum red-shifts with increasing aspect ratios. The solid lines correspond to the scattering spectra for $R = 1.6$ and 2.3. The scattering spectra overlap the emission spectra for the two nanorods, indicating a strong relationship between the emission and surface plasmon peak. Right: Confocal two-photon-induced emission images of vertically oriented gold nanorods ($R = 3.3$) with the light polarization oriented with the longitudinal axis and the transverse axis, as indicated by the white arrows (scale bars: 300 nm). Compared to the transverse excitation, which only shows weak residual background noise, the longitudinal excitation shows much larger enhanced emission. The inset shows microscopy images of the nanorods. Reproduced with permission from [106]. Copyright 2005 APS.

that of spheres due to the direct excitation of the surface plasmon in the near-infrared region. It is strongly enhanced when excited along the long axis (Fig. 6C, right images). The TPL response originates from the sequential excitation of an intraband transition from just below the Fermi level, followed by a second d-band excitation to where the hole was created by the first excitation. PL occurs when the remaining electron and hole radiatively combine. By locally exciting regions along the length of the nanorod, while simultaneously monitoring the PL from the entire rod, Imura et al.[84] were able to determine the portions of the rod that yielded the strongest response. The spatial distribution obtained mapped out the plasmon mode. Thus, where the plasmon shows the strongest internal electric field, it also shows the strongest PL.

It is noteworthy that the aforementioned investigations provided incentive to carry out studies that examined the influence that plasmonic nanoparticles have on the PL originating from adjacent semiconductor nanostructures. CdSe quantum dots are well known for their PL properties. They are also well known for their fluorescence properties. However, colloidal solutions comprising these quantum dots in close contact with gold nanorods showed a three order of magnitude decrease in the fluorescence.[107] Both energy transfer and electron transfer processes could result in the observed quenching phenomenon, but they are differentiated by the fact that energy transfer processes are sensitive to the amount of overlap between the emission spectrum of the quantum dot and the absorption spectrum of the gold nanorods while electron transfer does not. By experimentally varying the extent of this overlap through a variation in the nanorod aspect ratio, Nikoobakht et al.[107] found that the quenching originated from an electron transfer between the excited CdSe nanoparticle and the conduction band of the gold nanorod in concert with a simultaneous transfer of an electron near the gold Fermi level with a hole in the CdSe quantum dot. Lee et al.[108] observed luminescence quenching from CdTe nanowires when covered with a nanoshell of gold. This, however, is not the case as the gold shell was separated from the semiconductor by a 5 nm thick layer of protein molecules. This separation distance was thick enough to severely limit the efficient electron transfer processes, whose probability decreases exponentially with the donor–acceptor distance, but thin enough to allow for surface plasmon–exciton coupling, which decays as R^{-6}. Under these conditions, the authors observed a fivefold increase in the emission quantum yield of the CdTe nanowires. In a follow-up publication,[109] they varied the distance between gold nanospheres and CdTe nanowires and observed a shift in the emission spectra that depended on the separation distance, an effect that may prove useful in the fabrication of biosensors.

2.1.6. Nonlinear Optical Properties of Gold Nanorods

At low light intensities, a material's dielectric polarization responds linearly to the electric field of the light. Deviations from this behavior at higher intensities give rise to nonlinear optical effects. Materials that exhibit substantial nonlinearities offer great functionality when dealing with the high irradiances readily available from many laser systems. Since plasmonic resonances give rise to intense local electromagnetic fields and nanorods give the largest field enhancements,[91,92] it should not be surprising that Au nanorods support substantial nonlinearities and could thus prove quite useful in potential applications in this field.

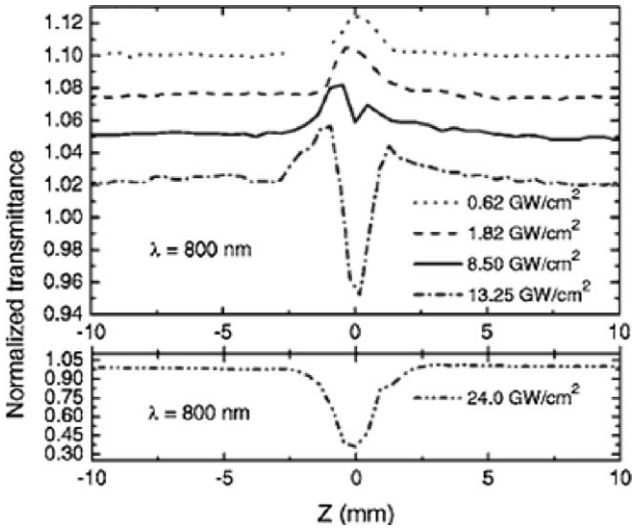

Figure 7. *Z*-scan measurements showing the normalized transmittance of gold nanorods as the sample is translated along the axis of propagation through various distributions of irradiance having maxima at $Z = 0$. Note that the optical nonlinearities give rise to increased absorption at $Z = 0$ for the 0.62 and 1.82 GW cm^{-2} data, but shows diminished transmittance for higher values of irradiance. Reproduced with permission from [110]. Copyright 2006 APS.

One of the most basic tests of optical nonlinearity is the so-called *Z*-scan. In this measurement the sample under study is translated through a gradient of intensities made available along a focused laser beam's axis of propagation (i.e., the *Z*-axis). Nonlinearities can, thus, be identified as deviations from a flat-line response in a plot of the normalized transmittance versus *Z*. Saturable and reverse-saturable absorption are terms commonly ascribed to a nonlinear response associated with increased and decreased transmittance, respectively. Figure 7 shows *Z*-scan data carried out on solution-based Au nanorods at $\lambda = 800$ nm, a wavelength near the longitudinal plasmon mode.[110] As expected, the data shows substantial nonlinearities. Unexpected is the transformation from a saturable to a reverse-saturable response as the irradiance exceeds 5 GW cm^{-2}. Such behavior likely arises from two competing nonlinear processes. It is noteworthy that similar results have been observed for gold[111] and platinum nanospheres.[112]

While the solution-based work shows obvious optical nonlinearities, it does not provide a complete picture when compared to studies on individual metal nanoparticles.[113,114] Isolating single rods removes inhomogeneous broadening and allows for the measurement of an anisotropic nonlinear response, which can prove to be much greater than that of nanorod ensembles.[113] Also showing anisotropy is the collective response from aligned nanorods embedded in a silica matrix, formed through the directional bombardment of nanospheres with heavy ions.[115] Lamarre et al.[116] used such samples to conduct a systematic study of the polarization-dependent nonlinear effects. Their study, based on $\lambda = 532$ nm irradiances below 5 GW cm^{-2}, yielded a nonlinear saturable absorption, where the nonlinear absorption coefficient was 5.7 times larger along the long axis of the nanorod. Their results also provided convincing evidence that nanorods show superior nonlinearities to those of nanospheres.

In a somewhat related, but alternate approach to the generation of nonlinear properties using gold nanorods, Dickson et al.[117] fabricated a photonic crystal comprising an array of substrate-based vertically aligned nanorods embedded in a polymer (poly-3BCMU) well known for its nonlinear properties. The strong electric fields produced through the excitation of the gold plasmons were able to induce nonlinearities in the surrounding polymer matrix.

These early stage investigations into the nonlinear optical properties of gold nanorods have given credence to their potential use in such applications as optical limiting devices, sensor protection, and as components in all-optical circuitry. In order to explore their full potential, advances will be required in fabrication techniques, such that aligned nanorods are produced with control over spacing, aspect ratio, and orientation. Success in this regard could yield tunable, polarization-dependent nonlinear devices.

2.2. Nonradiative Photothermal Properties

2.2.1. Photophysical Processes

The absorbed light is converted into heat by the particle via a series of photophysical processes that have been extensively studied by the El-Sayed group and some other workers using ultrafast dynamics.[20–22,44,118–122] Basically, these photophysical processes start with a fast loss of phase of the coherently excited electrons on the few femtosecond timescale. This is followed by energy loss to the phonon bath, and the electrons and holes cascade down the energy scale by electron–phonon processes on the order of 0.5–1 ps (Fig. 8A and B). The relaxation process is size- and shape-independent and also independent for both the transverse or longitudinal surface plasmon in the rods.[123] This strongly confirmed the lack of involvement of the surface phonons in the relaxation of the hot electrons. The lattice cools off by passing its heat to the surrounding medium via phonon–phonon relaxation within ~100 ps. The last process leads to the complete cooling of the whole nanoparticle.

During the rapid heating of the particle lattice after laser excitation, a coherent vibrational mode can be impulsively excited resulting in transient absorption signal oscillations. This is because the volume of the particle lattice changes periodically upon the laser heating of the particle. As a result, electron density decreases and increases with the same periods leading to the SPR wavelength maximum red- and blue-shifting with respect to that at lattice equilibrium position. Hartland and co-workers[27,29] studied the coherent vibrational motion of gold nanospheres and nanorods. The nanospheres show a vibrational period of ~5 ps with an inverse proportional relationship between the period and the radius of the particle. The nanorods have a vibrational period of ~50 ps, which changes linearly with the length of the rod (Fig. 8C and D). It also depends on the probe wavelength because the sample has a broad inhomogenous width. The phases change by 180° when probed at the red and blue sides of the longitudinal surface plasmon band. The plasmon coupling on the lattice motion has also been observed by Huang et al.[124] in their studies on the coherent motion of nanodisk pairs on lithographic prepared samples.

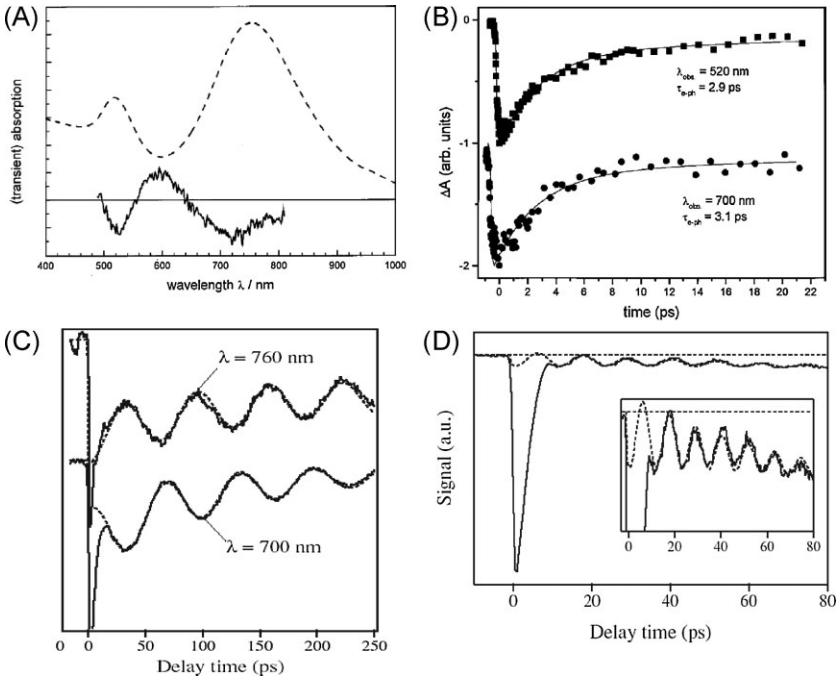

Figure 8. A) Transient absorption spectra of gold nanorods showing the bleach of the transverse and longitudinal bands of gold nanorods with an aspect ratio of 3.8. The positive absorption is due to a broadening of the two bands at higher electronic temperature, induced by a femtosecond laser pulse. B) Plasmon photon-bleach recovery of gold nanorods used for the measurement of electron–phonon relaxation time, $\tau_{e\text{-}ph}$. C) Transient absorption data for the gold nanorods obtained by exciting with near-UV pump laser pulses and probing the longitudinal plasmon band. The nanorods have a length of 61 ± 5 nm and width of 21.5 ± 1.9 nm. The extensional vibrational oscillation shows a period of ~50 ps, and the phase is reversed by 180° when probed at the blue (700 nm) and red (760 nm) side of the SPR band. D) Transient absorption data for the gold nanorods obtained by exciting with near-IR pump laser pulses and probing the transverse plasmon band. The breathing mode oscillation shows a period of ~11 ps. The nanorods have the same dimension as in C. A,B) Reproduced with permission from [20]. Copyright 2000 Taylor & Francis Ltd. C,D) Reproduced with permission from [27]. Copyright 2006 Annual Reviews.

2.2.2. Photothermal Reshaping and Fragmentation

The lattice heating by the electrons and cooling by the surrounding medium is a competitive process. If the heating rate is much faster than the cooling rate, heat can be accumulated within the lattice causing a temperature rise of the nanoparticle in a short time. This temperature increase could be sufficient enough to lead to particle structural changes if the structural change, such as shape transformation and particle fragmentation, takes the time on the scale between the lattice heating and cooling timescales.

In 1999, Link et al.[123,125] found that nanorods melted into near spherical particles of comparable volumes at moderate energies using a 100-fs laser at 800 nm and fragmented into smaller spheres when using a high-energy 7-ns laser or the higher energy of the 100-fs laser. The energy threshold of the fs laser for a single rod melting was determined to be around 60 fJ, and it was increased by a factor of 100 when a nanosecond laser was used due to the less efficient and slower heating process.[126] Using pump-probe fs transient absorption spectroscopy, they measured the bleaching rate of the longitudinal surface plasmon absorption as the nanorods melted into spheres and found that it took about 35 ps to transform a nanorod into a sphere.[127] Using high-resolution TEM, they found that this photothermal melting begins with the formation of defects inside the nanorods, followed by surface diffusion and reconstitution, a different process from thermal melting, which starts at the surface.[128]

Different from laser photothermal reshaping, Mohamed et al.[129] reported the reshaping of gold nanorods with micelles by dissolving the micelles with heat. Because long micelles dissolve at a lower temperature than shorter micelles, the precipitation of long rods leads to a decrease in the average length of the rods remaining in solution and a blue-shift of the longitudinal absorption maximum. This provides a simple method to reshape the size distribution of gold nanorods.

3. Synthesis

Shape-controlled synthesis has received widespread interest due to the importance of anisotropic nanoparticles in their structural, optical, electronic, magnetic, and catalytic properties, as well as their potential applications.[130–132] Although the modern synthesis of spherical gold nanoparticles is dated back to 1857 by Faraday,[47] fabrication of colloidal gold nanorods emerged only during the past decade. Fortunately, great advancement has been achieved for obtaining nanorods with high yield, quality, and uniformity. In this review, various synthetic approaches are described in terms of bottom-up and top-down techniques.

3.1. Bottom-Up Methods

3.1.1. Seed-Mediated Growth Method

Typical Protocols: The seed-mediated growth method is the most popular method for the synthesis of colloidal gold nanorods due to their simplicity of the procedure, high quality and yield of nanorods, ease of particle size controlling, and flexibility for structural modifications. The method is dated back to 1989 when Wiesner and Wokaun[133] reported the formation of anisometric gold colloids by adding gold nuclei to $HAuCl_4$ growth solutions. The nuclei were formed by reduction of $HAuCl_4$ with phosphorus, and the growth of gold nanorods was initiated with the addition of H_2O_2.

The current concept of seed-mediated chemical growth is originated in 2001 by Jana et al.[134] who prepared colloidal gold nanorods by the addition of citrate-capped small gold nanospheres to a bulk $HAuCl_2$ growth solution obtained by the reduction of $HAuCl_4$ with ascorbic acid in the presence of cetyltrimethylammonium bromide (CTAB) surfactant and silver ions. Ascorbic acid can only reduce gold ions to gold atoms in the presence of metal nanoparticles that catalyze the reduction

reaction. The method is extended and improved by the same group with a three-step procedure in the absence of silver nitrate for long rod synthesis up to an aspect ratio of 25.[135–137] In the typical procedure, first-stage gold nanorods are used as seeds for second growth, which are sequentially used as seeds for third growth.[138] The drawback of this method is the large fraction of gold nanospheres produced, which requires time-consuming centrifugation steps to separate the rods from the spheres. It is also found that the addition of nitric acid in the third seeding growth medium facilitates the formation of high-aspect-ratio gold nanorods with increased monodispersity and yield.[139]

In 2003, Nikoobakht and El-Sayed[37] made two modifications to this method: replacing sodium citrate with a stronger CTAB stabilizer in the seed formation process and utilizing silver ions to control the aspect ratio of gold nanorods. This protocol includes two steps: i) synthesis of seed solution by the reduction of auric acid in the presence of CTAB with ice-cold sodium borohydride and ii) the addition of the seed solution to the Au^{+} stock solution in the presence of CTAB which is obtained by the reduction of $HAuCl_4$ with ascorbic acid. Silver nitrate is introduced to the gold solution before seed addition to facilitate the rod formation and to tune the aspect ratio as well. This method produces high yield gold nanorods (99%) with aspect ratios from 1.5 to 4.5 and avoids repetitive centrifugations for sphere separation. The overgrowth can be stopped by simple centrifugation or arrested by adding sodium sulfide.[140]

To grow nanorods with higher aspect ratios, a co-surfactant, benzyldimethylhexadecylammonium chloride (BDAC) is introduced in the original growth solution. This binary surfactant system produces nanorods with aspect ratios of up to 10 by changing the silver concentrations.[37] (Fig. 9) With the Pluronic F-127 co-surfactant system, the aspect ratio can increase up to 20 with reasonable monodispersitivity.[141] To grow nanorods with a desired aspect ratio, one can gradually add the gold growth solution to the nanorod solution after the first stage of the nanorod growth at a rate of 1.0 mL per 20 min to induce continuous rod growth.[37] Aspect ratios of up to 70 have been reported by fourth additions of growth medium with increased volumes accompanied by shape changes from fusiform into 1D rods.[142]

In both methods, the yield, monodispersity, size, and fine shape of gold nanorods are affected by many parameters, such as seed concentration, size, structure, ascorbic acid concentration, temperature, pH, the gold precursor concentration, the surfactant concentration, the use of other surfactants, additives, solvent, and even the nanorod aging time.[37,138–156] Gold nanorods themselves can be used as seeds to obtain multishaped nanostructures.[157] In addition, the impurity of CTAB surfactant plays an important role in the nanorod growth. CTAB from different suppliers and different catalog numbers not only affects the aspect ratio of the nanorods, but also the yield and monodispersity, due to the existence of impurities.[158] Iodide contaminant has been found to be the key shape-directing element as it selectively binds to the Au(111) facet inducing formation of gold nanorods.[159]

Growth Mechanism: Two mechanisms have been proposed to explain the growth process of gold nanorods. One is the proposed surfactant-preferential-binding-directed growth by Murphy and co-workers[138,160] based on the high resolution TEM (HRTEM) images showing the structure of the rods and various factors affecting the rod formation process (Fig. 10A). The HRTEM and electron diffraction pattern show that gold nanorods prepared with citrate-capped seeds without silver ions are pentatetradedral twins.[160] They propose that intrinsic structural twinning in face-centered cubic (fcc) metallic nanoparticles causes symmetry breaking to produce anisotropic nanoparticles. The following anisotropic growth into nanorods is due to the preferential binding of the CTA^{+} headgroup to faceted seed nanoparticles on the {100} face as the gold atom spacing in this face is more comparable to the size of the surfactant head groups than that of the close-packaged[161] rod end. At the same time, Gail and Harmer[162] also observed twin defect structures on the {110} side surface. This is consistent with the well-known fact that the {110} face has a higher surface energy than other faces. As a result, CTAB binding is able to stabilize this face and consequently the crystal growth on this side is retarded and gold is deposited to the end facet leading to rod growth.

The other is the electric-field-directed growth mechanism proposed by Mulvaney and co-workers[155] (Fig. 10B). In this mechanism, $AuCl_4^{-}$ is bound to CTAB micelles and hence reduced to $AuCl_2$–CTAB micelles. This complex binds

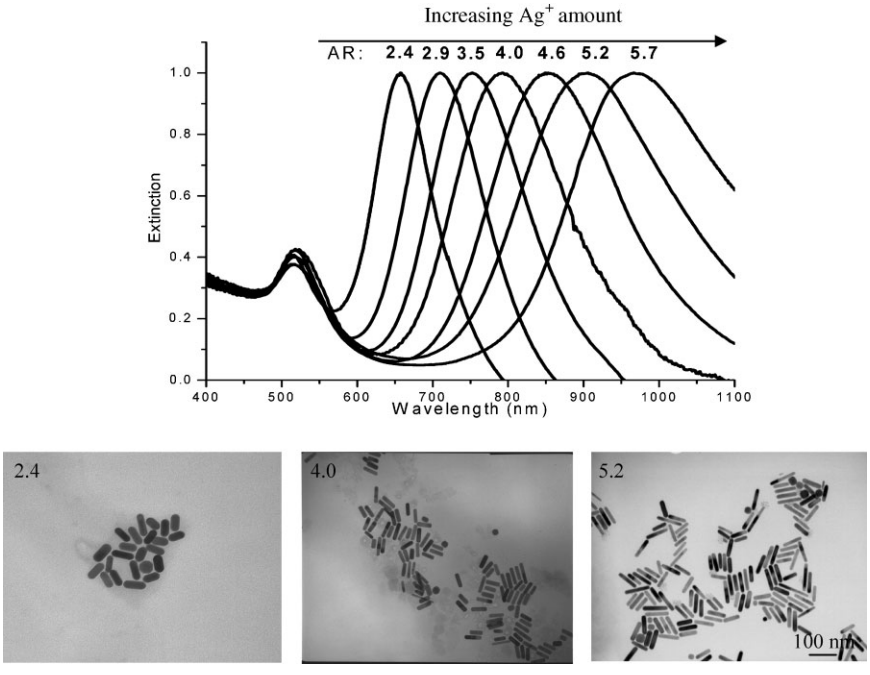

Figure 9. The tuning of aspect ratios of gold nanorods by varying the amount of silver ions in a CTAB and BDAC binary surfactant system in the two-step protocol. Increasing the amount of silver ions leads to gold nanorods of higher aspect ratios, which is consistent with the red-shifting surface plasmon resonance.

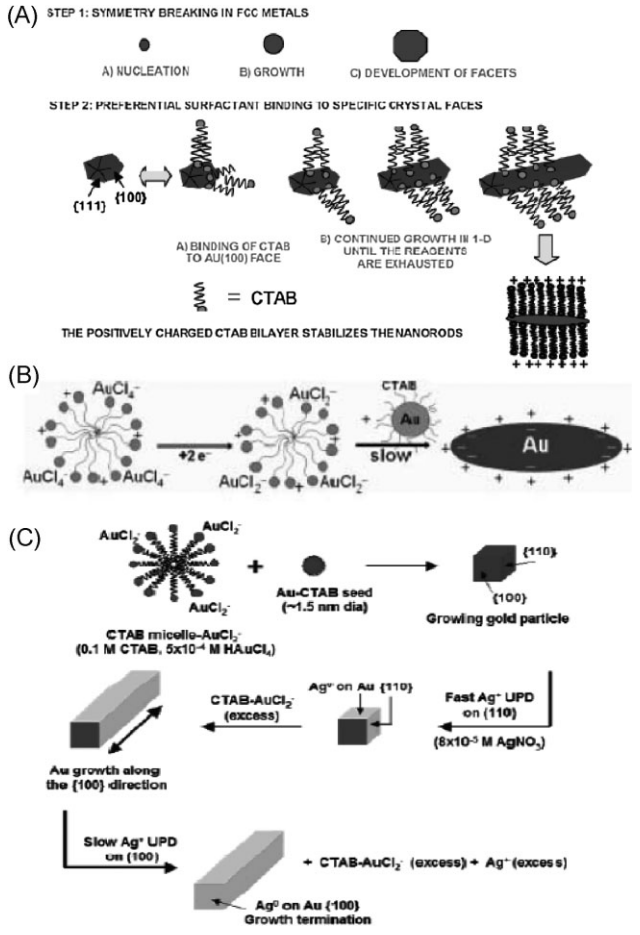

Figure 10. Mechanisms of seed-mediated growth of gold nanorods. A) Surfactant-preferential-binding mechanism in the absence of silver ions. The seed nanoparticles develop facets that are differentially blocked by the surfactant. Subsequent addition of metal ions to the exposed facet leads to growth of gold nanorods. Reproduced with permission from [138]. Copyright 2005 ACS. B) Electric-field-directed mechanism in the absence of silver ions. The $AuCl^{2-}$ ions bound to cationic micelles diffuse to seed nanoparticles at high points of curvature due to higher electric double layer gradient at these points and thus leads to nanoparticle growth in rod shape. Reproduced with permission from [155]. C) Mechanism for gold nanorod growth in the presence of silver ions. Ag^{+} is reduced to Ag^{0} at a metal substrate with a surface potential less than the standard reduction potential of Ag^{+}, called silver underpotential deposition (UPD). The deposition of silver on the side {110} facet is faster than on the end {100} facets due to lower reduction potential on the {110} facet. This inhibits the nanorod growth on the side face leading to preferential growth of gold at the ends. Increasing the silver concentration results in more silver deposition on the side facet and the nanorod growth of higher aspect ratio. Further increase of the silver concentration results in the silver deposition of whole rods and thus stopping nanorod growth. Reproduced with permission from [163]. Copyright 2006 ACS.

to the CTAB-capped seed particles through collisions which are controlled by the electric double layer between the positively charged seed and negatively charged $AuCl_2^-$ on the CTAB micelles. The collisions are faster at the tips than the sides of the seeds and thus facilitate the rod-shape growth. This mechanism did not explain how the initial tips of the seed nanoparticles are formed.

The role of silver ions in controlling the aspect ratio has been previously explained as adsorption of the Ag–Br pair to the different facets of gold nanoparticles which restricts particle growth.[134] Nikoobakht and El-Sayed[37] explained that the Ag–Br pairs decrease the charge density of bromide ions and thus decrease the repulsion of neighboring CTAB headgroups. This repulsion results in CTAB elongation and thus rod formation. Liu and Guyot-Sionnest[156] have systematically studied the roles of silver ions by comparing the structure difference using CTAB-capped and citrate-capped seeds. Their results show that the single-crystalline CTAB-capped seed leads to single-crystalline nanorods with {110} faces on the side and {100} on the flat end, while the multiply twinned crystalline citrate-capped seed grows into multiple twinned structures, specifically into pentatwinned bypyramidals. The deposition of gold atoms to the seed surface does not create a stacking default and therefore preserves the initial seed structures. Although Ag^{+} in the CTAB solution cannot be reduced to bulk silver atoms by ascorbic acid in acidic pH.[163] Ag^{+} can be reduced to Ag^{0} onto a metal substrate in the form of a metal monolayer at a potential much less than bulk reduction, known as underpotential deposition (UPD).[164] The reduction potential for silver deposition on surfaces is lower than that on {100} or {111}.[134] Based on these facts, Liu and Guyot-Sionnest[156] propose that silver deposition on the {110} side of the rods is faster than on the {100} ends due to the UPD effects and thus the seeds grow into nanorods.

Combining the UPD, electric-driving-directed, surfactant preferential binding models, and their quantization studies of metal contents in the silver-assisted nanorod growth, Orendorff and Murphy[163] proposed a silver UPD mechanism which clearly elucidates the growth process (Fig. 10C). $AuCl_2^-$ on the CTAB micelles diffuses to CTAB-capped seed spheres by electric field interactions, and the sphere symmetry is broken into different facets with preferential binding of CTAB onto the {110} facet. Silver ions deposit onto the {110} side facet with a faster rate than they do onto the {100} end facet, resulting in the particle growth into rod shape along the [110] direction. Complete deposition of silver ions on to {100} end facet stops the particle growth, which limits the method to make no longer than 100 nm nanorods. This mechanism is well supported by the fact that silver-assisted nanorods are shorter than those prepared in the absence of silver ions.[134] An increase in silver ions over a threshold concentration could not further increase the aspect ratio[37] due to the blocking of the end facet of the nanorods by silver metal deposition.

3.1.2. Electrochemical Method

Before the emergence of the seed-mediated chemical growth method, high yield of gold nanorods were mainly prepared by the electrochemical method, which was developed by Wang and co-workers in the 1990s.[165–167] They reported the formation of gold nanorods by extending their electrochemical method for the synthesis of metal clusters in reversed micelles. In this method, a gold metal plate anode and a platinum plate cathode are immersed in an electrolytic solution consisting of rod-inducing CTAB surfactant and co-surfactant tetradodecylammonium bromide (TOAB). The electrolysis results in the generation of gold ions in the form of $AuBr_4^-$ from a gold metal anode, which then complexes with the CTAB micelle and migrates to the cathode where gold ions

are reduced to gold atoms. A silver plate is gradually inserted into the solution to control the aspect ratio of the nanorods by the concentration and release rate of silver ions produced from the redox reaction between the gold ion and silver plate. Acetone and cyclohexane are added before electrolysis to facilitate the mixing of CTAB and TOAB and to assist the formation of rod-like CTAB micelles, respectively. Ultrasonication is required to dissipate the rods away from the cathode. CTAB forms a bilayer structure on the longitudinal surface of gold nanorods with the trimethylammonium headgroups of the first layer facing the gold surface.[168]

The structure of gold nanorods prepared by the electrochemical method depends on the aspect ratios and is also different from those fabricated by the seed-mediated method. Fcc metal nanocrystals could have {111}, {100}, and {110} facets. A combination of these facets controls the shape formation. As described in the previous section, gold nanorods grown by the seed-mediated growth method using citrate-seed without silver ions show {100} and {110} side faces with a {111} end face in a pentatwinned structure (Fig. 11A).[160,169] For the rods grown using CTAB-caped seed in the presence of silver ions, the rods are single-crystalline bearing {110} faces on the sides and {100} on the ends[156] (Fig. 11B). If the seed is replaced by citrate-capped nanoparticles, elongated pentatwinned bipyramidal nanoparticles instead of gold nanorods are formed.[156] For the nanorods grown by the electrochemical method, the HRTEM and electron diffraction studies by Wang et al.[170] show that short rods with an aspect ratio of 3–7 are single crystals without stacking faults, twins, or dislocations, and they are dominated by {100} and unstable {110} facets[171] with a [001] growth direction (Fig. 11C). The nanorods are capped by (001) and {111} facets of small areas at the ends. The long rods with an aspect ratio above 20 display one twin plane parallel to the [111] direction. The nanorods are dominated by {111} and {110} facets with a ⟨112⟩ growth direction. They also found that the spherical nanoparticles in the majority of the nanorod solution are multiply twinned and composed of {111} and {100} facets in the absence of the {110} facet which is the dominant facet in gold nanorods.

3.1.3. Other Methods

One other common synthetic method is photochemical reduction, the earliest method used to form colloidal gold nanorods.[172] In this method, auric acid is bound to rod-like cationic micelle surfactants to form ion pairs and then excited by UV light to reduce metal ions to form metals via electron transfer from metal ions to ligands.[173–176] It is proposed that the rod formation is due to a two-step aggregation process, i.e., metal nuclei aggregation to form primary particles and primary crystal aggregation to form rod-like structures due to specific crystal face stabilization by surfactant micelles.[174] Addition of sodium chloride electrolyte increases the percentage and length of the nanorods via the modification of the micellar size and particle crystallization process.[174] The presence of silver ions greatly improves nanorod yield and uniformity due to a similar mechanism involved in the seed-mediated growth method.[173] UV light at 300 nm leads to longer nanorods with narrower size distributions than 254 nm light, and increasing the light intensity accelerates the growth of gold nanorods.[175]

High yield and monodispersity of gold nanorods can also be produced with a one-step seedless method where sodium borate is directly added to the growth solution in the presence of silver ions, ascorbic acid, and CTAB surfactant to initiate particle nucleation and growth.[177,178] The aspect ratios of the nanorods can be controlled by changing the amount of sodium borate[177] or adjusting the temperature.[178] Other preparation methods include bioreduction,[179] X-ray irradiation, proton beam irradiation,[180] microwave reduction,[181] and solvothermal reduction.[182] These methods constitute good additions to the fabrication of colloidal gold nanorods although with less popularity. In addition, a template method, a common way to prepare aligned nanocomposites of desired materials, can also be used to make colloidal gold nanorods by separating nanoparticles from substrates and later dispersion in solvent.[183] This method has the advantages of making nanorods without capping molecules allowing for easy surface chemistry and precise controlling of the length, width, and uniformity of the nanorods by the solid template.

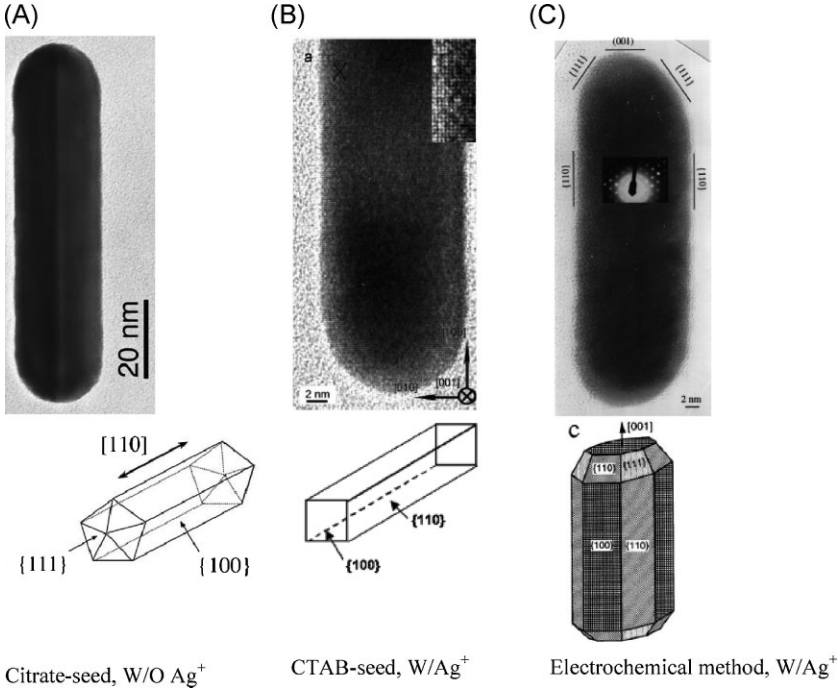

Figure 11. Crystal structures of gold nanorods obtained by different methods. A) Seed-mediated growth method using citrate-capped seed in the absence of silver ions. The nanorods have side faces of Au {100} or {110} and end faces of {111} in a pentatwinned structure. Reproduced with permission from [169]. Copyright 2004 ACS. B) Seed-mediated growth method using CTAB-capped seed in the presence of silver ions. The nanorods are single crystal bearing {110} faces on the sides and {100} on the ends. Reproduced with permission from [156]. Copyright 2005 ACS. C) Electrochemical reduction method. The nanorods with aspect ratio of 3–7 are single crystals dominated by {100} and {110} facets on the side and (001) and {111} facets at the ends. Reprinted with permission from [170]. Copyright 1999 Elsevier.

3.1.4. Surface Modifications

Surface modification with a layer of hard inorganic nanomaterials has the advantages of increasing stability, facilitating surface chemistry, tuning properties, and broadening practical applications. Silver modification has the potential of enhancing Raman scattering of the nanoparticles due to less plasmon damping in silver compared to gold.[184] Silver coating is generally conducted by the reduction of silver nitrate with ascorbic acid at base condition in the presence of gold nanorods and stabilizing agents such as citrate, CTAB, and polyvinylpyrrolindone (PVP).[185,186] Reduction of saturated silver chloride aqueous solution with hydroxyamine oxide could also chemically deposit a silver shell on gold nanorods.[187] The silver thickness can be controlled by tuning the concentration of the silver precursor and the mild reducing agents.[185] The silver layer can be selectively dissolved by hydrochloric acid to restore gold nanorods. A several-nanometer coating of the nanorods causes sharper, stronger, and blue-shifted surface plasmon absorption bands.[185–189] The Au/Ag core/shell nanorods are stable up to a couple of months due to the decomposition of the silver shell into silver nanoparticles with increased storage time which constitutes a drawback of the nanocomposite.[185]

Silicon coatings can passivate and thus further stabilize gold nanorods while allowing for simple surface chemistry with silane coupling agents and phase transfer to organic solvents. Simple addition of aqueous sodium silicate to gold nanorods, which have been mixed with 3-mercaptopropyl trimethoxysilane (MPTMS) or 3-mercaptopropyl triethoxysilane (MPTES) solution in advance, induces mesoporous silicon shell formation and thus a red-shift of the longitudinal SPR band due to the refractive index change of the nanorod-surrounding environment upon coating.[190,191] Homogenous coating with controllable shell thickness can be achieved by hydrolysis and condensation of tetraethoxy silane (TEOS) after layer-by-layer electrostatic deposition of polyelectrolytes to the original CTAB-capped gold nanorods.[192] Direct injection of TEOS to the CTAB-capped nanorod solution in basic condition without the use of a polymer intermediate layer is also reported to form thin and highly porous silica shells through silica oligomerization, aggregation, and promotion to the shell structure on the nanorods.[193]

Other hard coatings include iron oxide coating by coprecipitation of iron salts or electrostatic adsorption of iron oxide nanoparticles,[194] platinum coating by mild reduction of platinum salts with ascorbic acid,[195,196] and silver sulfide or selenide by exposing Au/Ag core/shell nanorods to sulfide or selenide salts in an oxidizing environment.[197] These coatings are promising in the applications of magnetic separation and imaging, catalysis, and optical nonlinearities, respectively.

3.2. Top-Down Methods and Site-Selective Patterning on Substrates

The placement of gold nanorods on well-defined areas of a substrate's surface, in a manner that renders them immobile, is important to numerous applications as well as to the integration of these nanostructures with wafer-based circuitry. Implementation often occurs through top-down approaches where gold films are formed over the entire substrate surface and then, through nanoscale patterning procedures, most of the film is removed leaving behind gold nanostructures in predetermined areas. Bottom-up approaches, where nanorod growth is initiated only for preselected areas, have been used, but to a lesser extent. In this section, progress will be described for top-down approaches where state-of-the-art lithographic methods are utilized and for bottom-up approaches that are initiated either by catalytic seeds or three-dimensional templates.

3.2.1. Lithographic Methods

Lithographic techniques are by far the most experimentally demanding fabrication methods used in the production of gold nanostructures. The most commonly utilized technique for this purpose is electron-beam lithography (EBL). The procedure begins by coating a substrate with an electron-sensitive resist that, when exposed to an electron beam, dissociates into smaller polymer segments that can be selectively removed with a developing agent. Thus, patterns written with an electron beam allow for the formation of nanometer-scale openings in the resist through which gold can be deposited. Both the remaining unexposed resist and the gold deposited on it are easily removed using acetone. This so-called lift-off technique can result in the formation of intricately shaped nanostructures with dimensional control on the tens of nanometer length-scale. An alternate top-down approach, commonly referred to as focused ion beam (FIB) lithography, utilizes a rastered ion beam, typically gallium, to sputter away unwanted portions of a continuous film leaving behind nanostructures of the desired shape. While both of these techniques allow for the production of nanostructures with unparalleled control over the size, shape, and alignment, they are impractical in terms of producing such structures on macroscopic-length scales. Other drawbacks of these techniques include the fact that the nanostructures are typically polycrystalline, dimensions less than 10 nm are not readily obtainable, and nanostructure adhesion to the substrate usually requires an intermediate layer of chromium or titanium.

Gold nanorod structures have been produced using both EBL[100,198,199] and FIB techniques.[100,200,201] Figure 12, taken from the work of Billot et al.,[198] shows scanning electron microscopy (SEM) images of arrays of gold nanorods fabricated to study the effect of nanorod length on the surface-enhanced plasmon resonances originating from these structures. The images demonstrate the capabilities of this lithographic technique in terms of nanostructure alignment as well as the degree of dimensional control. For the sake of completeness, it also pointed out that lithographic techniques are being extensively deployed in the fabrication of gold nanodisks in order to study and gain control over the interparticle coupling between tightly spaced pairs of disks.[4,94,95,202,203] Such structures have been used in the fabrication of nanometric optical tweezers[203] and can potentially be used as a ''plasmon ruler'' capable of determining nanoscale distances in biological systems on the basis of spectral shift.[4]

3.2.2. Catalytic Methods

Although nanorods on substrates can be obtained by various assembly processes from colloidal solution, which is described in

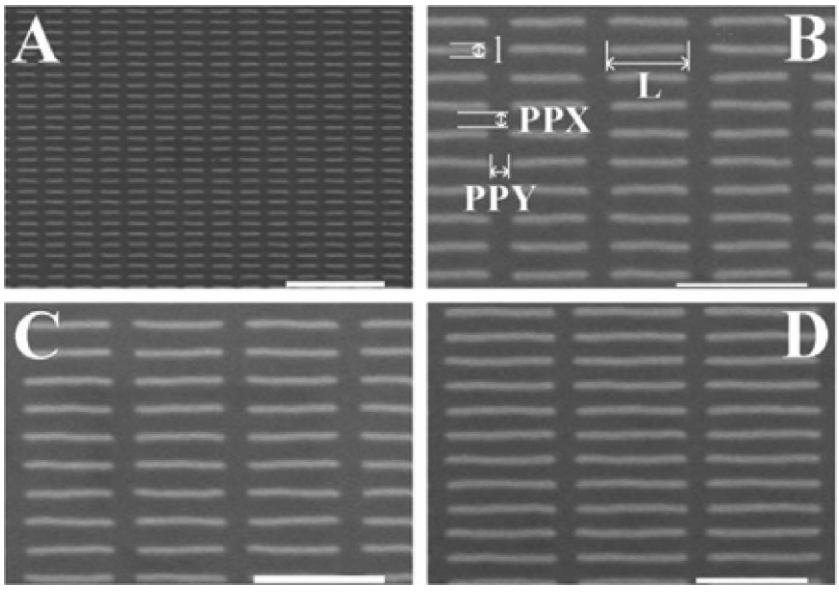

Figure 12. SEM images of nanorod arrays produced using EBL. All of the rods have widths, *l*, of 60 nm, heights of 50 nm, and lengths, *L*, of A) 420 nm, B) 620 nm, C) 720 nm, and D) 1 μm. The interparticle spacings, given by PPX and PPY, are 150 nm. The scale bars shown are 2 μm in length for A and 1 μm for B, C, and D. Reprinted with permission from [198]. Copyright 2006 Elsevier.

a previous section, a different approach is the use of catalytic seed nanospheres to directly grow one-dimensional rods on the substrates.[204] Such a method is a well-established technique for producing substrate-based semiconductor nanowires.[205] In the process reported by Taub et al.,[204] the substrate was first treated with a linker able to facilitate nanoparticle attachment to the surface. Once affixed, approximately 15% of the nanoparticles were able to promote nanorod growth when the substrate was placed in the aqueous solution. The remaining nanoparticles promoted a myriad of shapes including those that are spherical, triangular and hexagonal.

Subsequent reports describe alternate means of linking the nanoparticles to the surface[206,207] as well as the use of HgTe nanoparticles as the seed-material.[208] Mieszawska et al.[209] have taken this process one step further by using a microcontact printing technique to attach the gold nanoparticles to the substrate's surface. In their process, gold nanoparticles were attached to the substrate using a stamp fabricated from a silicon wafer with micrometer-scale patterns etched into it. With only the raised portions of the stamp coming into contact with the substrate, only site-specific areas were able to support nanorod growth, while the substrate remained bare. Using adhesive tape, they were also able to remove a significant percentage of the oddly shaped nanostructures by taking advantage of the fact that they have poor adhesion to the substrate.

3.2.3. Template Method

Template methods involve the use of nanoporous track-etched polycarbonate or an anodized alumina membrane as the template where gold atoms are deposited by electrochemical reduction of a gold ion precursor in an electrochemical cell.[117,183,210–220] The subsequent chemical etching of the template membrane gives an ordered array of gold nanorods with the long axis normal to the substrate. The width of the nanorods is controlled by the pore diameter of the membrane template. Pore diameters of 5–200 nm can be prepared by the anodization of the aluminum metal in an acidic solution. The length of the rods is controlled by varying the amount of the gold deposited and thus the aspect ratio of the nanorods can be tuned accordingly. In a similar vein, CdTe nanorods[8,221,222] were used as a template upon which a thin gold nanoshell layer was deposited (Fig. 13). While gold showed plasmonic behavior, the CdTe showed enhanced hot electron relaxation rates for excitations that are resonant with the surface plasmon absorption.[8]

3.2.4. Other Methods

Interest in the site-selective patterning of nanostructures is obviously not limited to gold nanorods. As such, a number of innovative techniques are being developed for this purpose that have not, as of yet, been tried for the Au nanorod system. Nevertheless, they are certainly worthy of consideration. One of the most intriguing, due to its relative simplicity while at the same time allowing for the production of aligned nanostructures on centimeter-length scales, was developed by Whang et al.[223] In their process, they used standard Langmuir–Blodgett techniques to obtain uniformly spaced, horizontally aligned silicon nanowires on the surface of a substrate. These nanowires were then used as a shadow mask through which chromium metal was deposited, yielding a substrate surface with uniformly spaced 15 nm thick Cr metal lines. In another approach, through a somewhat involved EBL process, Melosh et al.[224] was able to obtain a silicon substrate coated with 20 nm wide parallel lines of platinum with a spacing of 60 nm. Deng and Mao[225] developed a template method where fluid flow over a substrate's surface resulted in the deposition and stretching of one-dimensional DNA strands. These strands, when exposed to palladium ions,

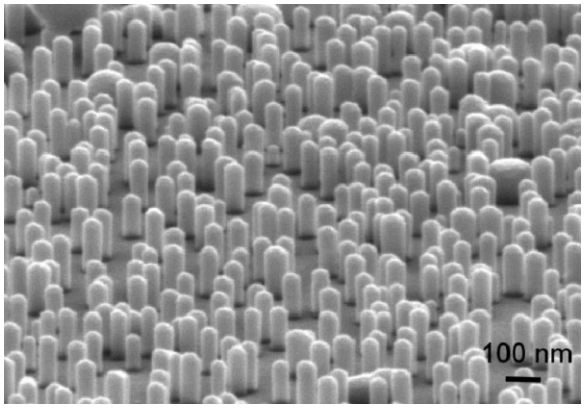

Figure 13. SEM image of gold nanoshells using CdTe nanowires as a template. Reproduced with permission from [8]. Copyright 2008 ACS.

acted as a template for Pd nanowire growth that yielded horizontally aligned 5 nm wide nanowires. Taken together, all of the results presented in this section, show both the promise and progress being made in techniques aimed at providing site-selective patterning of gold nanorods on substrates.

4. Assembly

Assembly of colloidal metallic, semiconducting quantum dots, or insulating inorganic particles into one-, two-, and three-dimensional superstructures has received increased interests over the last decade. This is due to their potential uses as smart materials and devices as they are characteristic of ordered structures with collective physical properties from the individual particles and the interparticle coupling. Assemblies can be liquid-crystal structures in solution, crystals, or precipitates separated from solution phase or ordered arrays supported on liquid or solid phase. Assembly approaches include spontaneous self-assembly, chemical driving assembly, template-directed patterning, and physical methods such as polymer stretching and electric field induction.

4.1. Self-Assembly

Spontaneous self-assembly of colloidal nanoparticles depends on the particle shape, size distribution, and capping molecules. While spherical nanoparticles require a narrow size distribution (polydispersity smaller than 5%), anisotropic nanoparticles can self-assemble into various patterns with some degree of polydispersity.[226] Self-assembly of gold nanorods was firstly reported in 2000 by Nikoobakht et al.[227] who found large and aligned structures of gold nanorods on a copper TEM grid after air drying a drop of nanorod solution on the grids or drying the rod solution with the grid immersed halfway. The arrays are especially formed in the vicinity of the region where the solution and grid intersect. They explained that the assembly is due to the increased lateral capillary forces between particles as a consequence of water evaporation during the drying process. The parallel alignment is proposed to result from higher and later capillary forces along the length of the assembled nanorods rather than the width. Surfactant concentration, ion strength, particle concentration, particle size distribution, and the presence of spherical particles can all affect the quality and final form of the assembly. Xu et al.[228] found that the nanorods prefer to pack together and therefore separated from spherical particles when a drop of rod–sphere mixture solution was slowly dried on a silicon wafer in a water vapor atmosphere to slow down the drying rate of the sample. This self-selective behavior is also explained according to the capillary force interactions between the particles and remarkable shape-dependence of the self-assembly process. Recently, Kawamura et al.[229] found that surfactant concentration plays a critical role in the ways of nanorod assembly. The nanorods are linearly and loosely aligned in a head-to-tail style if the as-prepared solution is centrifuged twice while a densely aligned 2D parallel assembly of the nanorods is observed after three rounds of centrifugation. They also show strong surface-enhanced Raman signals from the linear head-to-tail assembly while no enhancement for the parallel assembly. This is due to the higher field at the end portion of the nanorods compared to the side of the particle.

Later Jana et al.[230] observed the spontaneous formation of liquid crystal structures composed of aligned gold nanorods in a side-on fashion in concentrated solution with higher aspect ratios (13–18) by a polarizing microscope. The CTAB surfactant was found to be the key factor as only appropriate surfactant concentrations could lead to the crystal structures. As two nanorods approach, the expulsion of the outerlayer charged headgroup and counter ions of the surfactant can result in the hydrophobic tail portion of the surfactant toward the solvent. As a consequence, the two nanorods are attracted together in a side fashion due to hydrophobic interactions while minimizing hydrophobic–hydrophilic interactions with water. According to Onsager's theory,[231] these superstructures are thermodynamically stable because the gain in translational entropy is larger than the loss of the orientation entropy from the particle alignment. Due to the dependence of the assembly on the particle anisotropy and polydispersity, the assembly was found useful for shape- and size-separation in a mixture of nanorods with different aspect ratios, spheres, and other shapes of nanoparticles.[232] This is because with the increasing of the assembly mass, the liquid crystals can precipitate out of solution. Long rods precipitate more easily than short rods, followed by platelets particles, enabling step-by-step particle separation of different shapes.

4.2. Chemically Driven Assembly

Different from self-assembly that depends on the capping surfactant interactions to form a side-on fashion alignment, the chemically driven assembly method can program the assembly either in an end-to-end or side-by-side way via the soft modification of the rod surface with small molecules or a polymer. These molecules drive the rods together through intermolecular interactions, and the rod alignment is determined by the location of the molecules either on the end for linear assembly or on the side for parallel assembly.

4.2.1. End-to-End Assembly

As the side face of gold nanorods are densely capped by the CTAB capping molecules through strong Au–N bonds probably via Br bridging,[168] replacement of this surfactant layer with other ligands such as thiolated chemicals is significantly challenging. Heating and sonication[233,234] or the use of ion exchange resin exchanging environment[235] might help a full ligand exchange, but in most cases chemical binding occurs only on the bare end faces. The rationale for the end-to-end assembly is mostly based on the bifunctional small molecules with thiols on one end available for rod binding and a functional group on the other end for intermolecular interaction. Examples of thiolated bifunctional molecules are biotin disulfide,[236] thioalkylcarboxylic,[237–240] α,ω-alkanedithiols,[241] and thiolated DNA.[242] The end-to-end assemblies into chain structures using these molecules are realized by streptavidin bridging, hydrogen bonds, Au–S bonds, and DNA hybridization, respectively. In the work by Chang et al.,[243] gold nanorods were functionalized with thioacetic acid

at the ends and further conjugated to anti-mouse immunoglobulin G IgG) via 1-ethyl-3-(3-dimethylaminopropyl)-carbodiimide (EDC) coupling reaction. The addition of mouse IgG having two binding sites initiated rod linking and linear chains up to 3 μm. This was obtained by stepwise increasing the concentration of mouse IgG (Fig. 14A). Other methods are by the Huisgne 1,3-cycloaddition reaction[244] and crown ether derivatives.[245]

A new way to assemble rods into finite superstructure was reported by Khanal and Zubarev[246] who obtained ring-like assemblies by modifying gold nanorods with polystyrene arms. They first fully exchanged the CTAB with 4-mercaptophenol by dropwise addition of the thiols in tetrahydrofuran (THF) solution to an aqueous rod solution. The thiolated rods were then covalently coupled to carboxybiphenyl-terminated polystyrene. Decreasing the concentration of the rod/polymer hybrid solution resulted in isolated rings of single rods (Fig. 14B). The ring formation is based on the ''breath figures'' mechanism that takes advantage of water microdroplets condensed on the surface of nonpolar solvents from humid air. The polystyrene shell stabilizes the rods in solution during water evaporation until they are packed around the circumference of the water droplets. When the polymer is only bound to the end face of the nanorods, Nie et al. reported the observation of rings, bundles, chains, and bundled chains of the nanorods.[247]

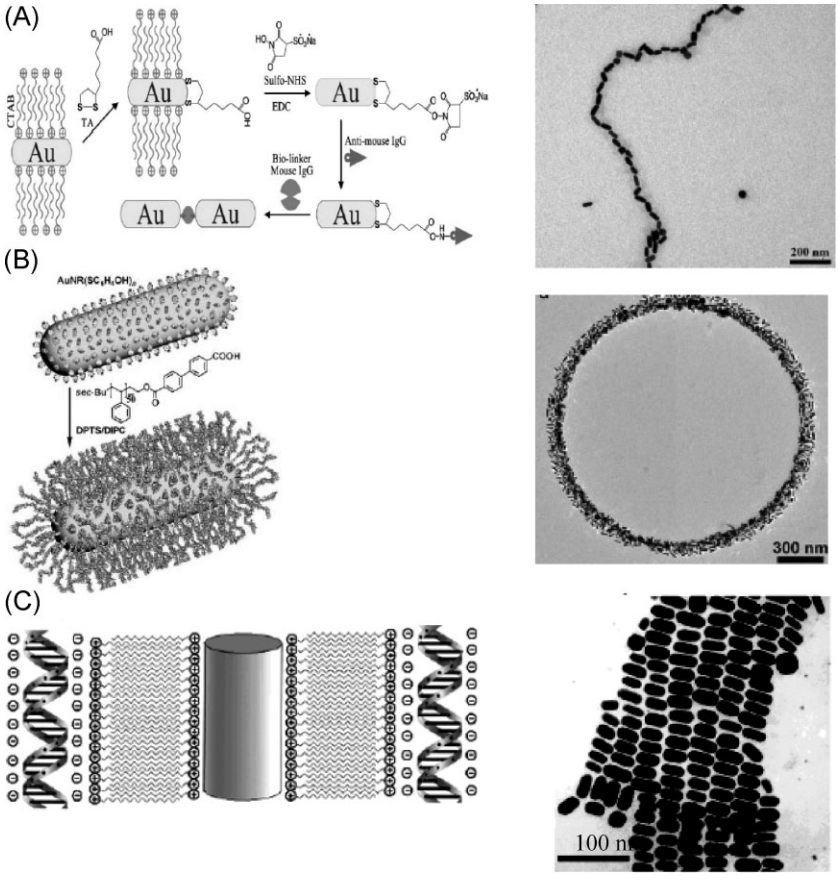

Figure 14. Assembly of gold nanorods to linear chains (A), rings (B), and parallel stacks (C). A) Reproduced with permission from [243]. Copyright 2005 RSC. B) Reproduced with permission from [246]. C) Reproduced with permission from [161]. Copyright 2007 ACS.

4.2.2. Side-by-Side Assembly

The first chemically driven assembly of gold nanorods was reported by Dujardin et al.[248] who assembled gold nanorods in parallel stacks by DNA hybridization. Thiolated oligonucleotides replace the CTAB capping molecules via Au–S bonds, and the assembly is initiated by DNA duplexation arising from the addition of the complementary strand either on rods in the two-strand system or a third strand that duplexes the two strands on the rods in the three-strand system. One disadvantage of this method is the interference of the electrostatic interaction between negatively charged DNA and positively charged rods as well as the difficulty for ligand exchange of the CTAB capping molecules. The studies of Pan et al.[161] show that the nanorods can be directly assembled into one- and two-dimensional structures via the electrostatic interaction between DNA and rods (Fig. 14C). Such assemblies via charge interaction were also demonstrated by Orendorff et al.[249] using adipic acid, by Jain et al.[97] using citrate molecules, and by Sreeprasad et al.[250] using dimercaptosuccinic acid. In a different way, Gole and Murphy[251] coated gold nanorods with the poly(acrylic acid) (PAA) polymer leaving a layer of free carboxylic acids for the binding of biotin–PEO–amine (where PEO is polyethylene oxide) through EDC-catalyzed carboxidine reaction. The addition of streptavidine induces rod assembly due to their multiple binding to biotin on the nanorods.

The other way to assemble gold nanorods is the use of solvent evaporation similar to self-assembly, but the CTAB surfactant is exchanged with other ligands before the assembly. Nakashima et al.[245] exchanged the CTAB surfactant with 1,2-dipalmitoyl-*sn*-glycero-3-phosphothioethanol (DPPTE) and observed one- and two-dimensional arrays after chloroform evaporation of the rod solution on a silicon substrate. In the two-dimensional structures, the nanorods are orientated in either a lateral or perpendicular pattern depending on the interfacial hydrophobicity or hydrophilicity of the silicon substrate. Rods treated with mercaptopropyltrimethoxysilane (MPS) and subsequently octadecyltrimethoxysilane (ODS) are also found to be able to form 2D and 3D ordered superstructures after solvent evaporation.[252] At low concentration of the hydrophobic rods, the nanorods are aligned parallel to the substrate, and increased concentrations lead to perpendicular hexagonal array.

4.3. Polymers as Hosts for Gold Nanorod Alignment

Using surface chemical directing, gold nanorods can be assembled to other types of nanostructures, such as gold colloid[253] and carbon nanotubes,[254] to form hybrid nanomaterials. The integration of gold nanorods

with polymer beads is very interesting due to their potential application in drug delivery. Microgel beads, mainly poly(-*N*-isopropylacrylamide) (NIPAM) as well as its acrylic acid form,[255–258] are widely used due to their unique thermal responsive properties. Gold nanorods are loaded onto the bead surface or inside the particle by electrostatic interactions. The laser heating of the hybrid due to the light-to-thermal energy conversion by the nanorods induces the microgel deswelling and thus drug releasing while the microgel swells back to its original volume when the laser is turned off.

The integration of gold nanorods with polymer film enables the rod alignment by the stretched-film method. As firstly demonstrated by van der Zande et al.[259] and later studied by others,[38,260,261] orientation of the nanorods was easily obtained by simple mechanical stretching of poly(vinyl alcohol) (PVA) film in which the colloid nanorods were embedded during the polymer preparation. With the electric field of the light parallel or perpendicular to the rod alignment direction, only the longitudinal band or the transverse band can be excited or detected by absorption or scattering. When the nanorods are incorporated in a symmetric block copolymer film of poly(styrene-*b*-methyl methacrylate) (PS-*b*-PMMA), the nanorods were sequestered and lined in the lamellar PMMA planes by solvent evaporation.[262] The nanorods show an interesting concentration gradient from the substrate to the surface of the film.

Other than the polymer alignment, an electric field is used to induce the alignment of nanorods in solution. The electro-optical effects studied by van der Zande et al.[263] show that at low electric field strengths the rod absorption is linearly dependent on the square of the electric field strength, but at sufficiently high electric field strengths the absorption reaches saturation. They also found that the anisotropy in electric polarizability depends on the square root of the particle length.

5. Biological and Biomedical Applications

Because of their exceptional radiative and nonradiative properties, gold nanorods have emerged as a new type of nanostructure for a wide range of biological and biomedical applications including biosensing, biomedical imaging, gene and drug delivery, disease detection, diagnosis, and therapy. For potential clinical trials, it is necessary to understand their potential risks to human health and the environment. In vitro studies on the toxicity of gold nanoparticles of different size, shape, and surfactant showed that while free CTAB molecules are detrimental to human cells, bound CTAB molecules are not toxic.[264] Since free CTAB molecules can be separated by centrifugation or dialysis membrane, the use of gold nanorods for in vivo and clinical studies is expected to be quite safe. In another case, the surface of gold nanorods can be modified such that CTAB is either replaced or covered by known compatible molecules. For example, Yamada and co-workers[265] found that the PC-modified (PC = phosphatidylcholine) nanorods show much low cytotoxicity than the twice-centrifuged CTAB-capped nanorods. Chan and co-workers'[266] studies on the effects of surface chemistry on cellular uptake, toxicity, and gene expression show that PDADMAC-coated (PDADMAC = poly(diallyldimethylammonium chloride)) gold nanorods have negligible impact on cell function. The PSS-coated (PSS = poly(4-styrenesulfonic acid)) gold nanorods do not pose observable toxicity either.[266] One other common modification to reduce toxicity of gold nanorods while increasing nanorod biocompatibility is the ligand exchange with polyethyleneglycol (PEG) polymers by simply mixing mPEG-SH with the nanorod solution for hours.[267]

5.1. Bioconjugation

Currently conjugation of biomolecules to gold nanorods can be divided into four different methodologies: direct ligand exchange, the use of a biofunctional linker, surface coating, and electrostatic adsorption (Fig. 15). Like other types of gold nanoparticles, thiol exchange is the most common way to replace the original capping molecules since the metal–sulfur bond is known to be the strongest bond compared to other general functional groups (i.e.,

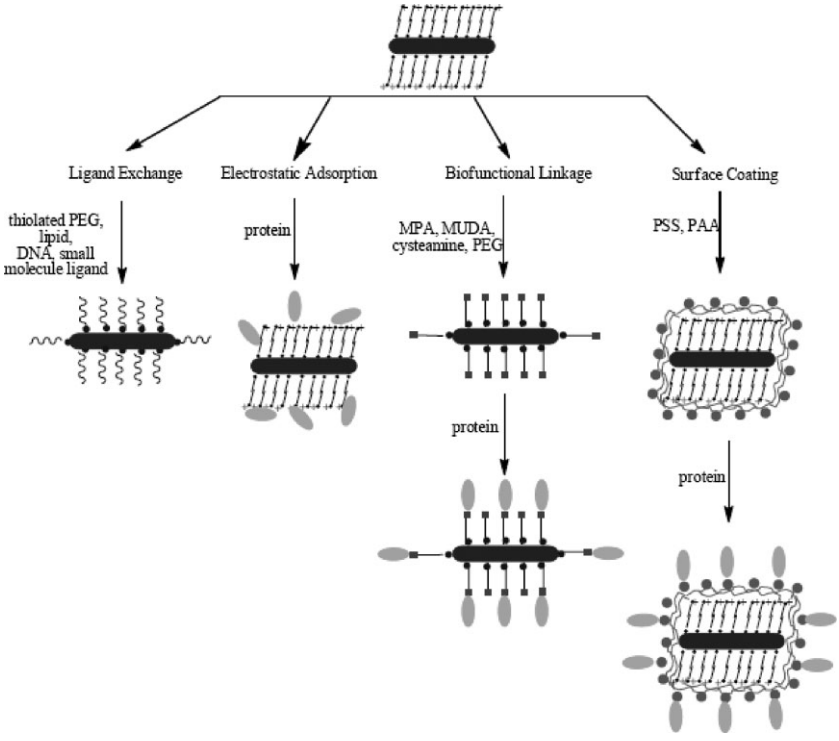

Figure 15. Schematic illustration of biconjugation methods for gold nanorods. Biomolecules can be conjugated to gold nanorods by four approaches: direct ligand exchange of the CTAB capping molecules with the biomolecules; electrostatically adsorbed onto the capping molecules; via a biofunctional linker which binds to gold at one end and to biomolecules on the other end; or a functionalized coating of molecules that are electrostatically adsorbed onto the capping molecules while binding to biomolecules at their sites of functional groups.

amines, carboxylic acids, alcohols, and phosphors). Biomolecules, such as PEG,[267–270] DNA,[248,271] lipids,[272] and small molecule ligands for cellular biomarkers,[273] are firstly functionalized with an alkythiolated linker and then bound to gold nanorods through Au–S bonds after few hours of reaction. For complete exchange, sonication and heating might be required to take the CTAB off while preventing the nanoparticles from aggregation. The success of the ligand exchange reaction can be examined by using the Raman peak of the biomolecules especially the Au–S bonds around 260 cm^{-1},[267] by the stability of the bioconjugates in buffered solution or by the change of zeta potential.

For some biomolecules, such as antibodies and proteins, thiolation is complicated by the fact that molecules are too large to reach the gold surface due to the dense packing of the CTAB double layers. The use of small biofunctional molecules such as 3-mercaptopropionic acid (MPA), 11-mercaptoundecanoic acids (MUDA),[233,235,274] and cysteamine[268] are useful in these studies. As most thiol molecules are not water-soluble, the use of organic solvents (such as ethanol and chloroform) and phase extraction are needed. This places challenges for the modification as gold nanorods are facile to aggregate in organic solvents. A smart way to successfully displace CTAB molecules with MUDA was reported by Dai et al.[235] who conducted the exchange reaction inside an ion-exchange resin. The polymer resin beads were firstly loaded with gold nanorods via capillary force and then suspended in a MUDA chloroform solution. The ligand exchange reaction took place inside the polymer beads, and the thiolated nanorods diffused out of beads into the chloroform solution. The chloroform was dried and the nanorods could be dissolved in aqueous or organic solvents.

Another bioconjugation approach is to coat the nanorods with polymeric molecules that react with the biomolecules. Polyelectrolytes can be deposited onto a substrate[275,276] or particles[277–279] layer by layer via consecutive electrostatic adsorption to manipulate surface properties. Coating gold nanorods with anionic poly(sodium-4-styrenesulfonate) (PSS) polyelectrolytes not only reverses the positive surface charge of the nanorods to negative, but also enables antibody adsorption onto the polymer via hydrophobic interactions.[280,281] PAA adsorption can induce carboxylic acid groups on the surface of the nanorods and protein or amine-terminated small molecules can be thereafter covalently conjugated to the nanorods via the EDC-mediated coupling reaction.[251] Compared to the method of bifunctional linkage that requires ligand exchange, this method is easier, faster, and more efficient, but the stability of the electrostatic interaction is questionable for long-time storage or when used for in vivo application.

The easiest way to adsorb charged proteins, such as antibodies, is the electrostatic interaction. At pH higher than the isoelectric point (p*I*), the protein is negatively charged, and therefore it can be directly adsorbed to gold nanorods via electrostatic attraction. However, the protein/rod ratio needs be optimized to avoid the aggregation of the nanoparticles due to charge neutralization while ensuring high loading of the protein onto the nanorods. Cortie and co-workers[282] used this method to conjugate antibodies to murine macrophage cells in their photothermal studies and achieved a lower laser threshold than comparative studies. This is probably due to high loading of the gold nanorods by this method.

5.2. Biosensing

5.2.1. Surface Plasmon Resonance Sensing

As described previously, the SPR frequency depends on the dielectric constant of the surrounding medium. The dependence arises from the resonance condition at $\varepsilon_r = -(1 - n^{(i)}) \times \varepsilon_m / n^{(i)}$,[54] where $n^{(i)}$ is a depolarization factor with the value of 1/3 for spheres. This gives a negative value for the real part of the dielectric constant of the metal. According to the approximate linear relationship between the real part of the dielectric constant of gold and the wavelength,[55] increasing the dielectric constant, ε_m (or the refractive index, $n_m = \varepsilon_m^{1/2}$) of the surrounding medium leads to a red-shift of the SPR wavelength. Therefore, the SPR wavelength, either by absorption or scattering, provides great opportunity to monitor the changes of the local environment of the nanoparticle and thus can be used for sensing.[283] The sensitivity, defined as the plasmon shift per refractive index unit (RIU) change ($d\lambda_{SPR}/dn_m$), depends on the shape of the nanoparticles as reflected in the shape factor of $(1 - n^{(i)})/n^{(i)}$. A high-value shape factor gives higher sensitivity. This indicates that anisotropic nanoparticles give higher sensitivity than spherical nanoparticles. As described by Lee and El-Sayed,[71] a narrow plasmon bandwidth is also important for the SPR responses. Silver offers a sharper SPR band as a result of the smaller dephasing time of its coherent plasmonic excitation compared to gold. Silver nanotriangle array on a substrate has been demonstrated as an efficient system for chemical and biosensing applications by Van Duyne and co-workers.[284–287]

Gold nanorods are highly suited for plasmon sensing due to the high-value shape factor (surface curvature). Yu and Irudayaraj[233] have demonstrated a multiplex biosensor assay using the different responses of gold nanorods to different targets. Human, rabbit, and mouse IgG were conjugated to gold nanorods of different aspect ratios via a MUDA linker, and the binding events of these three molecular probes to their respective complements (anti-IgGs) were monitored and differentiated by the different shifts of the SPR wavelength of the nanorods. The limit of detection is found to be on the nanomolar scale. Using a mathematical model, they quantified the binding events and measured the binding constants. In a different study, they functionalized the rods with Fab segments of IgG only at the ends via a MUDA bifunctional linker, and they could detect multiplex anti-IgGs according to the different distinct response of the absorption spectrum to those targets.[288] In another study, they are able to simultaneously detect multiplex surface markers of breast cancer cells by using the antibody-conjugated gold nanorod molecular probes.[234] Plasmonic spectra of gold nanorods clearly show the profiling of three surface markers by the recognition of gold nanorod probes of three different aspect ratios. Biomolecular protein recognition based on the scattering wavelength shift from single gold nanorod were also reported.[289] Spectral shifts as small as a half nanometer were detected from a single gold nanorod by dark field microscopy upon binding of streptavidin for a 1 nM concentration. Single molecular DNA detection was also reported using dark field microscopy of gold nanorod sensors linked to F1-ATPase motors.[290]

In addition to biosensing based on the changes of the refractive index of the surrounding medium, the SPR wavelength

dependence on the proximity of other nanoparticles has also been widely used for detection of DNA, antigens, and disease biomarkers.[291] The use of the metal particle pair as a distance probe has also been tested on some biological systems based on the difference of the dark field imaging and spectroscopy in response to the interparticle distance.[292] The distance dependence of plasmon coupling induced by a biomolecule assembly can, in turn, be used as a rapid tool for the detection of the molecules. As shown by Wang et al.,[293] the SPR shift due to side-by-side assembly makes the nanorods sensitive reporters of h-IgG binding at the nanogram level.

Different from the use of surface plasmon-based sensing, Liu et al.[294] reported a one-step homogeneous immunoassay for cancer biomarker detection by taking advantage of the size changes of the nanoparticles upon antigen detection. The mixing of gold nanorods conjugated to capture antibody and gold nanospheres conjugated to detection antibody specific for the free prostate-specific antigen (f-PSA) initiates the agglutination of the nanoparticles, which can be monitored with dynamic light scattering.

5.2.2. Surface-Enhanced Raman Scattering Molecular Sensing

Raman scattering (inelastic photon scattering), first observed by Raman and Krishnan in 1928,[295] provides the most detailed information about the chemical and molecular information of target molecules compared to other optical spectroscopies, such as absorption, scattering and fluorescence.[296,297] It has been used for biological detection since the first interpretable laser-excited Raman spectrum of lysozyme by Lord and Yu in 1970.[298–302] It is well known that most biological molecules have small Raman scattering cross-sections and thus very weak Raman signals. Strong resonance Raman (laser frequency is in resonance with the electronic transition of a molecule) has frequently been used to get enhanced signals for chromo-proteins, but it has the disadvantage of photochemical damage when UV and visible lasers are used. Further, strong fluorescence from these systems interferes and prevents recording of good Raman signals.

An alternative method is the enhancement of Raman scattering by a roughened metal surface, known as surface-enhanced Raman scattering (SERS), which can enhance the signal by six orders of magnitude.[91] Since its discovery by Fleischmann et al.[303] on pyridines adsorbed on a roughened silver electrode, SERS has been extensively used and reviewed from fundamental mechanisms to biomedical applications.[304–320] Very recently, Nie and co-workers[321] showed that SERS from tumors in mice can be obtained by using the Raman tag of dye molecules adsorbed onto spherical gold nanoparticles. This study advanced the development of SERS from bench to in vivo applications and offered the possibility for future clinical cancer diagnosis based on Raman spectroscopic detection.

SERS results from one or two mechanisms: the long-range electromagnetic field due to the SPR and the short-range chemical enhancement. Electric field considerations of individual nanoparticles show that the Raman intensity depends on the distance between the molecule and the metal surface and the particle radius of curvature.[307] This indicates that for large SERS enhancement, besides the distance proximity to the metal surface, particle shape plays an important role due to the lightening-rod effect. As demonstrated by Nikoobakht et al.,[322] enhancement factors on the order of 10^4–10^5 were observed for adsorbed molecules on the nanorods while no such enhancement was observed on nanospheres under similar conditions. Optimal enhancement is found to be on the length scale of 20–100 nm.[323] Enhancement factors are a factor of 10–10^2 greater for nanorods when the longitudinal plasmon band and excitation source spectrum overlap compared to when they do not.[324] Such strong SERS enhancement, together with the facile tuning of the SPR band by the aspect ratio for optimal overlapping with the excitation laser, especially the harmless red laser, are the reasons for the increasing interests in the use of gold nanorods as SERS probes in chemical and biological studies in recent years.[322,323,325,326] One example are the studies by Oyelere et al.[326] who observed Raman bands from the nucleus of both cancer and noncancer cells. In this study, nucleus localization signal (NLS) peptide was conjugated to gold nanorods via a thioazide linker, and the incubation of the conjugates with cells led to dominant accumulation of the nanorods inside the cellular nucleus. Using a micro-Raman spectrometer with excitation at 785 nm, DNA backbone vibration and guanine Raman bands from a single cell were obtained. The normal and cancer cells show fingerprint differences which could be useful for molecular cancer diagnosis. One thing should also be pointed out is that silver nanoparticle or silver-coated gold nanoparticle show 10–10^2 times stronger enhancement due to a stronger molar extinction coefficient[323] and less plasmon damping compared to gold.

Nanorod aggregation,[327–329] two-dimensional film,[330–333] and assembly, especially end-to-end assembly,[229] offer further enhancement due to plasmon coupling between particles. In the recent studies by Huang et al.,[334] the assembly of gold nanorods by cancer cells due to the binding of the anti-EGFR-conjugated rods to the overexpressed EGFR (epidermal growth factor receptor) on the cancer cell surface gives highly enhanced, sharp, and polarized SERS, while no SERS is observed from the majority of the normal cells. This gives a diagnostic tool for cancer.

5.3. Molecular Imaging

Molecular imaging is defined as ''a technique which directly or indirectly monitors and records the spatiotemporal distribution of molecular and cellular processes for biochemical, biologic, diagnostic, or therapeutic applications.''[335] It visualizes molecular or genetic phenomena in live cells, tissue, organs, and whole organisms.[336] Prototype techniques include magnetic resonance imaging (MRI) and spectroscopy (MRS), positron emission tomography (PET) and single-photon emission-computed tomography (SPECT), ultrasound, and optical imaging. Nanoplatforms offer promising imaging probes or contrast agents for these techniques due to their unique optical, electronic, magnetic, and structural properties not available for individual molecules or bulk materials.[337] Compared to conventional contrast agents—such as radionucleotide in PET and SPECT, gadolinium compounds in MRI, and dye molecules in optical fluorescence imaging—nanoparticles have unique features. The size, shape, composite, and structure dependent properties

enable availability of a broad range of nanoplatforms as imaging contrast agents, such as semiconductor quantum dots, plasmonic nanoparticles, magnetic nanoparticles, carbon nanotubes, and nanoparticles.[338,339] Nanoparticles have the characteristics of large surface area offering molecular multifunctionality for simultaneous disease targeting, imaging, diagnostic, and therapeutic applications. Further, they are photoresistant and stable, offering long time operation for optical imaging. Plasmonic nanoparticles, generally spherical and rod shaped gold and silver nanoparticles, Si/Au nanoshells, and gold nanocages are efficient contrast agents in optical imaging based on their unique light–particle interaction process (i.e., the excitation of SPR by light). This SPR enhances all linear and nonlinear optical properties and thus offers multiple imaging modalities including light scattering,[280,283,340,341] optical coherence tomography (OCT),[342] extinction,[270,343] photothermal,[344–346] two-photon luminescence,[104,281,347] multiphoton imaging,[348] harmonic generation,[349] and photoacoustic imaging.[350–355]

As the scattering cross-section of gold nanoparticles is millions of orders of magnitude stronger than that of the emission from fluorescent dye molecules,[60] they are well suited for biomedical imaging using a reflectance confocal microscope and in vivo imaging using optical coherence microscope.[356–362] In the case of white light illumination using simple dark field microscopy which is more facile for in vitro cellular imaging[341,363] or self-built sideway illumination,[364,365] the particles scatter most strongly around the surface plasmon wavelength maximum making them individually visualized with a color that is dependent on the particle size and shape.[70,366] Like gold nanoshells[367] and nanocages,[368] gold nanorods offer the advantage of light scattering in the near-infrared (NIR) region, as their SPR is located in that spectral region. Huang et al.[280] demonstrated that gold nanorods can be used for cancer diagnosis by using anti-EGFR antibodies that bind homogenously and predominately to cancer cells due to EGFR overexpression on such cells (Fig. 16A). Ding et al.[369] used dark field light scattering to image and monitor the receptor-mediated uptake of nanorods into HeLa cells. Nucleus targeting and imaging have also been achieved by conjugating the nanorods to the NLS (Fig. 16B).[326] For potential in vivo imaging, Oldenburg et al.[370] demonstrated that gold nanorods less than 50 nm in length offer good contrast agents with little backscattering albedo appropriate for the highly scattering tissue phantom. The sensitivity is comparable to the in vivo transmission imaging based on the strong absorption ability.[270]

An alternative technique for highly scattering tissue is the fluorescence imaging. Based on the strongly enhanced two-photon-induced luminescence, individual gold nanorods are well distinct under femtosecond NIR laser excitation.[85,104,347] Actually, Wang et al.[104] have shown that single gold nanorods can be detectable in the mouse ear blood vessel by two-photon excitation. Other studies show that TPL signals of gold nanorods are three orders of magnitude stronger than those from the two-photon autofluorescence of cells and tissue, which make them highly efficient contrast agents for cancer imaging.[281] The nanorod targeting of cancer biomarkers on the cytoplasm membrane or their internalization into the cell cytoplasm by receptor-mediated endocytosis can be well differentiated by the TPL signals from the rods (Fig. 16C and D).[371] While semiconductor quantum dots show stronger, narrower, and more tunable emission offering much more sensitive and efficient imaging, gold nanorods have the advantage of photothermal therapy with the imaging modality at the same time.

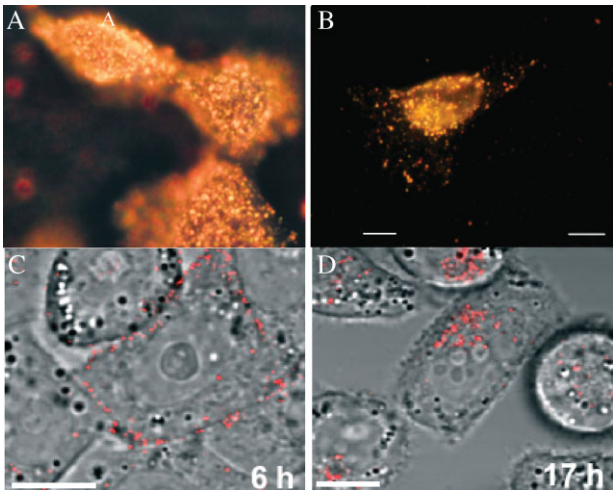

Figure 16. Molecular imaging of live cells using gold nanorods. A) Light scattering imaging of cancerous hematopoietic stem cells (HSC) with anti-EGFR-conjugated gold nanorods located on cytoplasm membrane. Scale bar: 15 μm. Reproduced with permission from [280]. Copyright 2006 ACS. B) Light scattering imaging of cancerous HSC with NLS-conjugated gold nanorods located inside cell nucleus. Scale bar: 15 μm. Reprinted with permission from [326]. Copyright 2007 ACS. C,D) Two-photon-induced luminescence imaging of KB cancer cells with folate-conjugated gold nanorods located on cytoplasm membrane after 6 (C) and 17 h (D) of incubation. (The KB cancer cell line is known to overexpress certain folate receptors). Reproduced with permission from [371]. Scale bar: 10 μm.

Photoacoustic tomography (PAT) is the use of absorbed laser pulse light by a target to induce rapid thermal expansion of the target and thus create acoustic waves (ultrasonic emission), which is detected by ultrasonic transducers to form images. It is based on the optical absorption contrast while combining ultrasound resolution. Therefore, the absorption efficiency of the target directly determines the amplitude of the generated photoacoustic signal. Gold nanorods greatly enhance the contrast in this technique due to the high efficiency of the surface plasmon absorption (absorption cross-section on the order of 10^9 cm^2) in the NIR region where tissue absorption is low. Their potential power for both in vitro and in vivo optoacoustic imaging has been demonstrated by few studies. Li et al.[350,351] imaged the cancer biomarker HER2 on MBT2 cells and CXCR4 on HepG2 by conjugating the nanorods to corresponding antibodies. Kim et al.[354] differentiated inflamed cells from control cells by using the gold nanorods conjugated to anti-intercellular adhesion molecule-1 (ICAM-1) for the targeting of overexpressed ICAM-1 on inflammatory cells. Their ability in the detection of prostate cancer has also been demonstrated by the same group.[353] The nanorod distribution under the skin of nude mice can be well identified at concentrations as low as 125 μM.[352] Chamberland et al.[355] have shown the improvement of the PAT imaging of a rat

tail joint after direct injection of etanercept-conjugated gold nanorods.

5.4. Gene and Drug Delivery

Due to the risk of cytotoxicity and immunologic responses of conventional virus-mediated gene delivery, the search for nonviral gene vectors is indispensible. In the context of synthetic nanocarriers,[372–375] gold nanorods started to catch attention in recent years.[271,376,377] The current strategy is to use the shape transformation of gold nanorods under exposure to NIR laser pulses to result in the DNA release due to surface atom rearrangement (Fig. 17).[271] In the work by Niidome and co-workers,[376] plasmid DNA is adsorbed to PC-modified gold nanorods by electrostatic interaction and their release is tested by illuminating the PC–nanorod–DNA solution with the fundamental light of a Q-switched Nd:YAG laser. The DNA release was verified by gel electrophoresis. In vitro assays show that 1% of the DNA molecules is released and 0.5% is active.[377] In the work by Wu and co-workers,[271] the thiolated gene of enhanced green fluorescence protein (EGFP) is covalently conjugated to gold nanorods. The heating by a Q-switched Nd:YLF laser not only causes shape transformation of the nanorods, but also breaks the Au–S bonds due to thermal and electron heating of the particles. Induced EGFR expression in HeLa cells after laser exposure to the EGFR–gold nanorod incubated cells are specifically observed. This study demonstrated the feasibility of the remote control of gene expression with an optical switch mediated by gold nanorods.

Integrating gold nanorods with polymer materials could lead to drug release under NIR laser irradiation. One example is the use of gold nanorod/PNIPAAm core/shell nanohybrids by Wei et al.[378] to manipulate norvancomycin delivery with NIR light (PNIPAAm = poly(N-isoproylacrylamide). Laser irradiation induces heating of the gold nanorods and the adjacent temperature-responsive polymer materials. The polymer undergoes shrinkage under temperature increases and thus the drug is released.

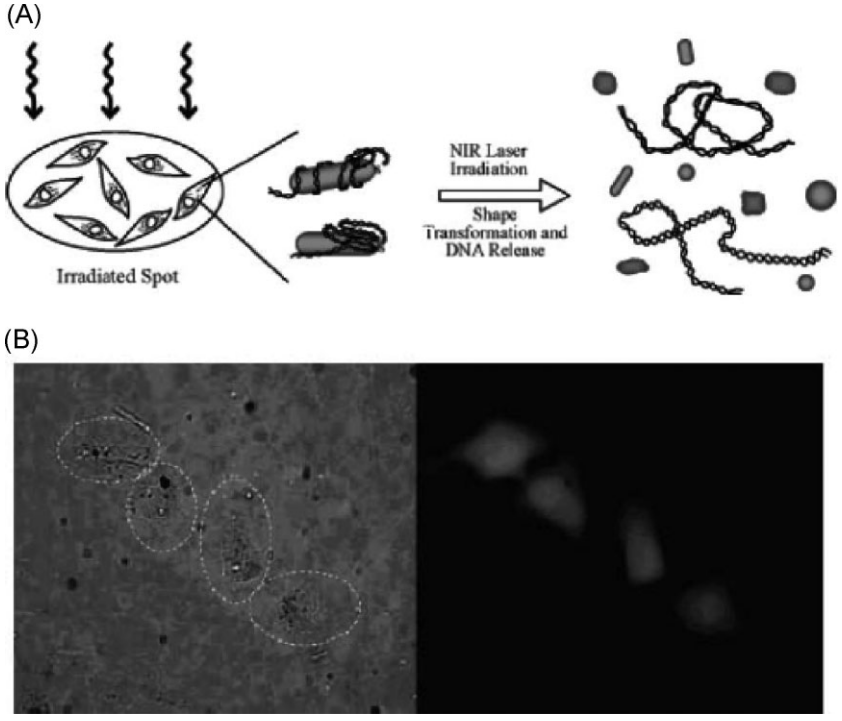

Figure 17. Gene delivery using gold nanorods. A) Schematic illustration of the gene delivery process inside live cells using DNA–GNR conjugates with the assistance of NIR irradiation. Under laser irradiation, gold nanorods undergo shape transformation that resulted in the release of EGFP DNA. B) Expressing of EGFP inside cells after laser irradiation. Left: bright field images. Right: the confocal image showing GFP expression. Reproduced with permission from [271]. Copyright 2006 ACS.

5.5. Photothermal Therapy of Cancer

Current plasmonic nanoparticles for photothermal therapy of cancer are gold nanospheres, nanorods, nanoshells, and nanocages.[24] Compared to other types of nanoscale photothermal absorbers (e.g., carbon nanotubes[379]), the plasmonic nanoparticles enable dual imaging/therapy functions. The latter three types of plasmonic nanoparticles are more popular as they absorb light in the NIR window (650–900 nm[36]) where light penetration is optimal due to minimal absorption by water and hemoglobin in the tissue. The recent interest in the use of gold nanorods comes from the advantages of their facile synthesis, excellent stability, small size, high absorption efficiency, and tunable absorption in the biological window.

5.5.1. Cancer Targeting and Diagnosis

To induce local heating and destruction of the cancer and tumor region without affecting surrounding healthy cells and tissue, the nanoparticles have to be specifically delivered to the desired targets. It is known that cancer targeting can be achieved in two ways. One way is by passive targeting, taking advantage of the enhanced permeation and retention (EPR) effects of nanoparticles with controlled size in tumor tissue, which is characteristic of leaky vasculatures (pore size of 20–500 nm[380]) and an impaired lymphatic drainage system.[381–383] The nanoparticles are generally coated with hydrophilic polymers to avoid their uptake by the reticuloendothelial system and protein adsorption in blood circulation.[384–386] For gold nanorods, the PEG polymer is widely used, and they are conjugated to the nanoparticles via covalent binding between the functional thiol group of the polymer and gold surface.[267,269,270] The complete replacement of CTAB molecules by the PEG molecules is questionable. However, the generally used PEG 5000 molecules have a hydrodynamic length of 10 nm.[321] This is longer than that of the CTAB bilayer (4 nm,[250]) and the brush conformation of the polymer could form a crosslinked layer outside of the undisplaced

CTAB molecules. This shears the potential nonspecific protein adsorption of the positively charged CTAB capping molecules. It also stabilizes the nanorods in a high-ionic-strength environment as well.[267] The other way is by active targeting using conjugated compounds that specifically bind to cancer biomarkers via lectin–carbohydrate, ligand–receptor, and antibody–antigen interactions.[387] Antibodies,[280,350,388] folate,[273,371] or deltorphin molecules[389] are conjugated to gold nanorods either via noncovalent[280,350] or covalent binding[273,371,388,389] to specifically target receptors overexpressed on the cancer cells.

5.5.2. Photothermal Therapy

In 2003, two groups initiated plasmonic photothermal therapy (PPTT) for cancer. One is Lin and co-workers[390] who photolyzed lymphocytes cells using spherical gold nanoparticles in combination with a pulsed visible laser. The other is Halas and co-workers[391] who photodestructed breast carcinoma cells and tumors in mice using silica/gold core/shell nanoparticles coupled with a continuous wave (CW) NIR laser. Three years later, El-Sayed and co-workers[280] conducted the PPTT of human oral cancer cells in the NIR region using gold nanorods by extending their previous work using gold nanospheres in visible region.[392,393] In this study, gold nanorods were conjugated to anti-EGFR antibodies enabling selective photothermal therapy due to their preferential binding onto human oral cancer cells. A CW Ti/Sappire NIR laser with a wavelength at 800 nm, overlapping with the SPR absorption maximum of the gold nanorods (aspect ratio of 3.9), was used for the photoirradiation of the cells immunolabeled with the nanorods. Using the trypan blue cell death staining and variable laser energies, they found that the cancer cells required half the laser energy (10 W cm^{-2}, Fig. 18A) to be photothermally damaged as compared to the normal cells (20 W cm^{-2}) (Fig. 18B). In their recent studies using a mouse model,[270] the nanorods were conjugated to mPEG-SH 5000 and injected into mice both intravenously and subcutaneously. Using the transmission imaging of the NIR laser with a customized camera, the tumor can be well identified after nanorod accumulation either via intravenous or subcutaneous injections (Fig. 18C). The spectral profiling of the images clearly shows the difference in the particle targeting efficiency between the two administration methods. After exposure to a CW red laser at 808 nm with an energy of 1 W cm^{-2} for 10 min, tumor volumes in both delivery methods did not grow while the untreated tumor kept growing at a rapid rate (Fig. 18D). The intravenous treated tumors show lower PPTT efficiency due to lower amount of gold nanorods inside the tumor as shown in the NIR imaging. In the case of pulse laser irradiation, Niidome and co-workers[394,395] found that it could induce cell death, but successive irradiation causes reshaping of the nanorods into nanospheres to prevent further cell death.

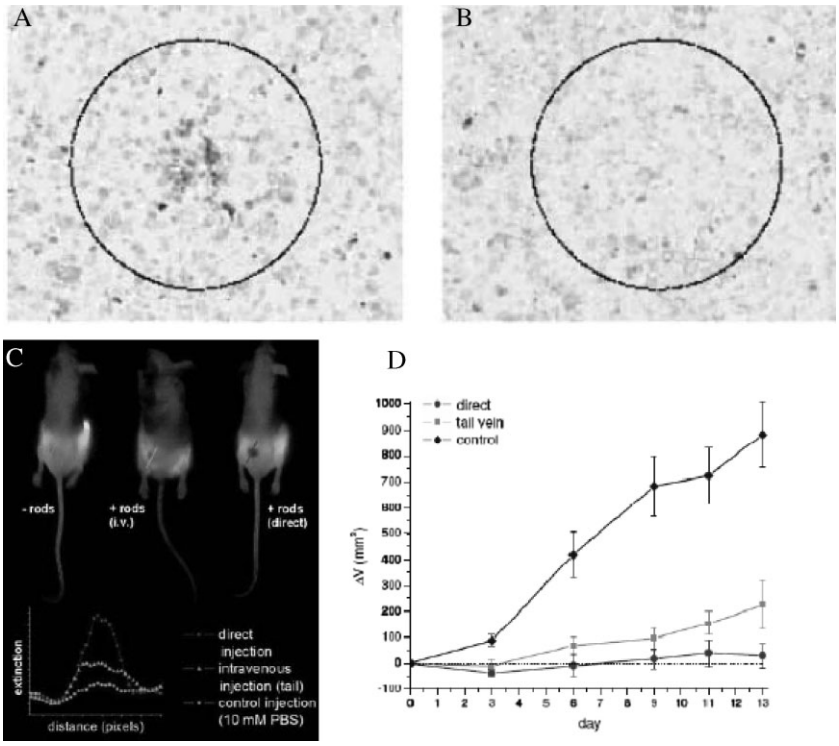

Figure 18. A,B) Selective in vitro photothermal cancer therapy using gold nanorods. The HaCat normal (A) and HSC-3 cancer (B) cells are incubated with anti-EGFR/gold nanorod conjugates and then exposed to NIR laser at wavelength of 800 nm. At 10 W cm^{-2}, the cancer cells within the laser spot undergo irreversible photodestruction (A) while the normal cells are not affected (B). Reproduced with permission from [280]. Copyright 2006 ACS. C,D) In vivo NIR tumor imaging and therapy using gold nanorods. The tumors are identified by a black spot under NIR illumination due to the light absorption by the nanorods that are administrated into the tumor either intratumorally or intravenously. NIR irradiation of the nanorod-treated tumors leads to significant inhibition of the tumor growth rate compared to control tumors (i.v. is intravenous; PBS is phosphate buffered saline solution). Reprinted with permission from [270]. Copyright 2008 from Elsevier.

For the spectroscopic monitoring of gold nanorods in vivo, Niidome and co-workers[269] have designed a spectrometer equipped with an integrating sphere to record the SPR band of gold nanorods in a mouse abdomen. The mouse is placed on a PMMA plate and the integrating sphere collected scattered light from the mouse abdomen and thus the absorbed light by the nanorods is recorded by a photomultiplier tube detector. The absorption spectrum of PEGlyated gold nanorods in the mouse abdomen was obtained 3.5 s after tail vein injection, and the nanorod accumulation increased at 30 min without aggregation. This method could be well used for the quantitative monitoring of nanoparticle circulation in the blood stream and their accumulation in the tumor.

The photothermal heat generation by laser irradiation of the nanorods in cells has been calculated by Cortie and co-workers[282] in their studies on the photothermal destruction of murine macrophage cells. Based on a conductive heat-transfer model, their results show that the effective temperature increases on the cells at a laser influence of 30 J cm^{-2} is on the order of

10 °C. This suggests that heat stress caused the death of the cells instead of mechanical perforation of their membrane.

The photothermolysis mechanism elucidated by Wei and Cheng groups[371] departs away from the simple hyperthermia assumption. Their studies show that the laser energy used to destroy the cells when the nanoparticles are located on the cytoplasm membrane is 10 times lower than that required when the nanoparticles are internalized inside the cytoplasm. The energy required for a fs laser is 10-fold lower than that by using a CW laser. Based on these results and staining of cell membrane integrity, cell viability, and actin filaments, they found that the cell death is initiated by the disruption of the plasma membrane. Subsequent influx of calcium ions induces membrane blebbing and damage of actin filaments. Obviously, apoptosis is the route of cell destruction by the laser heating of gold nanorods.

6. Conclusion and Outlook

Gold nanorods have thus shown exceptional optical properties suitable for a wide range of applications with a recent blossom in cancer diagnosis and treatment. As seen by current photothermal therapeutic studies, the nanorods could be advanced to clinical trials in the near future. Nonetheless, like any other new material, a number of parameters have to be addressed in detail before approval by the Food and Drug Administration (FDA). The main factors are toxicity, biodistribution, and the fate of the nanoparticles after in vivo administration. We anticipate that it will take up to 10 years for the translation stage. Another future research direction could be optically controlled gene delivery. Current research on this area is based on the shape change of nanorods to release DNA. However, if sensing DNA is hybridized to an anti-sensing sequence that is chemically bound onto the gold surface, mild laser heating without shape changes could unhybridize the duplex to release DNA. This is a very promising way for gene delivery as the releasing action can be manually powered by light, acting as on and off switch. The third promising research direction would be their use for in vivo spectroscopic tumor detection. The combination of small-molecule Raman reporters (generally organic dye molecules) and an enhancing substrate of gold nanorods would make single-molecule in vivo SERS detection possible.

Acknowledgements

We thank the Department of Energy, Office of Basic Energy (DE-FG02-97 ER 14799) for support. XH acknowledge Emory-Georgia Cancer Nanotechnology Center for the distinguished CCNE fellowship.

Received: September 18, 2009
Published online:

[1] R. Narayanan, M. A. El-Sayed, *J. Phys. Chem. C* **2005**, *109*, 12663.
[2] R. Narayanan, M. A. El-Sayed, *Chim. Oggi* **2007**, *25*, 84.
[3] U. Heiz, U. Landman, *Nanocatalysis*, Springer, Heidelberg **2006**.
[4] P. K. Jain, W. Huang, M. A. El-Sayed, *Nano Lett.* **2007**, *7*, 2080.
[5] S. Nie, S. R. Emory, *Science* **1997**, *275*, 1102.
[6] K. Kneipp, Y. Wang, H. Kneipp, L. T. Perelman, I. Itzkan, R. R. Dasari, M. S. Feld, *Phys. Rev. Lett.* **1997**, *78*, 1667.
[7] A. Biesso, W. Qian, M. A. El-Sayed, *J. Am. Chem. Soc.* **2008**, *130*, 3258.
[8] S. Neretina, W. Qian, E. Dreaden, M. El-Sayed, R. A. Hughes, J. S. Preston, P. Mascher, *Nano Lett.* **2008**, *8*, 2410.
[9] W. Huang, W. Qian, P. K. Jain, M. A. El-Sayed, *Nano Lett.* **2007**, *7*, 3227.
[10] K. Kneipp, H. Kneipp, I. Itzkan, R. R. Dasari, M. S. Feld, *J. Phys. Condens. Matter.* **2002**, *14*, R597.
[11] C. A. Mirkin, *Inorg. Chem.* **2000**, *39*, 2258.
[12] B. M. Reinhard, M. Siu, H. Agarwal, A. P. Alivisatos, J. Liphardt, *Nano Lett.* **2005**, *5*, 2246.
[13] B. Reinhard, S. Sheikholeslami, A. Mastroianni, A. P. Alivisatos, J. Liphardt, *Proc. Natl. Acad. Sci. USA* **2007**, *104*, 2667.
[14] C. Sönnichsen, B. M. Reinhard, J. Liphard, A. P. Alivisatos, *Nat. Biotechnol.* **2005**, *23*, 741.
[15] P. K. Jain, M. A. El-Sayed, *J. Phys. Chem. C* **2007**, *111*, 17451.
[16] P. K. Jain, M. A. El-Sayed, *Nano Lett.* **2007**, *7*, 2854.
[17] P. K. Jain, M. A. El-Sayed, *J. Phys. Chem. C* **2008**, *112*, 4954.
[18] P. K. Jain, X. Huang, I. H. El-Sayed, M. A. El-Sayed, *Acc. Chem. Res.* **2008**, *41*, 1578.
[19] C. Tabor, R. Murali, M. A. Mahmoud, M. A. El-Sayed, *J. Phys. Chem. A* **2009**, *113*, 1946.
[20] S. Link, M. A. El-Sayed, *Int. Rev. Phys. Chem.* **2000**, *19*, 409.
[21] M. A. El-Sayed, *Acc. Chem. Res.* **2001**, *34*, 257.
[22] S. Link, M. A. El-Sayed, *Annu. Rev. Phys. Chem.* **2003**, *54*, 331.
[23] C. H. Loo, A. Lin, L. R. Hirsch, M. H. Lee, J. Barton, N. J. Halas, J. West, R. A. Drezek, *Technol. Cancer Res. Treat.* **2004**, *3*, 33.
[24] X. Huang, P. K. Jain, I. H. El-Sayed, M. A. El-Sayed, *Lasers Med. Sci.* **2007**, *39*, 747.
[25] A. Habenicht, M. Olapinski, F. Burmeister, F. P. Leiderer, J. Boneberg, *Science* **2005**, *309*, 2043.
[26] W. Huang, W. Qian, M. A. El-Sayed, *J. Am. Chem. Soc.* **2006**, *128*, 13330.
[27] G. V. Hartland, *Annu. Rev. Phys. Chem.* **2006**, *57*, 403.
[28] W. Huang, M. A. El-Sayed, *Eur. Phys. J. Spec. Top.* **2008**, *153*, 325.
[29] G. V. Hartland, M. Hu, O. Wilson, P. Mulvaney, J. E. Sader, *J. Phys. Chem. B* **2002**, *106*, 743.
[30] W. Huang, W. Qian, M. A. El-Sayed, *Nano Lett.* **2004**, *4*, 1741.
[31] W. Huang, W. Qian, M. A. El-Sayed, *J. Phys. Chem. C* **2005**, *109*, 18881.
[32] M. Hu, J. Chen, Z. Y. Li, L. Au, G. V. Hartland, X. Li, M. Marqueze, Y. Xia, *Chem. Soc. Rev.* **2006**, *35*, 1084.
[33] A. J. Haes, D. A. Stuart, S. Nie, R. P. Van Duyne, *J. Fluoresc.* **2004**, *14*, 355.
[34] S. J. Oldenburg, R. D. Averitt, S. L. Westcott, N. J. Halas, *Chem. Phys. Lett.* **1998**, *288*, 243.
[35] Y. Sun, B. T. Mayers, Y. Xia, *Nano Lett.* **2002**, *2*, 481.
[36] R. Weissleder, *Nat. Biotechnol.* **2001**, *19*, 316.
[37] B. Nikoobakht, M. A. El-Sayed, *Chem. Mater.* **2003**, *15*, 1957.
[38] C. J. Murphy, C. J. Orendorff, *Adv. Mater.* **2005**, *17*, 2173.
[39] G. Mie, *Ann. Phys.* **1908**, *25*, 377.
[40] M. Kerker, *The Scattering of Light and Other Electromagnetic Radiation*, Academic Press, New York **1969**.
[41] G. C. Papavassiliou, *Prog. Solid State Chem.* **1980**, *12*, 185.
[42] C. F. Bohren, D. R. Huffman, *Absorption and Scattering of Light by Small Particles*, Wiley, New York **1983**.
[43] U. Kreibig, M. Vollmer, *Optical Properties of Metal Clusters*, Springer, Berlin **1995**.
[44] S. Link, M. A. El-Sayed, *J. Phys. Chem. B* **1999**, *103*, 8410.
[45] L. M. Liz-Marzan, *Mater. Today* **2004**, *7*, 26.
[46] P. K. Jain, X. Huang, I. H. El-Sayed, M. A. El-Sayed, *Plasmonics* **2007**, *2*, 107.
[47] M. Faraday, *Philos. Trans.* **1857**, *147*, 145.
[48] J. A. Creighton, D. G. Eadon, *J. Chem. Soc. Faraday Trans.* **1991**, *87*, 3881.
[49] A. M. Schwartzberg, T. Y. Olson, C. E. Talley, J. Z. Zhang, *J. Phys. Chem. B* **2006**, *110*, 19935.

[50] J. Chen, B. Wiley, Z. Y. Li, D. Campbell, F. Saeki, H. Cang, L. Au, J. Lee, X. Li, Y. Xia, *Adv. Mater.* **2005**, *17*, 2255.
[51] R. Bukasov, J. S. Shumaker-Parry, *Nano Lett.* **2007**, *7*, 1113.
[52] Y. Sun, B. Mayers, Y. Xia, *Nano Lett.* **2003**, *3*, 675.
[53] E. Hao, R. C. Bailey, G. C. Schatz, J. T. Hupp, S. Li, *Nano Lett.* **2004**, *4*, 327.
[54] R. Gans, *Ann. Phys.* **1915**, *47*, 270.
[55] S. Link, M. B. Mohamed, M. A. El-Sayed, *J. Phys. Chem. B* **1999**, *103*, 3073.
[56] S. Link, M. A. El-Sayed, *J. Phys. Chem. B* **2005**, *109*, 10531.
[57] A. Brioude, X. C. Jiang, M. P. Pileni, *J. Phys. Chem. B* **2005**, *109*, 13138.
[58] B. Yan, Y. Yang, Y. Wang, *J. Phys. Chem. B* **2003**, *107*, 9159.
[59] S. Eustis, M. A. El-Sayed, *J. Appl. Phys.* **2006**, *100*, 044324.
[60] P. K. Jain, K. S. Lee, I. H. El-Sayed, M. A. El-Sayed, *J. Phys. Chem. B* **2006**, *110*, 7238.
[61] L. D. Landau, E. M. Lifshitz, *Electrodynamics of Continuous Media*, 2nd edition, Elsevier Science & Technology, Oxford, UK **1984**.
[62] H. C. van de Hulst, *Light Scattering by Small Particles*, Wiley, NewYork **1957**.
[63] L. Qiu, T. A. Larson, D. K. Smith, E. Vitkin, S. Zhang, M. D. Modell, I. Itzkan, E. B. Hanlon, B. A. Korgel, K. V. Sokolov, L. T. Perelman, *IEEE J. Sel. Top. Quantum Electron.* **2007**, *13*, 1730.
[64] K. S. Lee, M. A. El-Sayed, *J. Phys. Chem. B* **2005**, *109*, 20331.
[65] F. M. Purcell, C. R. Pennypacker, *Astrophys. J.* **1973**, *186*, 705.
[66] B. T. Draine, *Astrophys. J.* **1988**, *333*, 848.
[67] B. T. Draine, J. J. Goodman, *Astrophys. J.* **1993**, *405*, 685.
[68] B. T. Draine, P. J. Flatau, *J. Opt. Soc. Am. A* **1994**, *11*, 1491.
[69] B. T. Draine, in *Light Scattering by Nonspherical Particles: Theory, Measurements, and Geophysical Applications* (Eds: M. I. Mishchenko, J. W. Hovenier, L. D. Travis) Academic Press, NY **2000**, p. 131.
[70] C. Sönnichsen, T. Franzl, T. Wilk, G. V. Plessen, J. Feldmann, *Phys. Rev. Lett.* **2002**, *88*, 077402.
[71] S. K. Lee, M. A. El-Sayed, *J. Phys. Chem. B* **2006**, *110*, 19220.
[72] H. Chen, X. Kou, Z. Yang, W. Ni, J. Wang, *Langmuir* **2008**, *24*, 5233.
[73] G. Raschke, S. Kowarik, T. Franzl, C. Sönnichsen, T. A. Klar, J. Feldmann, A. Nichtl, K. Kurzinger, *Nano Lett.* **2003**, *3*, 935.
[74] C. Sönnichsen, S. Geier, N. E. Hecker, G. von Plessen, J. Feldmann, H. Ditlbacher, B. Lamprecht, J. R. Krenn, F. R. Aussenegg, V. Z. H. Chan, J. P. Spatz, M. Moller, *Appl. Phys. Lett.* **2000**, *77*, 2949.
[75] C. Novo, D. Gomez, J. Perez-Juste, Z. Zhang, H. Petrova, M. Reismann, P. Mulvaney, G. V. Hartland, *Phys. Chem. Chem. Phys.* **2006**, *8*, 3540.
[76] M. Hu, C. Novo, A. Funston, H. Wang, H. Staleva, S. Zou, P. Mulvaney, Y. Xia, G. V. Hartland, *J. Mater. Chem.* **2008**, *18*, 1949.
[77] S. Berciaud, L. Cognet, P. Tamarat, B. Lounis, *Nano Lett.* **2005**, *5*, 515.
[78] J. Becker, I. Zins, A. Jakab, Y. Khalavka, O. Schubert, C. Sönnichsen, *Nano Lett.* **2008**, *8*, 1719.
[79] K. Ueno, S. Juodkazis, V. Mizeikis, D. Ohnishi, K. Sasaki, H. Misawa, *Opt. Express* **2007**, *15*, 16527.
[80] E. K. Payne, K. L. Shuford, S. Park, G. C. Schatz, C. A. Mirkin, *J. Phys. Chem. B* **2006**, *110*, 2150.
[81] H. Okamoto, K. Imura, *J. Mater. Chem.* **2006**, *16*, 3920.
[82] K. Imura, H. Okamoto, *Opt. Lett.* **2006**, *31*, 1474.
[83] K. Imura, T. Nagahara, H. Okamoto, *J. Chem. Phys.* **2005**, *122*, 154701.
[84] K. Imura, T. Nagahara, H. Okamoto, *J. Phys. Chem. B* **2005**, *109*, 13214.
[85] K. Imura, T. Nagahara, H. Okamoto, *J. Am. Chem. Soc.* **2004**, *126*, 12730.
[86] L. Douillard, F. Charra, Z. Korczak, R. Bachelot, S. Kostcheev, G. Lerondel, P.-M. Adam, P. Royer, *Nano Lett.* **2008**, *8*, 935.
[87] K. Imura, T. Nagahara, H. Okamoto, *J. Phys. Chem. B* **2004**, *108*, 16344.
[88] K. Imura, H. Okamoto, *Phys. Rev. B* **2008**, *77*, 041401.
[89] J. T. Krug, G. D. Wang, S. R. Emory, S. M. Nie, *J. Am. Chem. Soc.* **1999**, *121*, 9208.
[90] J. I. Gersten, *J. Chem. Phys.* **1980**, *72*, 5779.
[91] E. Hao, G. C. Schatz, *J. Chem. Phys.* **2004**, *120*, 357.
[92] E. Hao, G. C. Schatz, J. T. Hupp, *J. Fluoresc.* **2004**, *14*, 331.
[93] M. B. Mohamed, V. Volkov, S. Link, M. A. El-Sayed, *Chem. Phys. Lett.* **2000**, *317*, 517.
[94] W. Rechberger, A. Hohenau, A. Leitner, J. R. Krenn, B. Lamprecht, F. R. Aussenegg, *Opt. Commun.* **2003**, *220*, 137.
[95] K. H. Su, Q. H. Wei, X. Zhang, J. J. Mock, D. R. Smith, S. Schultz, *Nano Lett.* **2003**, *3*, 1087.
[96] M. Gluodenis, C. A. Foss, *J. Phys. Chem. B* **2002**, *106*, 9484.
[97] P. K. Jain, S. Eustis, M. A. El-Sayed, *J. Phys. Chem. B* **2006**, *110*, 18243.
[98] R. Atkinson, W. R. Hendre, G. A. Wurtz, W. Dickson, A. V. Zayats, P. Evans, R. J. Pollard, *Phys. Rev. B* **2006**, *73*, 235402.
[99] G. A. Wurtz, W. Dickson, D. O'Connor, R. Atkinson, W. Hendren, P. Evans, R. Pollard, A. V. Zayats, *Opt. Express* **2008**, *16*, 7460.
[100] E. J. Smythe, E. Cubukcu, F. Capasso, *Opt. Express* **2007**, *15*, 7439.
[101] A. Mooradian, *Phys. Rev. Lett.* **1969**, *22*, 185.
[102] S. Eustis, M. A. El-Sayed, *J. Phys. Chem. B* **2005**, *109*, 16350.
[103] C. Z. Li, K. B. Male, S. Hrapovic, J. H. T. Luong, *Chem. Commun.* **2005**, 3924.
[104] H. Wang, T. B. Huff, D. A. Zweifel, W. He, P. S. Low, A. Wei, J. X. Cheng, *Proc. Natl. Acad. Sci. USA* **2005**, *102*, 15752.
[105] J. P. Wilcoxon, J. E. Martin, F. Parsapour, B. Wiedenman, D. F. Kelley, *J. Chem. Phys.* **1998**, *108*, 9137.
[106] A. Bouhelier, R. Bachelot, G. Lerondel, S. Kostcheev, P. Royer, G. P. Wiederrecht, *Phys. Rev. Lett.* **2005**, *95*, 267405.
[107] B. Nikoobakht, C. Burda, M. Braun, M. Hun, M. A. El-Sayed, *Photochem. Photobiol.* **2002**, *75*, 591.
[108] J. Lee, A. O. Govorov, J. Dulka, N. A. Kotov, *Nano Lett.* **2004**, *4*, 2323.
[109] J. Lee, P. Hernandez, J. W. Lee, A. O. Govorov, N. A. Kotov, *Nat. Mater.* **2007**, *6*, 291.
[110] H. I. Elim, J. Yang, J.-Y. Lee, J. Mi, W. Ji, *Appl. Phys. Lett.* **2006**, *88*, 083107.
[111] R. Philip, G. R. Kumar, N. Sandhyarani, T. Pradeep, *Phys. Rev. B* **2000**, *62*, 13160.
[112] Y. Gao, X. Zhang, W. Li, H. Liu, Y. Wang, Q. Chang, W. Jiao, Y. Song, *Opt. Commun.* **2005**, *251*, 429.
[113] M. Pelton, M. Liu, S. Park, N. F. Scherer, P. Guyot-Sionnest, *Phys. Rev. B* **2006**, *73*, 155419.
[114] O. L. Muskens, N. D. Fatti, F. Vallee, *Nano Lett.* **2006**, *6*, 552.
[115] S. Roorda, T. van Dillen, A. Polman, C. Graf, A. van Blaaderen, B. J. Kooi, *Adv. Mater.* **2004**, *26*, 235.
[116] J. M. Lamarre, F. Billard, C. H. Kerboua, M. Lequime, S. Roorda, L. Martinu, *Opt. Commun.* **2008**, *281*, 331.
[117] W. Dickson, P. R. Evans, G. A. Wurtz, W. Hendren, R. Atkinson, R. J. Pollard, A. V. Zayatz, *J. Microsc.* **2008**, *229*, 415.
[118] S. Link, C. Burda, Z. L. Wang, M. A. El-Sayed, *J. Chem. Phys.* **1999**, *111*, 1255.
[119] S. Link, C. Burda, M. B. Mohamed, B. Nikoobakht, M. A. El-Sayed, *Phys. Rev. B* **2000**, *61*, 6086.
[120] M. B. Mohanmed, S. A. Temer, S. Link, M. Braun, M. A. El-Sayed, *Chem. Phys. Lett.* **2001**, *343*, 55.
[121] S. Link, A. Furube, M. B. Mohamed, T. Asahi, H. Masuhara, M. A. El-Sayed, *J. Phys. Chem. B* **2002**, *106*, 945.
[122] S. Link, D. J. Hathcock, B. Nikoobakht, M. A. El-Sayed, *Adv. Mater.* **2003**, *15*, 5.
[123] S. Link, C. Burda, M. B. Mohamed, B. Nikoobakht, M. A. El-Sayed, *J. Phys. Chem. A* **1999**, *103*, 1165.
[124] W. Huang, W. Qian, P. K. Jain, M. A. El-Sayed, *Nano Lett.* **2007**, *7*, 3227.
[125] S. Link, C. Burda, M. B. Mohamed, B. Nikoobakht, M. A. El-Sayed, *J. Phys. Chem. B* **2000**, *104*, 6152.
[126] S. Link, M. A. El-Sayed, *J. Chem. Phys.* **2001**, *114*, 2362.
[127] S. Link, C. Burda, B. Nikoobakht, M. A. El-Sayed, *Chem. Phys. Lett.* **1999**, *315*, 12.
[128] S. Link, Z. L. Wang, M. A. El-Sayed, *J. Phys. Chem. B* **2000**, *104*, 7867.
[129] M. B. Mohamed, K. Z. Ismail, S. Link, M. A. El-Sayed, *J. Phys. Chem. B* **1998**, *102*, 9370.
[130] C. Burda, X. Chen, R. Narayanan, M. A. El-Sayed, *Chem. Rev.* **2005**, *105*, 1025.
[131] Y. Xia, N. J. Halas, *MRS Bull.* **2005**, *30*, 338.

[132] Y. Yin, A. P. Alivisatos, *Nature* **2005**, *437*, 664.
[133] J. Wiesner, A. Wokaun, *Chem. Phys. Lett.* **1989**, *157*, 569.
[134] N. R. Jana, L. Gearheart, C. J. Murphy, *Adv. Mater.* **2001**, *13*, 1389.
[135] N. R. Jana, L. Gearheart, C. J. Murphy, *J. Phys. Chem. B* **2001**, *105*, 4065.
[136] B. D. Busbee, S. O. Obare, C. J. Murphy, *Adv. Mater.* **2003**, *15*, 414.
[137] A. Gole, C. J. Murphy, *Chem. Mater.* **2004**, *16*, 3633.
[138] C. J. Murphy, T. K. Sau, A. M. Gole, C. J. Orendorff, J. Gao, L. Gou, S. E. Hunyadi, T. Li, *J. Phys. Chem. B* **2005**, *109*, 13857.
[139] H. Y. Wu, H. C. Chu, T. J. Kuo, C. L. Kuo, M. H. Huang, *Chem. Mater.* **2005**, *17*, 6447.
[140] D. A. Zweifel, A. Wei, *Chem. Mater.* **2005**, *17*, 4256.
[141] M. Iqbal, Y. Chung, G. Tae, *J. Mater. Chem.* **2007**, *17*, 335.
[142] H. M. Chen, H. C. Peng, R. S. Liu, K. Asakura, C. L. Lee, J. F. Lee, S. F. Hu, *J. Phys. Chem. B* **2005**, *109*, 19553.
[143] T. K. Sau, C. J. Murphy, *J. Phys. Chem. B* **2004**, *126*, 8648.
[144] T. K. Sau, C. J. Murphy, *Langmuir* **2004**, *20*, 6414.
[145] L. Gou, C. J. Murphy, *Chem. Mater.* **2005**, *17*, 3668.
[146] X. Kou, S. Zhang, C. K. Tsung, M. H. Yeung, Q. Shi, G. D. Stucky, L. Sun, J. Wang, C. Yan, *J. Phys. Chem. B* **2006**, *110*, 16377.
[147] X. C. Jiang, A. Brioude, M. P. Pileni, *Colloids Surf, A* **2006**, *277*, 201.
[148] X. D. Xu, M. B. Cortie, *Adv. Funct. Mater.* **2006**, *16*, 2170.
[149] A. Gulati, H. Liao, J. H. Hafner, *J. Phys. Chem. B* **2006**, *110*, 22323.
[150] H. J. Park, C. S. Ah, W. J. Kim, *J. Vac. Sci. Technol.* **2006**, *24*, 1323.
[151] H. Y. Wu, W. L. Huang, M. H. Huang, *Cryst. Growth Design* **2007**, *7*, 831.
[152] X. C. Jiang, M. P. Pileni, *Colloids Surf, A* **2007**, *295*, 228.
[153] E. Carb-Argibay, B. Rodriguez-Gonzalez, J. Pacifico, I. Pastoriza-Santos, J. Perez-Juste, L. M. Liz-Marzan, *Angew. Chem. Int. Ed.* **2007**, *46*, 8983.
[154] W. Ni, X. Kou, Z. Yang, J. Wang, *ACS Nano* **2008**, *2*, 677.
[155] J. Pérez-Juste, L. M. Liz-Marzán, S. Carnie, D. Y. C. Chan, P. Mulvaney, *Adv. Funct. Mater.* **2004**, *14*, 571.
[156] M. Liu, P. Guyot-Sionnest, *J. Phys. Chem. B* **2005**, *109*, 22192.
[157] C. Wang, T. Wang, Z. Ma, Z. Su, *Nanotechnology* **2005**, *16*, 2555.
[158] D. K. Smith, B. A. Korgel, *Langmuir* **2008**, *24*, 644.
[159] J. E. Millstone, W. Wei, M. R. Jones, H. Yoo, C. A. Mirkin, *Nano Lett.* **2008**, *8*, 2526.
[160] C. J. Johnson, E. Dujardin, S. A. Davis, C. J. Murphy, S. Mann, *J. Mater. Chem.* **2002**, *12*, 1765.
[161] B. Pan, D. Cui, C. Ozkan, P. Xu, T. Huang, Q. Li, H. Chen, F. Liu, F. Gao, R. He, *J. Phys. Chem.* **2007**, *111*, 12572.
[162] P. L. Gai, M. A. Harmer, *Nano Lett.* **2002**, *2*, 771.
[163] C. J. Orendorff, C. J. Murphy, *J. Phys. Chem. B* **2006**, *110*, 3990.
[164] E. Herrero, L. J. Buller, H. D. Abruna, *Chem. Rev.* **2001**, *101*, 1897.
[165] Y. Yu, S. S. Chang, C. L. Lee, C. R. C. Wang, *J. Phys. Chem. B* **1997**, *101*, 6661.
[166] S. S. Chang, C. W. Shih, C. D. Chen, W. C. Lai, C. R. C. Wang, *Langmuir* **1999**, *15*, 701.
[167] C. W. Shih, W. C. Lai, C. C. Hwang, S. S. Chang, C. R. C. Wang, *Met. Nanopart.* **2002**, 163.
[168] B. Nikoobakht, M. A. El-Sayed, *Langmuir* **2001**, *17*, 6368.
[169] M. Hu, P. Hillyard, G. V. Hartland, T. Kosel, J. Perez-Juste, P. Mulvaney, *Nano Lett.* **2004**, *4*, 2493.
[170] Z. L. Wang, M. B. Mohamed, S. Link, M. A. El-Sayed, *Surf. Sci.* **1999**, *440*, L809.
[171] Z. L. Wang, R. P. Gao, B. Nikoobakht, M. A. El-Sayed, *J. Phys. Chem. B* **2000**, *104*, 5417.
[172] K. Esumi, K. Matsuhisa, K. Torigoe, *Langmuir* **1995**, *11*, 3285.
[173] F. Kim, J. H. Song, P. Yang, *J. Am. Chem. Soc.* **2002**, *124*, 14316.
[174] E. Leontidis, K. Kleitou, T. Kyprianidou-Leodidou, V. Bekiari, P. Lianos, *Langmuir* **2002**, *18*, 3659.
[175] O. R. Miranda, T. S. Ahmadi, *J. Phys. Chem. B* **2005**, *109*, 15724.
[176] O. R. Miranda, N. R. Dollahon, T. S. Ahmadi, *Cryst. Growth Design* **2006**, *6*, 12.
[177] N. R. Jana, *Small* **2005**, *1*, 875.
[178] P. Zijlstra, C. Bullen, J. W. M. Chon, M. Gu, *J. Phys. Chem. B* **2006**, *110*, 19315.
[179] G. Canizal, J. A. Ascencio, J. Gardea-Torresday, M. José Yacamán, *J. Nanopart. Res.* **2001**, *3*, 475.
[180] Y. J. Kim, G. Cho, J. H. Song, *Nucl. Instr. Methods Phys. Res. B* **2006**, *246*, 351.
[181] Y. Zhu, X. Hu, *Chem. Lett.* **2003**, *32*, 1140.
[182] J. Cao, X. Ma, M. Zheng, J. Liu, H. Ji, *Chem. Lett.* **2005**, *34*, 730.
[183] B. M. I. van der Zande, M. R. Boehmer, L. G. J. Fokkink, C. Schoenenberger, *Langmuir* **2000**, *16*, 451.
[184] L. Lu, H. Wang, Y. Zhou, S. Xi, H. Zhang, J. Hub, B. Zhao, *Chem. Commun.* **2002**, 144.
[185] M. Liu, P. Guyot-Sionnest, *J. Phys. Chem. B* **2004**, *108*, 5882.
[186] C. C. Huang, Z. Yang, H. T. Chang, *Langmuir* **2004**, *20*, 6089.
[187] C. S. Ah, S. D. Hong, D. J. Jang, *J. Phys. Chem. B* **2001**, *105*, 7871.
[188] J. H. Song, F. Kim, D. Kim, P. Yang, *Chem. Eur. J.* **2005**, *11*, 910.
[189] J. Becker, I. Zins, A. Jakab, Y. Khalavka, O. Schubert, C. Sönnichsen, *Nano Lett.* **2008**, *8*, 1719.
[190] S. O. Obare, N. R. Jana, C. J. Murphy, *Nano Lett.* **2001**, *1*, 601.
[191] J. Pérez-Juste, M. A. Correa-Duarte, L. M. Liz-Marzán, *Appl. Surf. Sci.* **2004**, *226*, 137.
[192] I. Pastoriza-Santos, J. Pérez-Juste, L. M. Liz-Marzán, *Chem. Mater.* **2006**, *18*, 2465.
[193] I. Gorelikov, N. Matsuura, *Nano Lett.* **2008**, *8*, 369.
[194] A. Gole, J. W. Stone, W. R. Gemmill, H. C. zur Loye, C. J. Murphy, *Langmuir* **2008**, *24*, 6232.
[195] M. Grzelczak, J. Pérez-Juste, B. Rodríguez-González, L. M. Liz-Marzán, *J. Mater. Chem.* **2006**, *16*, 3946.
[196] M. Grzelczak, J. Pérez-Juste, F. J. García de Abajo, L. M. Liz-Marzán, *J. Phys. Chem. C* **2007**, *111*, 6183.
[197] M. Liu, P. Guyot-Sionnest, *J. Mater. Chem.* **2006**, *16*, 3942.
[198] L. Billot, M. Lamy de la Chapelle, A.-S. Grimault, A. Vial, D. Barchiesi, J.-L. Bijeon, P.-M. Adam, P. Royer, *Chem. Phys. Lett.* **2006**, *422*, 303.
[199] J. Grand, S. Kostcheev, J.-L. Bijeon, M. Lamy de la Chapelle, P.-M. Adam, A. Rumyantseva, G. Lérondel, P. Royer, *Synth. Met.* **2003**, *139*, 621.
[200] E. Cubukcu, E. A. Kort, K. B. Crozier, F. Capasso, *Appl. Phys. Lett.* **2006**, *89*, 093120.
[201] P. B. Dayala, F. Koyama, *Appl. Phys. Lett.* **2007**, *91*, 111107.
[202] J. R. Krenn, A. Dereux, J. C. Weeber, E. Bourillot, Y. Lacroute, J. P. Goudonnet, G. Schider, W. Gotschy, A. Leitner, F. R. Aussenegg, C. Girard, *Phys. Rev. Lett.* **1999**, *82*, 2590.
[203] A. N. Grigorenko, N. W. Roberts, M. R. Dickinson, Y. Zhang, *Nat. Photonics* **2008**, *2*, 365.
[204] N. Taub, O. Krichevski, G. Markovich, *J. Phys. Chem. B* **2003**, *107*, 11579.
[205] Y. Xia, P. Yang, Y. Sun, Y. Wu, B. Mayers, B. Gates, Y. Yin, F. Kim, H. Yan, *Adv. Mater.* **2003**, *15*, 353.
[206] Z. Wei, A. J. Mieszawska, F. P. Zamborini, *Langmuir* **2004**, *20*, 4322.
[207] H. Liao, J. H. Hafner, *J. Phys. Chem. B* **2004**, *108*, 19274.
[208] S. I. Shopova, C. W. Blackledge, A. T. Rosenberg, *Appl. Phys. Lett.* **2006**, *89*, 023120.
[209] A. J. Mieszawska, F. P. Zamborini, *Chem. Mater.* **2005**, *17*, 3415.
[210] M. J. Tierney, C. R. Martin, *J. Phys. Chem.* **1989**, *93*, 2878.
[211] C. A. Foss, Jr, G. L. Hornyak, J. A. Stockert, C. R. Martin, *J. Phys. Chem. B* **1992**, *96*, 7497.
[212] C. A. Foss, Jr, G. L. Hornyak, M. J. Tierney, C. R. Martin, *J. Phys. Chem.* **1992**, *96*, 9001.
[213] C. R. Martin, *Science* **1994**, *266*, 1961.
[214] C. A. Foss, Jr, G. L. Hornyak, J. A. Stockert, C. R. Martin, *J. Phys. Chem.* **1994**, *98*, 2963.
[215] C. R. Martin, *Chem. Mater.* **1996**, *8*, 1739.
[216] B. M. I. van der Zande, M. R. Boehmer, L. G. J. Fokkink, C. Schoenenberger, *J. Phys. Chem. B* **1997**, *101*, 852.
[217] J. C. Hulteen, C. R. Martin, *J. Mater. Chem.* **1997**, *7*, 1075.
[218] S. L. Pan, D. D. Zeng, H. L. Zhang, H. L. Li, *Appl. Phys. A* **2000**, *70*, 637.

[219] M. S. Sander, L. S. Tan, *Adv. Funct. Mater.* **2003**, *13*, 393.
[220] D. Losic, J. G. Shapter, J. G. Mitchell, N. H. Voelcker, *Nanotechnology* **2005**, *16*, 2275.
[221] S. Neretina, R. A. Hughes, J. F. Britten, N. V. Sochinskii, J. S. Preston, P. Mascher, *Nanotechnology* **2007**, *18*, 275301.
[222] S. Neretina, R. A. Hughes, G. A. Devenyi, N. V. Sochinskii, J. S. Preston, P. Mascher, *Nanotechnology* **2008**, *19*, 185601.
[223] D. Whang, S. Jin, C. M. Lieber, *Jpn. J. Appl. Phys.* **2004**, *43*, 4465.
[224] N. A. Melosh, A. Boukai, F. Diana, B. Gerardot, A. Badolato, P. M. Petroff, J. R. Heath, *Science* **2003**, *300*, 112.
[225] Z. Deng, C. Mao, *Nano Lett.* **2003**, *3*, 1545.
[226] N. R. Jana, *Angew. Chem. Int. Ed.* **2004**, *43*, 1536.
[227] B. Nikoobakht, Z. L. Wang, M. A. El-Sayed, *J. Phys. Chem. B* **2000**, *104*, 8635.
[228] Z. C. Xu, C. M. Shen, C. W. Xiao, T. Z. Yang, S. T. Chen, H. L. Li, H. J. Gao, *Chem. Phys. Lett.* **2006**, *432*, 222.
[229] G. Kawamura, Y. Yang, M. I. Nogamia, *Appl. Phys. Lett.* **2007**, *90*, 261908.
[230] N. R. Jana, L. A. Gearheart, S. O. Obare, C. J. Johnson, K. J. Edler, S. Mann, C. J. Murphy, *J. Mater. Chem.* **2002**, *12*, 2909.
[231] L. Onsager, *Ann. N. Y. Acad. Sci.* **1949**, *51*, 627.
[232] N. R. Jana, *Chem. Commun.* **2003**, 1950.
[233] C. Yu, J. Irudayaraj, *Biophys. J.* **2007**, *93*, 3684.
[234] C. Yu, H. Nakshatri, J. Irudayaraj, *Nano Lett.* **2007**, *7*, 2300.
[235] Q. Dai, J. Coutts, J. Zou, Q. Huo, *Chem. Commun.* **2008**, *2858*.
[236] K. K. Caswell, J. N. Wilson, U. H. F. Bunz, C. J. Murphy, *J. Am. Chem. Soc.* **2003**, *125*, 13914.
[237] N. Varghese, S. R. C. Vivekchand, A. Govindaraj, C. N. R. Rao, *Chem. Phys. Lett.* **2008**, *450*, 340.
[238] K. G. Thomas, S. Barazzouk, B. L. Ipe, S. T. S. Joseph, P. V. Kamat, *J. Phys. Chem. B* **2004**, *108*, 13066.
[239] X. Hu, W. Cheng, T. Wang, E. Wang, S. Dong, *Nanotechnology* **2005**, *16*, 2164.
[240] S. Zhang, X. Kou, Z. Yang, Q. Shi, G. D. Stucky, L. Sun, J. Wang, C. Yan, *Chem. Commun.* **2007**, 1816.
[241] S. T. S. Joseph, B. I. Ipe, P. Pramod, K. G. Thomas, *J. Phys. Chem. B* **2006**, *110*, 150.
[242] B. Pan, L. Ao, F. Gao, H. Tian, R. He, D. Cui, *Nanotechnology* **2005**, *16*, 1776.
[243] J. Y. Chang, H. Wu, H. Chen, Y. C. Ling, W. Tan, *Chem. Commun.* **2005**, 1092.
[244] R. Voggu, P. Suguna, S. Chandrasekaran, C. N. R. Rao, *Chem. Phys. Lett.* **2007**, *443*, 118.
[245] H. Nakashima, K. Furukawa, Y. Kashimura, K. Torimitsu, *Chem. Commun.* **2007**, 1080.
[246] B. P. Khanal, E. R. Zubarev, *Angew. Chem. Int. Ed.* **2007**, *46*, 2195.
[247] Z. Nie, D. Fava, M. Rubinstein, E. Kumacheva, *J. Am. Chem. Soc.* **2008**, *130*, 3683.
[248] E. Dujardin, L. B. Hsin, C. R. C. Wang, S. Mann, *Chem. Commun.* **2001**, 1264.
[249] C. J. Orendorff, P. L. Hankins, C. J. Murphy, *Langmuir* **2005**, 2022.
[250] T. S. Sreeprasad, A. K. Samal, T. Pradeep, *Langmuir* **2008**, *24*, 4589.
[251] A. Gole, C. J. Murphy, *Langmuir* **2005**, *21*, 10756.
[252] K. Mitamura, T. Imae, N. Saito, O. Takai, *J. Phys. Chem B* **2007**, *111*, 8891.
[253] S. Pierrat, I. Zins, A. Breivogel, C. Sonnichsen, *Nano Lett.* **2007**, *7*, 259.
[254] M. A. Correa-Duarte, J. Perez-Juste, A. Sanchez-Iglesias, M. Giersig, L. M. Liz-Marzan, *Angew. Chem. Int. Ed.* **2005**, *44*, 4375.
[255] I. Gorelikov, L. M. Field, E. Kumacheva, *J. Am. Chem. Soc.* **2004**, *126*, 15938.
[256] M. Das, N. Sanson, D. Fava, E. Kumacheva, *Langmuir* **2007**, *23*, 196.
[257] M. Karg, I. Pastoriza-Santos, J. Perez-Juste, T. Hellweg, L. M. Liz-Marzan, *Small* **2007**, *3*, 1222.
[258] A. Shiotani, T. Mori, T. Niidome, Y. Niidome, Y. Katayama, *Langmuir* **2007**, *23*, 4012.
[259] B. M. I. van der Zande, L. Pages, R. A. M. Hikmet, A. van Blaaderen, *J. Phys. Chem. B* **1999**, *103*, 5761.
[260] J. Pérez-Juste, B. Rodriguez-Gonzalez, P. Mulvaney, L. M. Liz-Marzán, *Adv. Funct. Mater.* **2005**, *15*, 1065.
[261] P. Zijlstra, J. W. M. Chon, M. Gu, *Opt. Express* **2007**, *15*, 12151.
[262] R. Deshmukh, Y. Liu, R. J. Composto, *Nano Lett.* **2007**, *7*, 3662.
[263] B. M. I. van der Zande, G. J. M. Koper, H. N. W. Lekkerkerker, *J. Phys. Chem. B* **1999**, *103*, 5754.
[264] E. E. Connor, J. Mwamuka, A. Gole, C. J. Murphy, M. D. Wyatt, *Small* **2005**, *1*, 325.
[265] H. Takahashi, Y. Niidome, T. Niidome, K. Kaneko, H. Kawasaki, S. Yamada, *Langmuir* **2006**, *22*, 2.
[266] T. S. Hauck, A. A. Ghazani, W. C. W. Chan, *Small* **2008**, *4*, 153.
[267] T. Niidome, M. Yamagata, Y. Okamoto, Y. Akiyama, H. Takahashi, T. Kawano, Y. Katayama, Y. Niidome, *J. Controlled Release* **2006**, *114*, 343.
[268] P. C. Li, C. W. Wei, C. K. Liao, C. D. Chen, K. C. Pao, C. R. C. Wang, Y. N. Wu, D. B. Shieh, *Proc. SPIE* **2006**, *6086*, 60860M1.
[269] T. Niidome, Y. Akiyama, K. Shimoda, T. Kawano, T. Mori, Y. Katayama, Y. Niidome, *Small* **2008**, *4*, 1001.
[270] E. B. Dickerson, E. C. Dreaden, X. Huang, I. H. El-Sayed, H. Chu, S. Pushpanketh, J. F. McDonald, M. A. El-Sayed, *Cancer Lett.* **2008**, *269*, 57.
[271] C. C. Chen, Y. P. Lin, C. W. Wang, H. C. Tzeng, C. H. Wu, Y. C. Chen, C. P. Chen, L. C. Chen, Y. C. Wu, *J. Am. Chem. Soc.* **2006**, *128*, 3709.
[272] H. Nakashima, K. Furukawa, Y. Kashimura, K. Torimitsu, *Langmuir* **2008**, *24*, 5654.
[273] T. B. Huff, L. Tong, Y. Zhao, M. N. Hansen, J. X. Cheng, A. Wei, *Nanomedicine* **2007**, *2*, 125.
[274] C. Yu, L. Varghese, J. Irudayaraj, *Langmuir* **2007**, *23*, 9114.
[275] G. Dechor, *Science* **1997**, *277*, 1232.
[276] F. Caruso, K. Niikura, D. N. Furlong, Y. Okahata, *Langmuir* **1997**, *13*, 3427.
[277] D. I. Gittins, F. Caruso, *J. Phys. Chem. B* **2001**, *105*, 6846.
[278] H. Ai, M. Fang, S. A. Jones, Y. M. Lvov, *Biomacromolecules* **2002**, *3*, 560.
[279] A. Gole, C. J. Murphy, *Chem. Mater.* **2005**, *17*, 1325.
[280] X. Huang, I. H. El-Sayed, M. A. El-Sayed, *J. Am. Chem. Soc.* **2006**, *128*, 2115.
[281] N. J. Durr, T. Larson, D. K. Smith, B. A. Korgel, K. Sokolov, A. Ben-Yakar, *Nano Lett.* **2007**, *7*, 941.
[282] D. Pissuwan, S. M. Valenzuela, M. C. Killingsworth, X. Xu, M. B. Cortie, *J. Nanopart. Res.* **2007**, *9*, 1109.
[283] K. Aslan, J. R. Lakowicz, C. D. Geddes, *Curr. Opin. Chem. Biol.* **2005**, *9*, 538.
[284] M. D. Malinsky, K. L. Kelly, G. C. Schatz, R. P. Van Duyne, *J. Am. Chem. Soc.* **2001**, *123*, 1471.
[285] A. J. Haes, R. P. Van Duyne, *J. Am. Chem. Soc.* **2002**, *124*, 10596.
[286] A. J. Haes, W. P. Hall, L. Chang, W. L. Klein, R. P. Van Duyne, *Nano Lett.* **2004**, *4*, 1029.
[287] A. J. Haes, S. Zou, G. C. Schatz, R. P. Van Duyne, *J. Phys. Chem. B* **2004**, *108*, 6961.
[288] C. Yu, J. Irudayaraj, *Anal. Chem.* **2007**, *79*, 572.
[289] G. J. Nusz, S. M. Marinakos, A. C. Curry, A. Dahlin, F. Hook, A. Wax, A. Chilkoti, *Anal. Chem.* **2008**, *80*, 984.
[290] J. York, D. Spetzler, F. Xiong, W. D. Frasch, *Lab Chip* **2008**, *8*, 415.
[291] N. L. Rosi, C. A. Mirkin, *Chem. Rev.* **2005**, *105*, 1547.
[292] B. M. Reinhard, S. Sheikholeslami, A. Mastroianni, A. P. Alivisatos, J. Liphardt, *Nano Lett.* **2005**, *5*.
[293] C. Wang, Y. Chen, T. Wang, Z. Ma, Z. Su, *Chem. Mater.* **2007**, *19*, 5809.
[294] X. Liu, Q. Dai, L. Austin, J. Coutts, G. Knowles, J. Zou, H. Chen, Q. Huo, *J. Am. Chem. Soc.* **2008**, *130*, 2780.
[295] C. V. Raman, K. S. Krishnan, *Nature* **1928**, *121*, 501.
[296] E. B. Hanlon, R. Manoharan, T. W. Koo, K. E. Shafer, J. T. Motz, M. Fitzmaurice, J. R. Kramer, I. Itzkan, R. R. Dasari, M. S. Feld, *Phys. Med. Biol.* **2000**, *45*, R1.

[297] C. H. Liu, B. B. Das, L. S. Glassman, G. C. Tang, K. M. Yoo, H. R. Zhu, D. L. Akins, S. S. Lubicz, J. Cleary, R. Prudente, E. Celmer, A. Caron, R. R. Alfano, *J. Photochem. Photobiol. B: Biol.* **1992**, *16*, 187.
[298] R. C. Lord, N. T. Yu, *J. Mol. Biol.* **1970**, *50*, 509.
[299] A. S. Haka, K. E. Shafer-Peltier, M. Fitzmaurice, J. Crowe, R. R. Dasari, M. S. Feld, *Proc. Nat. Acad. Soc. USA* **2005**, *102*, 12371.
[300] D. Naumann, *Appl. Spectrosc. Rev.* **2001**, *36*, 239.
[301] A. Mahadevan-Jansen, R. Richards-Kortum, *J. Biomed. Opt.* **1996**, *1*, 31.
[302] R. Petry, M. Schmitt, J. Popp, *ChemPhysChem* **2003**, *4*, 14.
[303] M. Fleischman, P. J. Hendra, A. J. Mcquillan, *Chem. Phys. Lett.* **1974**, *26*, 163.
[304] D. L. Jeanmaire, R. P. Van Duyne, *J. Electroanal. Chem.* **1977**, *84*, 1.
[305] M. Albercht, J. A. Creighton, *J. Am. Chem. Soc.* **1977**, *99*, 5215.
[306] G. C. Schatz, *Acc. Chem. Res.* **1984**, *17*, 370.
[307] T. M. Cotton, J. H. Kim, G. D. Chumanov, *J. Raman Spectrosc.* **1991**, *22*, 729.
[308] I. Nabiev, I. Chourpa, M. Manfait, *J. Raman Spectrosc.* **1994**, *25*, 13.
[309] T. Vo-Dinh, *Trends Anal. Chem.* **1998**, *17*, 557.
[310] A. Campion, P. Kambhampati, *Chem. Soc. Rev.* **1998**, *27*, 241.
[311] L. A. Lyon, C. D. Keating, A. P. Fox, B. E. Baker, L. He, S. R. Nicewarner, S. P. Mulvaney, M. J. Natan, *Anal. Chem.* **1998**, *70*, 341R.
[312] K. Kneipp, H. Kneipp, I. Itzkan, R. R. Dasari, M. S. Feld, *Chem. Rev.* **1999**, *99*, 2957.
[313] C. L. Haynes, C. R. Yonzon, X. Zhang, R. P. Van Duyne, *J. Raman Spectrosc.* **2005**, *36*, 471.
[314] A. Kudelski, *Polish J. Chem.* **2005**, *79*, 1551.
[315] R. F. Aroca, R. A. Alvarez-Puebla, N. Pieczonka, S. Sanchez-Cortez, J. V. Garcia-Ramos, *Adv. Colloid Interface Sci.* **2005**, *116*, 45.
[316] J. A. Dieringer, A. D. McFarland, N. C. Shah, D. A. Stuart, A. V. Whitney, C. R. Yonzon, M. A. Young, X. Y. Zhang, R. P. Van Duyne, *Faraday Discuss.* **2006**, *132*, 9.
[317] E. C. Le Ru, E. Blackie, M. Meyer, P. G. Etchegoin, *J. Phys. Chem. C* **2007**, *111*, 13794.
[318] M. Y. Sha, H. Xu, S. G. Penn, R. Cromer, *Nanomedicine* **2007**, *2*, 725.
[319] I. Chourpa, F. H. Lei, P. Dubois, M. Manfaita, G. D. Sockalingum, *Chem. Soc. Rev.* **2008**, *37*, 993.
[320] M. D. Porter, R. J. Lipert, L. M. Siperko, G. Wang, R. Narayanana, *Chem. Soc. Rev.* **2008**, *37*, 1001.
[321] X. Qian, X. H. Peng, D. O. Ansari, Q. Y. Goen, G. Z. Chen, D. M. Shin, L. Yang, A. N. Young, M. D. Wang, S. Nie, *Nat. Biotechnol.* **2008**, *26*, 83.
[322] B. Nikoobakht, J. Wang, M. A. El-Sayed, *Chem. Phys. Lett.* **2002**, *366*, 17.
[323] N. R. Jana, T. Pal, *Adv. Mater.* **2007**, *19*, 1761.
[324] C. J. Orendorff, L. Gearheart, N. R. Janaz, C. J. Murphy, *Phys. Chem. Chem. Phys.* **2006**, *8*, 165.
[325] R. T. Tom, A. K. Samal, T. S. Sreeprasad, T. Pradeep, *Langmuir* **2007**, *23*, 1320.
[326] A. K. Oyelere, B. Chen, X. Huang, I. H. El-Sayed, M. A. El-Sayed, *Bioconjug. Chem.* **2007**, *18*, 1490.
[327] B. Nikoobakht, J. Wang, M. A. El-Sayed, *J. Phys. Chem. A* **2003**, *107*, 3372.
[328] C. Wang, Y. Chen, T. Wang, Z. Ma, Z. Su, *Adv. Funct. Mater.* **2008**, *18*, 355.
[329] Y. Wang, S. Guo, H. Chen, E. Wang, *J. Colloid Interface Sci.* **2008**, *318*, 82.
[330] M. Suzuki, Y. Niidome, N. Terasaki, K. Inoue, Y. Kuwahara, S. Yamada, *Jpn. J. Appl. Phys.* **2004**, *43*, L554.
[331] S. Yun, Y. K. Park, S. K. Kim, S. Park, *Anal. Chem.* **2007**, *79*, 8584.
[332] X. Hu, W. Cheng, T. Wang, Y. Wang, E. Wang, S. Dong, *J. Phys. Chem B* **2005**, *109*, 19385.
[333] A. Gole, C. J. Orendorff, C. J. Murphy, *Langmuir* **2004**, *20*, 7117.
[334] X. Huang, I. H. El-Sayed, W. Qian, M. A. El-Sayed, *Nano Lett.* **2007**, *7*, 1591.
[335] M. Thakur, B. C. Lentle, *Radiology* **2005**, *236*, 753.
[336] N. R. Jagannathan, *Curr. Sci.* **2007**, *92*, 1061.
[337] W. Cai, X. Chen, *Small* **2007**, *3*, 1840.
[338] K. T. Thurn, E. M. B. Brown, A. Wu, S. Vogt, B. Lai, J. Maser, T. Paunesku, G. E. Woloschak, *Nanoscale Res. Lett.* **2007**, *2*, 430.
[339] P. Sharma, S. Brown, G. Walter, S. Santra, B. Moudgil, *Adv. Colloid Interface Sci.* **2006**, *123–126*, 471.
[340] X. H. Huang, P. Jain, I. H. El-Sayed, M. A. El-Sayed, *Nanomedine* **2007**, *2*, 681.
[341] I. H. El-Sayed, X. Huang, M. A. El-Sayed, *Nano Lett.* **2005**, *5*, 829.
[342] S. A. Boppart, A. L. Oldenburg, C. Xu, D. L. Marks, *J. Biomed. Opt.* **2005**, *10*, 041208.
[343] A. G. Tkachenko, H. Xie, D. Coleman, W. Glomm, J. Ryan, M. F. Anderson, S. Franzen, D. L. Feldheim, *J. Am. Chem. Soc.* **2003**, *125*, 4700.
[344] D. Boyer, P. Tamarat, A. Maali, B. Lounis, M. Orrit, *Science* **2002**, *297*, 1160.
[345] L. Cognet, C. Tardin, D. Boyer, D. Choque, P. Tamarat, B. Lounis, *Proc. Natl. Acad. Sci. USA* **2003**, *100*, 11350.
[346] V. P. Zharov, D. O. Lapotko, *IEEE J. Sel. Top. Quantum Electron.* **2005**, *11*, 733.
[347] T. B. Huff, M. N. Hansen, L. Tong, Y. Zhao, H. Wang, D. A. Zweifel, J. X. Cheng, A. Wei, *Proc. SPIE—Int. Soc. Opt. Eng.* **2007**, *6448*, 64480D.
[348] D. Yelin, D. Oron, S. Thiberge, E. Moses, Y. Silberberg, *Opt. Express* **2003**, *11*, 1385.
[349] M. Lippitz, M. A. van Dijk, M. Orrit, *Nano Lett.* **2005**, *5*, 799.
[350] P. C. Li, C. W. Wei, C. K. Liao, C. D. Chen, K. C. Pao, C. R. C. Wang, Y. N. Wu, D. B. Shieh, *Proc. SPIE* **2006**, *6086*, 60860M.
[351] P. C. Li, C. W. Wei, C. K. Liao, C. D. Chen, K. C. Pao, C. R. C. Wang, Y. N. Wu, D. B. Shieh, *IEEE. Trans. Ultrason. Ferroelect. Freq. Control* **2007**, *54*, 1642.
[352] M. Eghtedari, A. Oraevsky, J. A. Copland, N. A. Kotov, A. Conjusteau, M. Motamedi, *Nano Lett.* **2007**, *7*, 1914.
[353] A. Agarwal, S. W. Huang, M. O'Donnell, K. C. Day, M. Day, N. Kotov, S. Ashkenazi, *J. Appl. Phys.* **2007**, *102*, 064701.
[354] K. Kim, S. W. Huang, S. Ashkenazi, M. O'Donnell, A. Agarwal, N. A. Kotov, M. F. Denny, M. J. Kaplan, *Appl. Phys. Lett.* **2007**, *90*, 223901.
[355] D. L. Chamberland, A. Agarwal, N. Kotov, J. B. Fowlkes, P. L. Carson, X. Wang, *Nanotechnology* **2008**, *19*, 095101.
[356] K. Sokolov, M. Follen, J. Aaron, I. Pavlova, A. Malpica, R. Lotan, R. Richartz-Kortum, *Cancer Res.* **2003**, *63*, 1999.
[357] K. Sokolov, J. Aaron, B. Hsu, D. Nida, A. Gillanwater, M. Follen, C. Macaulay, K. Adler-Storthz, B. Korgel, M. Discour, R. Pasqualini, W. Arap, W. Lam, R. Richartz-Kortum, *Technol. Cancer Res. Treat.* **2003**, *2*, 491.
[358] S. Kumar, K. Sokolov, R. Richards-Kortum, *Proc. SPIE—Int. Soc. Opt. Eng.* **2006**, *6095*, 609504.
[359] K. Sonia, R. Richards-Kortum, *Nanomedicine* **2006**, *1*, 23.
[360] N. Nitin, D. J. Javier, R. Richards-Kortum, *Bioconjug. Chem.* **2007**, *18*, 2090.
[361] J. Aaron, N. Nitin, K. Travis, S. Kumar, T. Collier, S. Y. Park, M. Jose-Yacaman, L. Coghlan, M. Follen, R. Richards-Kortum, K. Sokolov, *J. Biomed. Opt.* **2007**, *12*, 034007.
[362] D. J. Javier, N. Nitin, M. Levy, A. Ellington, R. Richards-Kortum, *Bioconjug. Chem.* **2008**, *19*, 1309.
[363] S. Kumar, N. Harrison, R. Richards-Kortum, K. Sokolov, *Nano Lett.* **2007**, *7*, 1338.
[364] J. Yguerabide, E. E. Yguerabide, *Anal. Biochem.* **1998**, *262*, 137.
[365] J. Yguerabide, E. E. Yguerabide, *Anal. Biochem.* **1998**, *262*, 157.
[366] C. J. Orendorff, T. K. Sau, C. J. Murphy, *Small* **2006**, *2*, 636.
[367] C. Loo, L. Hirsch, M. H. Lee, E. Chang, J. West, N. Halas, R. Drezek, *Opt. Lett.* **2005**, *30*, 1012.
[368] J. Chen, F. Saeki, B. J. Wiley, H. Cang, M. J. Cobb, Z. Y. Li, L. Au, H. Zhang, M. B. Kimmey, X. Li, Y. Xia, *Nano Lett.* **2005**, *5*, 473.
[369] H. Ding, K. T. Yong, I. Roy, H. E. Pudavar, W. C. Law, E. J. Bergey, P. N. Prasad, *J. Phys. Chem. C* **2007**, *111*, 12552.
[370] A. L. Oldenburg, M. N. Hansen, D. A. Zweifel, A. Wei, S. A. Boppart, *Opt. Express* **2006**, *14*, 6724.
[371] L. Tong, Y. Zhao, T. B. Huff, M. N. Hansen, A. Wei, J. X. Cheng, *Adv. Mater.* **2007**, *19*, 3136.
[372] M. D. Brown, A. G. Schätzlein, L. F. Uchegbu, *Int. J. Pharm.* **2001**, *229*, 1.

[373] M. R. Kumar, G. Hellermann, R. F. Lockey, S. S. Mohapatra, *Expert Opin. Biol. Ther.* **2004**, *4*, 1213.
[374] J. Dobson, *Gene Ther.* **2006**, *13*, 283.
[375] N. L. Rosi, D. A. Giljohann, C. S. Thaxton, A. K. R. Lytton-Jean, M. S. Han, C. A. Mirkin, *Science* **2006**, *312*, 1027.
[376] H. Takahashi, Y. Niidome, S. Yamada, *Chem. Commun.* **2005**, 2247.
[377] Y. Horiguchi, T. Niidome, S. Yamada, N. Nakashima, Y. Niidome, *Chem. Lett.* **2007**, *36*, 952.
[378] Q. Wei, J. Ji, J. Shen, *Macromol. Rapid Commun.* **2008**, *29*, 645.
[379] N. W. S. Kam, M. O'Connell, J. A. Wisdom, H. Dai, *Proc. Natl. Acad. Sci. USA* **2005**, *102*, 11600.
[380] A. G. Cuenca, H. Jiang, S. N. Hochwald, M. Delano, W. G. Cance, S. R. Grobmyer, *Cancer Lett.* **2006**, *107*, 459.
[381] H. F. Dvorak, J. A. Nagy, J. T. Dvorak, A. M. Dvorak, *Am. J. Pathol.* **1988**, *133*, 95.
[382] H. Maeda, *Adv. Enzyme Regul.* **2001**, *41*, 189.
[383] H. Maeda, J. Fang, T. Inutsuka, Y. Kitamoto, *Int. Immunopharma* **2003**, *3*, 319.
[384] F. F. Davis, *Adv. Drug Deliv. Rev.* **2002**, *54*, 457.
[385] H. Ringsdorf, *J. Polym. Sci, Part C: Polym. Symp.* **1975**, *51*, 135.
[386] S. M. Moghimi, A. C. Hunter, *Trends Biotechnol.* **2000**, *18*, 412.
[387] T. M. Allen, *Nat. Rev. Cancer* **2002**, *2*, 750.
[388] H. Liao, J. H. Hafner, *Chem. Mater.* **2005**, *17*, 4636.
[389] K. C. Black, N. D. Kirkpatrick, T. S. Troutman, L. Xu, J. Vagner, R. J. Gillies, J. K. Barton, U. Utzinger, M. Romanowski, *Mol. Imaging* **2008**, *7*, 50.
[390] C. M. Pitsillides, E. K. Joe, X. Wei, R. R. Anderson, C. P. Lin, *Biophys. J.* **2003**, *84*, 4023.
[391] L. R. Hirsch, R. J. Stafford, J. A. Bankson, S. R. Sershen, R. E. Price, J. D. Hazle, N. J. Halas, J. L. West, *Proc. Natl. Acad. Sci. USA* **2003**, *100*, 13549.
[392] I. H. El-Sayed, X. Huang, M. A. El-Sayed, *Cancer Lett.* **2006**, *239*, 129.
[393] X. Huang, P. K. Jain, I. H. El-Sayed, M. A. El-Sayed, *Photochem. Photobiol.* **2006**, *82*, 412.
[394] H. Takahashi, T. Niidome, A. Nariai, Y. Niidome, S. Yamada, *Chem. Lett.* **2006**, *35*, 500.
[395] H. Takahashi, T. Niidome, A. Nariai, Y. Niidome, S. Yamada, *Nanotechnology* **2006**, *17*, 4431.